UNIVERSIDADE DE SÃO PAULO

ESCOLA DE ENGENHARIA DE SÃO CARLOS

Programa de Pós-Graduação em Ciências da Engenharia Ambiental

TSENG CHIEN LING

A avaliação da qualidade ambiental de uma área degradada em recuperação e o processo de secagem de um solo brasileiro utilizando métodos não convencionais em escala micrométrica

São Carlos

2017

UNIVERSITY OF SÃO PAULO

SÃO CARLOS SCHOOL OF ENGINEERING

Graduate Program in Environmental Engineering Sciences

TSENG CHIEN LING

The environment qualities evaluation of a degraded area in recuperation and the drying process of a Brazilian soil using nonconventional methods at micrometric scale

São Carlos

2017

TSENG CHIEN LING

The environment qualities evaluation of a degraded area in recuperation and the drying process of a Brazilian soil using nonconventional methods at micrometric scale

Doctoral thesis submitted to São Carlos School of Engineering, University of São Paulo, in partial fulfillment of the requirements for the Degree of Doctor in Science: Environmental Engineering Science.

Advisor: Prof. Dr. Silvio Crestana

São Carlos

2017

Index card prepared by User Service at "Prof. Dr. Sergio Rodrigues Fontes Library" at EESC/USP

Tseng, Chien Ling
T882e The environment qualities evaluation of a degraded area in recuperation and the drying process of a Brazilian soil using nonconventional methods at micrometric scale / Tseng Chien Ling; advisor Silvio Crestana. -- São Carlos, 2017.

Doctoral(Thesis) - Graduate Program and Concentration area in Hydraulics and Sanitation Engineering. -- São Carlos School of Engineering, at University of São Paulo, 2017.

1. X-ray microtomography. 2. Gamma-ray granulometric analyzer. 3. Physical parameters. 4. Soil recovery. 5. Water I. Titulo.

FOLHA DE JULGAMENTO

Candidata: Licenciada **TSENG CHIEN LING.**

Título da tese: "A avaliação da qualidade ambiental de uma área degradada em recuperação e o processo de secagem de um solo brasileiro utilizando métodos não invasivos em escala micrométrica".

Data da defesa: 03/04/2017.

Comissão Julgadora: **Resultado:** Aprovada

Prof. Dr. **Silvio Crestana**
(Orientador)
(EMBRAPA)
APROVADO

Profa. Dra. **Marlene Cristina Alves**
(Universidade Estadual Paulista "Júlio de Mesquita Filho"/UNESP – Ilha Solteira) APROVADO

Dr. **Adolfo Nicolas Posadas Durand**
(Centro Internacional de Investigación Agroflorestal/ICRAF)
APROVADO

Prof. Dr. **André Luís Brasil Cavalcante**
(Universidade de Brasília/UnB)
APROVADO

Dr. **Carlos Manoel Pedro Vaz**
(EMBRAPA)
APROVADO

Coordenador do Programa de Pós-Graduação em Ciências da Engenharia Ambiental:
Prof. Associado **Frederico Fabio Mauad**

Presidente da Comissão de Pós-Graduação:
Prof. Associado **Luís Fernando Costa Alberto**

DEDICATION

To my grandparents Chin Tien and Feng [*in memoriam*], their love and affection are still present every day of my life.

To my parents Hui Ping and Hsiu Shih for believing and supporting unconditionally my choices, with deep love and wisdom.

ACKNOWLEDGMENT

I am grateful to God for constantly inspiring me to seek everything that I am not aware and at the same time to give me strength on this journey, even though it is sometimes sinuous, however, He always leaves surprises and hopes at the end of tunnel.

I am deeply grateful to my advisor Prof. Dr. Silvio Crestana for being my Bólè [one able to see, believe and explore my potentials] to became a scientist. Most importantly, I am very grateful for his friendship, guidance and patience from the first time I entered his office in 2010. He has always shown me the importance of the human side in a scientist and, at same time, showing the presence of lucidity, wisdom and serenity in all circumstances. That is in tune, with a famous phrase "Think big, Start small and Move fast".

I would like to express my sincere gratitude to Prof Marlene Cristina Alves and her team from UNESP, Ilha Solteira Campus – São Paulo States, for disposition and enthusiasm during collection and preparation of samples. Especially for her friendship and example of people who inspire love and care towards soil, as well as persistent spirit and laborious work to recover and care for this planet.

Thanks also to Embrapa Instrumentation - São Carlos – São Paulo States, to the space, equipment and full support to this work, for this is such a wonderful place, and it has become part of who I am today.

Thanks to São Carlos School of Engineering – University of São Paulo, through its Post Graduate Program in Environmental Engineering Science (PPG-SEA) for this great professional and personal growth opportunity.

To the Deparment of Mechanical Engineering of Federal University of Santa Catarina (EMC/UFSC) for the concession to use nano and microtomography and other equipment used during the experiment of this doctoral thesis.

I offer my most sincere thanks to Dr. Carlos Manoel Pedro Vaz, Dr. Adolfo Nicolas Posadas Durand, Dr. Ole Wendroth, Dr. Débora Marcondes Bastos Pereira Milori, Dr. João de Mendonça Naime and Dr. Ednaldo José Ferreira all of whom with their profound knowledge deeply contributed to this research offering me a new vision about sciences.

I would like to thank to lab technicians: Paulinho, Mattêo, Silviane, Alice, Adriana, Viviane, Joana, Seu Godoy, Jorge and Pedro Bonfim for informations and technical support on sample's preparation and equipment operation, especially for their help and meticulousness during the experiments.

I would like to thank Prof. Celso Fernandes, Dr. Anderson Camargo Moreira and Dr. Iara Frangiotti Mantovani for disposition and patience during experiment and, above all, their friendship and fallow up during my stay in Florianópolis.

I wish to thank Nelson e José Chiaretto from the secretariat of PPG-SEA; Karla, Élita, Kellen, Mirella, Liliane and Dilma from Embrapa Instrumentation for their attention and kindness to answer and solve all problems related to document processing in the course of this doctoral thesis.

Thanks to Ligia for her sisterhood and patience, for she was always there to help me unconditionally during my despair in Portuguese revision/correction. Above all, I am very grateful for her uncountable support to me during those moments of uncertainty and obstacles, as well as unique personal moments of my growth.

To André Luiz for his attention and competency to solve my computing problem, I am also very grateful for his encouragement and companionship to face together all the challenges presented along this journey.

Mariângela and André Sartori for their friendship and constant ironic humor, turning the most worrying and tense moments into inspiring moment, for the example of person they are, always perseverant and optimist to overcome the impossible.

My "eternal intern" Rodrigo Gounella for his commitment to the project and partnership during all my laboratory activities and, for his friendship and tranquility, which transformed the monotonous moments into a great fun and insight.

To Brianne, Adele and João Henrique for their friendship and great care in the translation and correction of the English text and for their example of person they are, always seeking to improve and increase their knowledge in different areas.

My uncle and aunt: Jei and Lai, although living abroad, they have always participated in my study journey with love and affection.

My dear parent: Hui Ping and Hsiu Shih, it is hard to find words able to totally measure my gratitude toward them. I am very touched by their confidence in my choices and mainly for being the foundation for me to go and fallow my chosen path; and above all for teaching me how I should look inside me and listen the voice of my heart and encourage me to follow this voice firmly and happily.

My adorable brother Yao Hsing, for his support and peculiar humor to transform my critical moments into laughs and thus helping me to carry on with total lightness and confidence.

To CNPq and CAPES for granting me scholarship and all financial support for this doctoral thesis.

Finally, my profound gratitude to all the above mentioned and those who directly or indirectly contributed to this work, because without them, I definitely would not have accomplished this step, which is very important to my life, as well as to get stronger to continue this journey.

Dream the impossible, then go out and make it happen!

- Gene Cernan

RESUMO

Tseng, C. L. **A avaliação da qualidade ambiental de uma área degradada em recuperação e o processo de secagem de um solo brasileiro utilizando métodos não-convencionais em escala micrométrica.** 2017. 182 f. Tese (Doutorado em Ciências da Engenharia Ambiental) - Escola de Engenharia de São Carlos, Universidade de São Paulo, São Carlos, 2007.

O solo é um recurso fundamental no meio ambiente, seu uso sustentável é vital para prover alimentos e consequentemente a continuidade da vida na Terra. No entanto, estado atual desse recurso no mundo encontra-se em condição crítica, logo as medidas de recuperação devem ser adotadas urgentemente, consequentemente a necessidade de métodos adequados para avaliação dessas medidas. O objetivo desse estudo é proporcionar uma avaliação holística sobre a arquitetura do solo em diferentes estados de recuperação, assim como sua interação com fluido no meio ambiente utilizando métodos não convencionais. Logo, foi organizado um pacote de ferramentas que permitam analisar a física solo no âmbito de geometria, morfometria e energia, proporcionando parâmetros físicos que indicam a qualidade física e ambiental; Em seguida esse pacote foi aplicado no estudo de seis tipos de manejos com diferentes estágios de desenvolvimento, envolvendo os parâmetros físicos derivados do pacote, mostrando assim a eficiência das técnicas de recuperação sob diferentes perspectivas; Assim foi realizado também a avaliação da dinâmica da água no solo em uma situação particular utilizando as mesmas ferramentas, proporcionando conhecimentos sobre o essa interação no meio ambiente ao longo do tempo. Finalmente, espera-se com esse trabalho novos olhares sobre esse recurso precioso no meio ambiente.

Palavras-chaves: Microtomografia de raios-X. Analisador granulométrico. Parâmetros físicos. Recuperação de solo. Água.

ABSTRACT

Tseng, C. L. **The environment qualities evaluation of a degraded area in recuperation and the drying process of a Brazilian soil using nonconventional methods at micrometric scale.** 2017. 182 p. Doctoral (Thesis in Environmental Engineering Sciences) - São Carlos School of Engineering, University of São Paulo, São Carlos, 2017.

Soil is a fundamental resource in the environment, its sustainable use is vital to food supply and, consequently, life continuity on the Earth. However, the currently status of this resource in the world is critical and, therefore, the need of soil recovery measures and methods to evaluate it is urgent. The aim of this study is to provide a holistic evaluation about soil architecture at different recovery states, as well as its interaction with fluid in the environment by using nonconventional methods. It was organized a tool package that allows to analyze soil physical at geometric, morphometric and energy scope, to show in a more efficient way, which physical parameters indicate the physical and environmental quality. Subsequently, this package was applied to the study of six types of managements in different stages of development by using of physical parameter derived from the package; It was also analyzed the efficiency of recovery techniques under different perspectives. In addition, the soil-water dynamic was evaluated in a particular condition by using the same tools, offering knowledge about this interaction in the environment along the time. Finally, it is expected that this work can bring new insight on preservation and recovery of this environmental resource.

Keywords: X-ray microtomography. Gamma-ray granulometric analyzer. Physical parameters. Soil recovery. Water.

SUMMARY

ACKNOWLEDGMENTS……..……11

RESUMO……17

ABSTRACT……..……..19

THESIS PRESENTATION……25

Objectives…….……27
General objectives……...……..27
Specific objectives…….…….……..……....……...27
Hypothesis…….……28

CHAPTER I…….……....29

GENERAL INTRODUCTION…….....29
1. Food security and land use in Brazil…….……..…30
2. The application of nuclear techniques in the study of degraded area recuperation – Selvíria (Mato Grosso do Sul State) - Brazil……..….32
3. Image analysis software for research…..……..……34
   Reference……35

CHAPTER II……..…….……37

A TOOL PACKAGE FOR SOIL PHYSICAL ANALYSIS BASED ON NONCONVENTIONAL TECHNIQUE……..……..37

Abstract……38
1. Introduction……...…39
2. Material and methods……40
3. Results and Discussion……..50
3.1 Design of Process……...……...…….50
3.2 Tools demonstration…….……56
4. Conclusion……....58

Reference……59

CHAPTER III……65

CHARACTERIZATION OF SOIL ARCHITECTURE UNDER DIFFERENT TYPES OF MANAGEMENT THROUGH ANALYTICAL TOOLS……65

Abstract……66

1. Introduction……67
2. Material and Methods……69
3. Results and Discussion……73

3.1 Microtomographic calibration……73

3.2 The particle size distribution……74

3.3 Porosity - ϕ_c and ϕ_t……75

3.4 Form Factor……78

3.5 Lacunarity……80

3.6 Relationship between total porosity (%) and lacunarity……82

4. Conclusion……82

Reference……83

CHAPTER IV……87

QUANTIFYING PHYSICAL AND STRUCTURAL SOIL PROPERTIES USING X-RAY MICROTOMOGRAPHY……87

Abstract……88

1. Introduction……89
2. Material and Methods……91
3. Results and Discussion……96

3.1 S Index and SWRC……96

3.2 Degree of Anisotropy……98

3.3 Euler-Poincaré number……99

3.4 Shannon Entropy……100

3.5 Soil Structure Visualization……101

3.6 Water Movement Pathways in Three-Dimensional Simulations……103

4. Conclusion……106

Reference……106

CHAPTER V……111

THE APPLICATION OF MULTIFRACTAL ANALYSIS IN MICROTOMOGRAPHY FOR EVALUATING RECOVERY TECHNIQUES AT A BRAZILIAN OXISOL
……111

Abstract……112

1. Introduction……113
2. Material and Methods……114
3. Results and Discussion……118

3.1 Multifractal spectrum……118

3.2 Entropy of system……122

3.3 Degree of multifractality (Δ)……124

3.4 Degree of asymmetry (A)……126

4. Conclusion……127

Reference……128

CHAPTER VI……133

CHARACTERIZATION OF WATER DYNAMICS PROCESS UNDER DRYING CYCLE IN A BRAZILIAN SOIL USING MICROTOMOGRAPHY DIGITAL PROCESSING……133

Abstract……134

1. Introduction……135
2. Material and Methods……136
3. Results and Discussion……144

3.1 Image quality……144

3.2 Physical parameters analysis……148

3.2.1 Shannon Entropy……149

3.2.2 Soil water retention curve……150

3.2.3 Soil porosity……151

3.2.4 Lacunarity……156

3.2.5 Euler-Poincaré number……157

3.2.6 Degree of anisotropy……158

3.2.7 Tortuosity 2D……160

3.2.8 Tortuosity 3D……162

4. Conclusion……..163
Reference……165

CHAPTER VII……..……171

FINAL REMARKS……..……..171
1. Main remarks…...…….……..……172
2. Suggestions for future research…….....173

APPENDIX I……..…175

APPLICATION OF COMPUTED TOMOGRAPHY TECHNIQUES AT MICRO AND NANOMETRIC RESOLUTION IN SOIL MATRIX INVESTIGATION…….175
Abstract……...176
1. Introduction……177
2. Material and Methods……178
3. Results and Discussion……179
3.1 Techniques potential……..…….179
3.2 Sample preparation for x-ray nanotomography……...……...180
4. Final consideration……..181
Reference……....181

THESIS PRESENTATION

This thesis is divided into three main topics: 1) Research and use of non-conventional tools for soil investigation in the environment; 2) Application of the tools package in the evaluation of recuperation process on degraded areas and 3) Investigation of water behavior within the soil in the micrometric scale along the time.

The thesis structure was developed in scientific paper format, which consists of five articles and one scientific note; two of the papers have been already submitted to international periodic and four of them are in final stage to be submitted soon.

Chapter 1 – Brief contextualization and motivation of this study shows the importance of soil preservation and appropriate use of methodology and instrumentation applied to the recuperation process evaluation of degraded areas in the environment.

Chapter 2 (Scientific paper) – **A tool package for soil physical analysis based on non-conventional techniques**: It is the use of techniques and methods for the study of soils physical parameters, involving soil morphometry, geometry and energy.

Chapter 3 (Scientific paper) – **Characterization of soil architecture under different types of management through analytical tools**: Application of tool package in the investigation of soils geometry under different types of management.

Chapter 4 (Scientific paper) – **The quantification of soil physical structural properties through X-ray microtomography**: Application of tool package to the investigation of soil morphometry under different types of management and the visualization of three planes and three-dimensional simulation of water pathway in the soil.

Chapter 5 (Scientific paper) – **The application of multifractal analysis in microtomography for evaluating recovery techniques of a Brazilian Oxisol**: Application of tool package in the investigation of soil energy under different types of management at two planes and three depths.

Chapter 6 (Scientific paper) – **Characterization of water dynamics process under drying cycle in a Brazilian soil using microtomography digital processing**: Quantification of physical parameters which are related to water movement in geometrical, morphometrical and energy extent scope along the time.

Chapter 7 – Final remarks about all topics studied during doctoral period and suggestions for future researches.

Appendix I (Scientific note) – **Application of computerized tomography technique in the micro and nanometric resolution in the investigation of soil matrix**: The preliminaries

results for soil study by means of non-conventional technology at multiscale, from micrometer to nanometer.

OBJECTIVES

General Objective

The main objective of this work is to provide a holistic perspective of tropical soil architecture through non-conventional methods to study soil physical quality and land use, as well as to investigate fluid dynamic of a non-saturated soil along the timeline employing X-ray microtomography.

Specific objectives

1) To provide physical parameters that allow evaluating soil architecture, including the geometry, the morphometry and energy at micro scale using X-ray microtomography;
2) To characterize physical differences between managements through digital image processing;
3) To quantify water dynamic over the time of a Brazilian oxisol at micro scale;
4) To afford internal structure simulation of a Brazilian Oxisol submitted in different managements and drying process.

HYPOTHSIS

This doctoral thesis is intended to explore two hypothesis, applying no-conventional methods to a Brazilian oxisol, under dry and unsaturated condition. The hypothesis are:

1) From the high-resolution tomographic images is possible to achieve qualitative and quantitative results that allow new understanding about a soil submitted to different managements, including the establishment of adequate physical parameters for this purpose.

2) Based on an unsaturated soil at drying process, it is possible to quantify, to simulate and to predict fluid dynamic over time, by using a high-resolution bench-top X-ray microtomography.

CHAPTER I

General Introduction

.

1. Food security and the land use in Brazil

Looking at the environmental changes at last decade, in global or local scale, it is recognized that, there is a great effort to answer or mitigate negative impacts consequences caused by human activities. However, the result have not been very positive in order to decelerate or reverse such impacts, considering that the record of the past five years showed that the humanity is living in critical thresholds (PROGRAMA DAS NAÇÕES UNIDAS PARA O MEIO AMBIENTE, 2012).

The population growth has been one of the main reasons for emergency of critical thresholds. Consequently, in order to meet the food needs of the population, it is necessary to produce more food. According to the latest FAO estimative (2015), there are 795 million undernourished people in the world, in other words, one in nine people does not have sufficient food to lead a healthy life.

Food production and food security are strongly dependent on soil resource. Nevertheless, as stated at "Status of The World's Soil Resource" report, nowadays, most parts of soils in the world are in median, poor or very poor condition and the tendency is to get worse. Erosion is one of the main contributor to this degradation process; there is still a possibility of losing more than 10% arable land, equivalent to 1.5 million km^2 of area of agricultural production, i.e. all arable land of India until 2050 if any intervention measure is adopted (FAO and ITPS, 2015).

To minimize degradation of vulnerable area, to recuperate degraded soil and to further improve knowledge about state and tendency of soil, all these measures must certainly be adopted in sustainable management practice today (FAO and ITPS, 2015).

Brazil is characterized by its competence in the agricultural sector. Technological development, agribusiness and Cerrado' (Brazilian Savannah) development programs (GUANZIROLI; BERENGUER, 2010) transformed Brazil into an important link in food security issue within the international context. Faced with long-term projections, Brazil shall contribute to a significant part to ensure food security in the world.

However, despite these promising perspective for agricultural sector growth of Brazil, the environmental consequences that could be triggered due to production necessity, are very worrying. For example, according to the Ministry of Agriculture data, the country currently has 50% of the farming land linked to pasture (INSTITUTO BRASILEIRO DE GEOGRAFIA E ESTATÍSTICA, 2007), none the less, around 32 million hectares of this area, is in some degradation stage (Figure 1).

Figure 1: Scenario 1 – With great optimism, pasture with some degree of degradation corresponds to 12.5 million hectares, i.e. 24% of total planted pasture at Cerrado; Scenario 2 – I was classified as the optimist, this area rises to around 18.4 million hectares, i.e. 35%; Scenario 3 – It was considered the most realistic, it was identified around 32 million hectares of degraded pasture, in other words, 60 % of planted pastures at Cerrado.

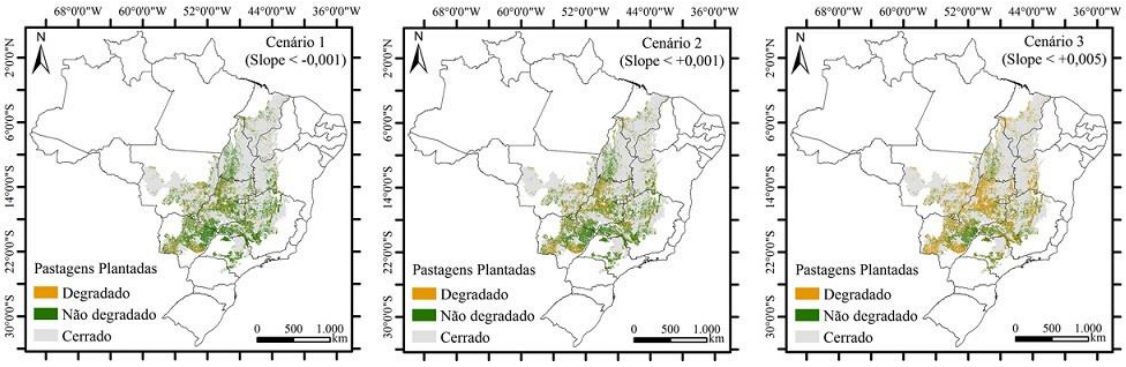

	Pastagem degradada	
UF	Milhões de hectares	Porcentagem (%)
BA	0,55	25
DF	0,03	26
GO	3,46	27
MA	0,36	21
MG	2,05	18
MS	2,86	25
MT	2,04	32
PI	0,18	38
PR	0,02	19
SP	0,40	16
TO	0,53	13
Total	**12,49**	**24**

	Pastagem degradada	
UF	Milhões de hectares	Porcentagem (%)
BA	0,85	39
DF	0,04	37
GO	5,25	42
MA	0,66	37
MG	3,05	26
MS	3,98	35
MT	2,77	44
PI	0,24	48
PR	0,03	28
SP	0,58	23
TO	0,94	22
Total	**18,37**	**35**

	Pastagem degradada	
UF	Milhões de hectares	Porcentagem (%)
BA	1,55	71
DF	0,07	60
GO	8,80	70
MA	1,30	74
MG	5,82	50
MS	6,52	58
MT	4,25	67
PI	0,34	68
PR	0,05	51
SP	1,09	42
TO	2,13	51
Total	**31,93**	**60**

Source: Andrade et al. (2016)

This degradation is understood as deterioration of edaphic properties, which is a result of inadequate management of the natural resource. In this way, it generates the loss of productive capacity of agricultural soil, the increase of fertilizer and agrotoxic use, depletion of water sources, siltation of rivers and reservoirs, natural collapses or by means of machinery and social problems (CAPECHE et al., 2008).

A number of measures to be adopted would be to rely on technology investment and intensification of agricultural practice. However, to avoid collateral effects of the intensification process, mainly environmental degradation, it should be used appropriate management practice, which would allow an increase in productivity,

It would also avoid erosion problems, increase carbon stock and, it would still recuperate vast degraded areas by pasture; i.e., to reverse the situation, it will be necessary a new paradigm for tropical countries with agricultural potential, seriously considering the soil sustainable use, taking into account climate changes and biodiversity conservation, together with food security issue (LAPOLA et al., 2013).

Thus, the presence and application of adequate instrumentation, equipments and methodology are becoming indispensable to evaluate agricultural activities performance and

effect in the environment. In particular, with regard to the physical parameters that constitutes soil architecture: soil's geometrical, morphometrical and energy characteristics and its association to the physical-hydro process, such as water and solute infiltration into the soil.

2. The application of nuclear techniques to the study of degraded area recuperation – Selvíria (Mato Grosso do Sul State) - Brazil

Cerrado (Brazilian Savannah) is the second largest biome of South America, which occupies 22% of Brazilian territory and it is the most important hotspot to biodiversity conservation in the world (MYERS et al., 2000). There is in the Cerrado area expansion of agricultural activity, due to favorable topology to mechanization, excellent physical properties and easily fertility correction using liming and fertilization, the biome predominant soil is Brazilian oxisol, which occupies almost 46% of the area, however, it is characterized by high degree of erosion susceptibility (EMBRAPA SOLOS, 2002).

For this research, the study was installed at Fazenda de Ensino e Pesquisa Produção Animal of Universidade Estatual Paulista (UNESP), Ilha Solteira campus; it is located along Paraná river, Selvíria city (Mato Grosso do Sul State); the local original vegetation is typical of Cerrado (Brazilian Savannah), the soil is dystrophic Brazilian oxisol and highly weathered. This site presents traces of the impact from Ilha Solteira Hydroelectric plant implantation, where 8.6 meters of soil was removed in the 1960's (BONINI ; ALVES, 2011; MARCHINI et al., 2015). Since then, the subsoil has been exposed (Figure 2) (DEMATTÊ, 1980; AGROPECUÁRIA-EMBRAPA, 2006). At the same time, the region also presents considerable agricultural activities; there is presence of pasture at various degrees of degradation.

Figure 2: Satellite image showing the experimental area

Source: Google Maps (2012)

In 1992 it has started the area recovery: Various techniques were implemented with positive results (Photography 1 to 8). Still, in terms of analysis, there is yet gaps to be better explored, mainly by using non-conventional techniques that allow investigation of soil physical properties, with utmost preservation of the soil architecture and its entire function in the nature.

Photography 1: Trench digging

Source: Author (2013)

Photography 2: Removing soil bloc from a trench

Source: Author (2013)

Photography 3: Soil from native forest – Cerrado (**NF**)

Source: Author (2013)

Photography 4: Recuperated soil (**RS**)

Source: Author (2013)

Photography 5: Recuperating soil (**G**)

Source: Author (2013)

Photography 6: Degraded soil (**D**)

Source: Author (2013)

Photography 7: Recuperating pasture soil (**RP**)

Source: Author (2013)

Photography 8: Degraded pasture soil (**DP**)

Source: Author (2013)

Therefore, the use of nuclear techniques in the environmental and agricultural Science in the characterization of soil structure has become useful qualitative and quantitative analysis. For this study, it was applied automatic gamma-ray granulometry analyzer and X-ray microtomography to obtain a serial of soil physical parammeter: bulk density, particle density, granulometry distribution, soil physical quality index, water retention curve, porosity, form factor, lacunarity, Euler-Poincaré, degree of anisotropy, tortuosity, Shannon entropy and random-walk simulation of water pathway into the soil, all of which will be better illustrated in the next chapter.

3. Image analysis software for soil research

There are various available image analysis software today. Although they are not intended only for soil study, however, they are widely used due to their practicality and to the possessing principles. Among the digital image processing software used by soil scientist, it is worth highlighting: Mathematic, ImageJ, CT-Analyser, Matlab, Avizo Fire and other softwares less frequently used: Macroview, 3D-Doctor, Amide, etc (TAINA; HECK; ELLIOT, 2008). Based on the mentioned software, it was elaborated some standards of comparison between five software highlighted, with the intention of selecting the most appropriate to this present study, which are software cost, accessibility, adaptation, openness code, online technical support, academic frequent use and 3D visualization of the object in study.

Then, from the requirements of this research and considering financial support, we choose CTAn (CT-Analyser), ImageJ, Mathematica, R and MASS, consisting in a total of five software to complete the research. Each of them was properly designed to investigate a different function during the analysis. Besides the mentioned standards of comparison, it was also taken into consideration the time available for the learning process of the software and

the previous experience in the software manipulation in the scientific work. The application of each software will be explained in the next chapters.

Reference

ANDRADE, R. G. et al. Recuperação de pastagens no cerrado. **AgroANALYSIS**, v. 36, n. 2, p. 30-32, 2016.

BONINI, S. B. AND ALVES, M. C. Recovery of soil physical properties by green manure, liming, gypsum and pasture and spontaneous native species[1]. **Revista Brasileira de Ciência do Solo**, v. 35, n. 4, p. 1397-1406, 2011.

CAPECHE, C. et al. Degradação do solo e da água: impactos da erosão e estratégias de controle. In: TAVARES, S. R. de L et al. **Curso de recuperação de áreas degradadas:** a visão da ciência do solo no contexto do diagnóstico, manejo, indicadores de monitoramento e estratégias de recuperação. Rio de Janeiro: Embrapa Solos, 2008. cap. 5, p. 105-132.

DEMATTÊ, J. L. I. **Levantamento detalhado dos solos do campus experimental de Ilha Solteira**. Piracicaba: ESALQ/USP, 1980.

EMBRAPA SOLOS. **Relatório técnico e plano de monitoramento do Projeto de Recuperação de Áreas Degradadas**. Rio de Janeiro: [s.n.], 2002.

EMPRESA BRASILEIRA DE PESQUISA AGROPECUÁRIA. **Manual de métodos de análise de solo**. 2. ed. rev. e atual. Rio de Janeiro: Centro Nacional de Pesquisa de Solos, 2006.

FAO (2015) Status of the World's Soil Resources. FAO, Rome. www.fao.org/3/a-i5199e.pdf (accessed 15.01.17)

GUANZIROLI, C.; BERENGUER, M. O. Experiências recentes em agronegócio e desenvolvimento rural sustentável bem sucedidas no Brasil. Brasília: IICA, 2010. Disponível em: <http://www.iicabr.iica.org.br/wp-content/uploads/2014/03/experiencias_recentes.pdf> Acesso em: 15 jan. 2017.

INSTITUTO BRASILEIRO DE GEOGRAFIA E ESTATÍSTICA. **Manual Técnico de Pedologia**. 2. ed. Rio de Janeiro: [s.n.], 2007. (Manuais Técnicos em Geociências, número 4). Disponível em: <http://biblioteca.ibge.gov.br/visualizacao/livros/liv37318.pdf >. Acesso em: 15 jan. 2017.

LAPOLA, D. M. et al. Pervasive transition of the Brazilian land-use system. **Nature Climate Change**, v. 4, n. 1, p. 27-35, 2014.

MARCHINI, D. C., et al. Matéria orgânica, infiltração e imagens tomográficas de Latossolo em recuperação sob diferentes tipos de manejo. **Rev. Bras. Eng. Agríc. Amb**, v. 19, p. 574-580, 2015.

MYERS, N., MITTERMEIER, R. A., MITTERMEIER, C. G., DA FONSECA, G. A., & KENT, J. Biodiversity hotspots for conservation priorities. **Nature**, v.403(6772), p. 853-858, 2000

PROGRAMA DAS NAÇÕES UNIDAS PARA O MEIO AMBIENTE. **Resumo para Formuladores de Política**. [S.l.: s.n.], 2012. Disponível em: < http://www.portalodm.com.br/dnfile/ywljrjbj5lamlbdjxawj/pdf/publicacoes/1/geo-5---panorama-ambiental-global.pdf>. Acesso em: 15 jan. 2017.

TAINA, I. A.; HECK, R. J.; ELLIOT, T. R. Application of X-ray computed tomography to soil science: a literature review. **Canadian Journal of Soil Science**, v. 88, n. 1, p. 1-19, 2008.

CHAPTER II

A tool package for soil physical analysis based on nonconventional techniques

TSENG, C. L., FERREIRA, E. J., CRESTANA, S.

A TOOL PACKAGE FOR SOIL PHYSICAL ANALYSIS BASED ON NONCONVENTIONAL TECHNIQUES

Tseng, C. L.[a], Ferreira, E. J. [b], Crestana, S.[b]

[a]University of São Paulo, "São Carlos School of Engineering " 400 Avenida Trabalhador São-carlense, CEP: 13566-590 São Carlos, São Paulo, Brazil.

[b]Embrapa Instrumentation, 1452, Rua XV de Novembro, CEP: 13560-970, São Carlos, São Paulo, Brazil.

ABSTRACT

The soil is an open and complex system in the environment; its complexity in quantification has always been a challenge to scientific community, from equipment and methods selection to appropriate attribute for each case. In view of that, the work purpose is to present a package tool from nonconventional techniques to obtain and investigate physical attributes of the soil, by correlating soil's morphometric, geometric and energetic characteristic. For that, it was prepared a design of the process to obtain a series of physical attributes both quantitative and qualitative. The process involves from sample preparation, data/image acquisition to data/image processing. It also pursued the correlation between attributes by dendrogram, classifying them in characteristic groups according to their similarity and thus representing the physical interaction system in an integrated manner. Finally, it is expected to contribute with a synthesized tool package to the study of soil use in the environment.

Keywords: Soil. Analysis tools. Physical attributes. X-ray microtomography. Analyzer granulometric.

1. Introduction

The soil is a system consisting of three common phases in the nature: solid, liquid and gaseous, where the physical, chemical and biological interaction occur; this system is vital to ensure Earth's performance and resilience. It is fundamental to have new investigation and interpretation perspective about nature phenomenon, which relates to soil study in the environment, as it is an open and dynamic complex system, which has not been adequately treated.

For the past few years, with technological advances enabling equipment that allows acquisition of various soil physical attributes in nonconventional way, such as analyzer granulometric (NAIME et al., 2001) and x-ray tomography (PETROVIC et al., 1982, HAINSWORTH and AYLMORE, 1983, CRESTANA, et al. 1985), which were used in this work; both provide data acquisition in a short time and intact preservation of samples in comparison to conventional methods.

Vaz et al. (2014) showed the advantages and limitation of benchtop X-ray microtomographic technique in soil vardose zone research; Recently, Jarvis et al. (2016) used a high-resolution X-ray tomography to investigate the connectivity and structural porous network of a cultivated soil and, Zhang et al. (2015) characterized the preferential flux of a cracked paddy soil by using an X-ray tomography.

In spite of the rapid evolution of the equipment, the need of adequate analysis software is also indispensable in order to extract the required data. Therefore, in this research it was used the following software: Qualisolo, CT-Analyser, ImageJ, R, MASS, Data-Viewer, CTVox and Mathematica to extract the physical attributes, to visualize different soil plane and to simulate soil in tridimensional; It was also used online UPGMA dendrogram (Unweighted Pair Group Method with Arithmetic Mean) to describe the correlation between the attributes. All these steps will be presented in-depth in next.

Although theses physical attributes can be obtained from conventional methods, such as particles sizes distribution, water retention curve (VARANDAS, 2011, NADERI-BOLDAJI and KELLER, 2016), S index of soil physical quality (ANDRADE et al. 2009 and MARIA et al., 2010) and porosity (PIRES, et al. 2014 and BOTTINELLI et al. 2016), the advantage of nonconventional technique is that they allow attributes to be acquired with preservation of sample originality and more efficiency.

There are other inherent and important characteristics in soil comprehension such as physical attributes, which are provided by software, even though they are not so common in

soil investigation. Among them, there can be highlighted: Degree of anisotropy (ZHAO et al. 2017), Euler-Poincaré number (SANDIN et al., 2017), Feret diameter (KATUWAL et al., 2015), form factor (PASSONI et al., 2014 e MUNKHOLM, et al. 2016), lacunarity (MARTÍNEZ et al., 2016), tortuosity (SHANTI et al., 2014), Shannon entropy (GAUR and MOHANTY, 2013), system entropy, degree of multifractality and asymmetry (POSADAS et al. 2003 and MARINHO et al., 2016). Furthermore, it proposed in this work tools that allows the visualization of different soil plane (PEREIRA and CRUVINEL, 2015), the three dimensional simulation of soil internal structure and, the random walk of particles into the soil (NAKASHIMA and KAMIYA, 2007).

Overall, it was verified that soil attributes are always selected and used separately, in counterpoint to interconnected phenomena that occurred in nature. Therefore, this work aims to provide a tool package from nonconventional techniques for soil physical investigation, through the correlation of soil's morphometric, geometric and energetic characteristics and, this package is presented in a demonstration. It is expected this tool package to operate as a synthesis to facilitate future investigations in a more integrated and compatible way with soil reality.

2. Material and methods

2.1 Study area and sampling

The study area is located at Selvíria town (Mato Grosso do Sul State - Brazil), on the right bank of Paraná River. The typical whether is Aw according to Köppen; with 1370mm of annual precipitation and 75% of air relative humidity. In this research it was used one soil sample of Brazilian native forest (Cerrado) (Figure 1), it is a red dystrophic latosol (EMBRAPA SOLOS, 2013) with clayey textural class at 40.08% of clay, 7.67% of silt and 52.25% of sand.

Figure 1 - Brazilian native forest (Cerrado) at Selvíria city (Mato Grosso do Sul States) – Brazil.

Source: Author (2013).

2.2 Design of process

The design of process is focused on the organization of a tool package, whose function is to extract results that indicate soil physical properties, both quantitative and qualitative, considering the time, the cost and the user accessibility. The methodology implemented in this experiment consisted of two main lines and three steps (Figure 2). The qualitative part is represented by microtomography visualization in different plane and, tridimensional simulation; the quantitative part shows numerical values and its interpretation from the extracted data.

Figure 2 - Process of design flowchart

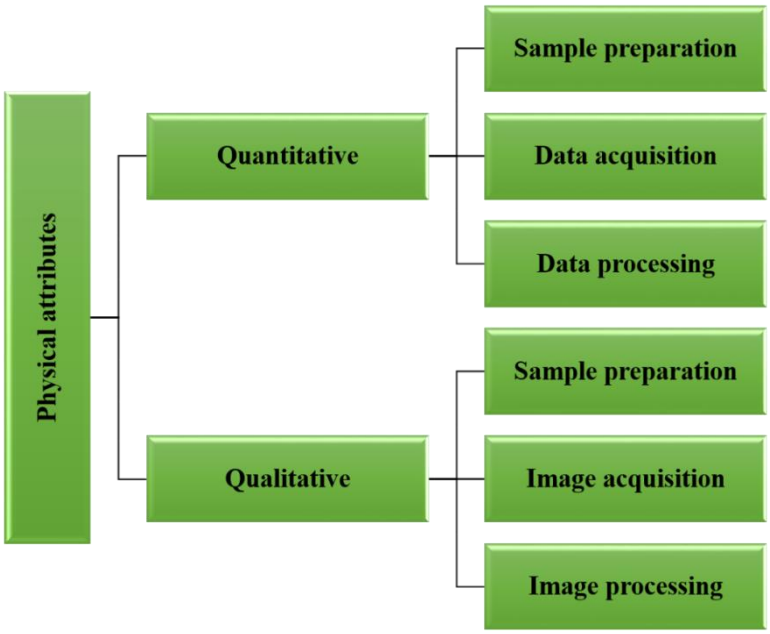

Source: Author (2016).

2.3 Sample preparation

2.3.1 Automatic gamma-ray granulometric analyzer

Initially, the disturbed soil samples were dried in oven at 105ºC during 24 hours and sieved through 2.0 mm mesh to remove gravel and rest of plant's roots; next, it was done the readings and measurements of sample mass attenuation coefficient. After that, it was prepared 40g of dried soil, adding 10mL of sodium hydroxide solution (NaOH – 1N) and distilled water. This solution was then transferred to agitator type Wagner and shook it for 16 hours continuously aiming to obtain total particles dispersion. Afterward, the sample solution was shifted to rectangular acrylic cuvette and filled up to the recommended level with distilled water. Finally, the sample was placed in the equipment for measurement.

2.3.2 X-ray microtomography

In a block of soil from field, it was inserted a 8mm x 15mm (internal diameter x height) acrylic tube and a sample was removed. After that, the sample was dried in oven at 105ºC during 42 hours and, sealed with Prafilm to avoid absorption of humidity along the experiment.

2.4 Data/image acquisition – equipment used

2.4.1 Automatic gamma-ray granulometric analyzer

The granulometric analyzer is an equipment developed by Embrapa Instrumentation – São Carlos (Figure 3), which uses the gamma-ray attenuation principle (modified Beer-Lambert's law) to determine particles sizes distribution during the water sedimentation process (Stockes' laws) (VAZ et al., 1992 and NAIME et al., 2001).

Figure 3 - Automatic gamma-ray granulometric analyzer of Embrapa Instrumentation's laboratory.

Source: Author (2015).

After granulometric analyzer readings, the sample went through fraction step in order to improve the precision of larger particles. For this, the sample was sieved with the aid of water

and a set of sieves with decreasing diameter. The sieved portion was dried in stove for 24 hours and weighed. Lastly, the result was inserted in equation (1) and a new configuration in granulometric curve was obtained.

$$\text{Fraction} = \frac{M_{rec+ds} - M_{rec}}{40} \quad (1)$$

Where, M_{rec} means recipient mass and M_{ds} is dried soil mass.

2.4.2 X-ray microtomography

The tomographic image acquisition and the reconstruction were conducted using a high-resolution X-ray microtomography, granted by Embrapa Instrumentation – São Carlos (Figure 4).

Figure 4 - X-ray microtomography - 1172, belonging to Nuclear Techniques Laboratory

Source: Author (2015).

As tomographic projections acquisition parameters it was used 100kV of voltage, 100 uA of current, Al+Cu filter, 4.96 μm of spatial resolution, 360º rotation, frame average of 5 and 0.3º of step. After that, tomographic projections were reconstructed with aid of NRcon software with a total 500 images, using 5 of smoothing, 10 of ring artifact correction and 60% of beam-hardening correction, all of them ware calibrated with Hounsfield unit (CRESTANA, et al., 1985 and VAZ et al., 2011).

2.5 Data/image processing – Software and methods used

2.5.1 Qualisolo

Qualisolo software (NAIME et al., 2004) is a program implemented to automatic application of Arya and Paris model (1981) validated to Brazilian soil (VAZ, et al. 2005). To run the program a bulk density value and granulometric table, which was obtained from the

analyzer of topic 2.4.1, must be inserted in the program interface and asked to be calculated (Figure 5).

Figure 5 - Qualisolo interface program.

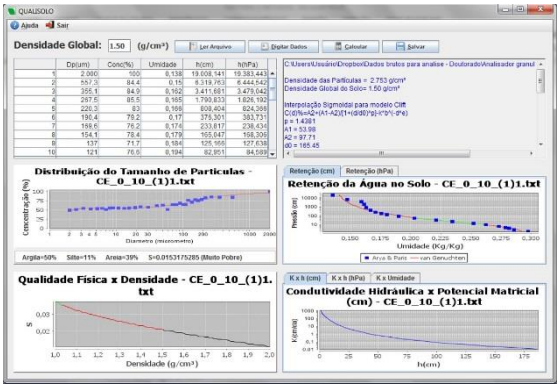

Source: Author (2015)

The program will provides four graphics: a) the relation of particles sizes distribution; b) the water retention curve; c) Soil physical quality (S index) versus density and, d) hydraulic conductivity versus matrix potential, however, only items a) and b) ware used in this work. At same time, the program also provides S-index of soil physical quality at txt. table, as well as $\theta_{residual}$ and $\theta_{saturated}$; From here, it is possible to estimate permanent wilting point, field capacity and available water capacity.

a) particles sizes distribution

It is obtained from Stokes' law and Clift model (NAIME and VAZ, 2007);

b) water retention curve

Arya & Paris model (1981) was used basis on two concepts: 1) capillarity equation, which relates matrix potential to radius of pores; 2) the calculation of water content, from the particles size distribution (VAZ et al., 2005 ; NAIME et al., 2001);

c) soil physical quality index

The soil physical quality or S index is determined indirectly from Arya & Paris model (1981) is represented by equation (2). According to Dexter (2004), when S value is higher than 0.035, it indicates good quality; 0.0202 < S < 0.035 means poor and S = 0.020 is a very poor soil

$$S = -n\,(\theta_s - \theta_r)\left[1 + \frac{1}{m}\right]^{-(1+m)} \quad (2),$$

where θr and θs are contents of residual water and saturated soil, respectively, n and m (m = 1-1/n) are a fitting parameter without physical significance.

2.5.2 CT-Analyser

It is software developed by Skyscan (Figure 6), granted by Embrapa Instrumentation is used as image pretreatment; this software binarized all images using Otsu method (1975). After that, CT-Analyser estimated the following values: a) porosity; b) degree of anisotropy and c) Euler-Poincaré number (MANUAL FOR BRUKER-MICRO CT - CT Analyser, 2013).

Figure 6 - CT-Analyser interface in-process of a set of microtomographic.

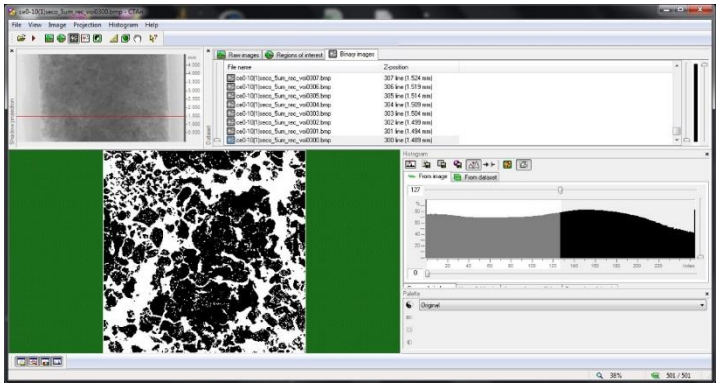

Source: Author (2015)

a) porosity

The porosity obtained by digital method was acquired from the binarized microtomographic. Subsequently, the 2D porosity value was calculated from the division of empty spaces by total identified area for each slice of image. Finally, it was applied the integral cauculus to estimate pores area of all slices, i.e., the total 3D porosity;

b) degree of anisotropy (DA)

It is a measure that quantifies if the pores are directionally dependent. The Mean Intercept Length concept (MIL) and the analysis of eigenvalues are used to calculate DA. To obtain DA in three dimension, the MIL distribution is described in an ellipsoid on three axis in the format of a tensor (HARRIGAN and MANN, 1984). The tensor, on the other hand is a simple number that measures DA, where value 1 means totally anisotropy and 0 isotropy (SKYSCAN, 2015);

c) Euler-Poincaré number

Euler-Poincaré number is a pore space connectivity index in three dimension (VOGEL and KRETZSCHMAR, 1996), is represented by equation (3); it is composed by separated object numbers (β_0), i.e, the pores; connectivities number (β_1) and closed cavities number (β_2). Therefore, all 3D components used in CT-Analyser software are given by (VOGEL, 2002; KATUWAL, et al., 2015 ; SKYSCAN, 2015):

$$\chi(X) = \beta 0 - \beta 1 + \beta 2 \qquad (3)$$

In short, Euler-Poincaré number is inversely proportional to connectivity value (ROZENBAUM et al., 2012).

2.5.3 ImageJ

It is an image processing software performing at Java environment (Figure 10) and it is an open source; today it is available to operate at Windows, Mac OS, Mac OS X and Linux environment. This software helped to provide the fallowing values: a) Feret diameter; b) form factor. Currently, there are more than 500 plugins available to use, such as FracLac and Geodesic plugin, which were used to calculate c) lacunarity and d) system bidimensional tortuosity (FERREIRA and RASBAND, 2012; KARPERIEN, 2007; LEGLAND, 2016).

a) Feret diameter

Feret diameter is calculated as the greatest distance between two points of a delimited area (FERREIRA and RASBAND, 2012), i.e. pore diameter; this measurement will serve as input to determine the form factor;

b) form factor

The form factor is obtained from the equation (4). From here, pores form are divided into five classes: 1) fissure (F≤ 0.2); 2) elongated dissected pores (F = 0.21-0.4); 3) isometricality dissected pores (F = 0.41-0.6); 4) slightly dissected pores (F = 0.61-0.8) and 5) round pores (F = 0.81-1.0) (, 2009);

$$F = \left(\frac{4\pi A}{P^2} + \frac{D}{L}\right)/2 \qquad (4)$$

where A is área of pore, p is perimeter, D and L means major and minor axis linear pore dimensions, respectively.

c) lacunarity

FracLac plugin was used in this study, which is a ImgeJ program extension (Figure 7) that uses "Gliding box" algorithm (ALLAIN and CLOITRE, 1991; KARPERIEN, 2007) to obtain the lacunarity with binarized pixel intensity average. Finally, the algorithm provides a lacunarity log-log graphic versus different "Gliding box" sizes (PLOTNICK et al., 1996);

Figure 7 - FracLac plugin interface.

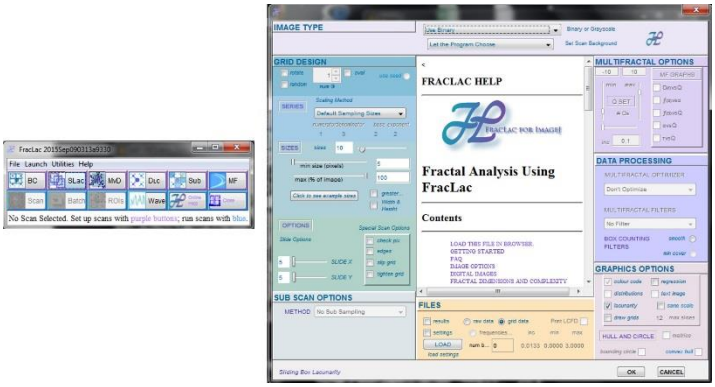

Source: Author (2016)

d) tortuosity

The ijGeodesics plugin of ImageJ software allows to calculate the geodesic distance, in other words, the greatest distance between two points of object (length of pores canal) from a binarized image. The value allows to calculate the tortuosity and it is based in the ratio between the geodesic distance and Euclidian (the shortest distance between two points), pixel by pixel (LEGLAND, 2011; SHANTI et al. 2014);

$$\text{Tortuosity} = \frac{\text{Geodesic distance}}{\text{Euclidian distance}} \qquad (5)$$

2.5.4 R – "Entropy Package"

The "Entropy Package" developed at R program language interface is an open source and it provides various Shannon entropy estimators. For this work, it was selected one representative tomographic image, which was transforms pixel by pixel in a table format (txt.) according to its grayscale. Once the table was obtained, it was adopted a Maximum Likelihood (ML) estimator of "Entropy Package" (HAUSSER and STRIMMER, 2012), whose estimator is a simple and widely used to calculate Shannon entropy (Figure 8).

Figure 8 - R interface and entropy package script

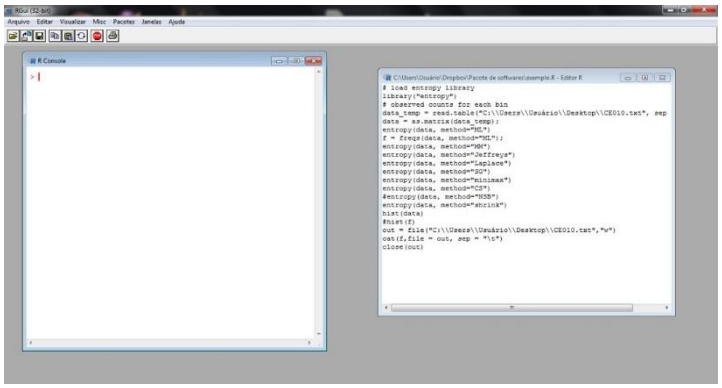

Source: Author (2016)

2.5.5 MASS (Multifractal Analysis & Scaling System)

It is a program developed by Centro Internacional de La Papa (CIP) (Figure 9) – Peru and is not public domain. The version used in this study was a result of partnership between CIP and Embrapa Instrumentation, which was used to calculate a) entropy and b) degree of multifractality and asymmetry of the system (JORGE et al., 2008). The system entropy calculation is derived from multifractal concept, which is appropriate to characterize mass spatial arrangement of complex system, at same time, it is able to solve local density problem (POSADAS, et al. 2003 ; LAFOND, et al., 2012).

a) entropy

In establishing the adequate parameters at MASS, the software will provide a multifractal spectrum, where its axis y (f(α)) is equivalent to the system entropy, at the same time, the software offers a table with all spectrum values, which are obtained from Rènyi (D_q) by using Legendre transformation (SZCZEPANIAK and MACEK, 2008);

b) degree of multifractality and asymmetry

Based on multifractal equation, it was possible to calculate the degree of multifractality (Δ), asymmetry (A) and their respective graphics (SZCZEPANIAK and MACEK, 2008).
They are essential values that characterize the multifractality and the system heterogeneity. The equations are given respectively by (HALSEY, et al., 1986):

$$\Delta \equiv \alpha_{max} - \alpha_{min} = D_{-\infty} - D_{\infty} = \left| \frac{\log(1-p)}{\log l_2} - \frac{\log(p)}{\log l_1} \right| \qquad (6)$$

$$A = \frac{\alpha_0 - \alpha_{min}}{\alpha_{max} - \alpha_0} \qquad (7)$$

where α is the Lipschitz-Holder exponent; p is probability of the measure; l is box size and D is fractal dimension.

The singularity spectrum is maximum when f(α0) = 1.

Figure 9 - MASS software interface and multifractal spectrum

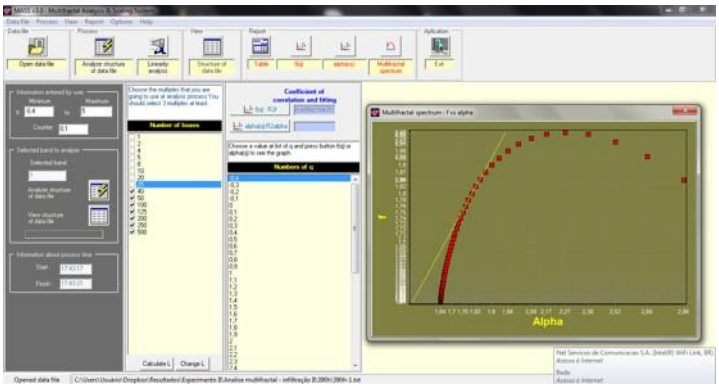

Source: Author (2016)

2.5.6 Dendrogram

UPGMA (Unweighted Pair Group Method with Arithmetic Mean) (SOKAL, 1958) on-line was used to make hierarchic analysis, i.e., physical parameters cluster by its structural similarity. At first, it was used Pearson coefficient and pair-to-pair variables to generate the correlation matrix. Subsequently, the negative correlations were replaced by absolute values, as for physical parameters analysis of this work it is not relevant if the correlation is direct or inverse (negative), but most importantly, if there is a strong correlation between parameters. Finally, the data were inserted in a dendrogram generating algorithm providing a "hierarchical tree".

2.5.7 Wolfram Mathematica

It was used a package of algorithm developed by Nakashima and Kamiya (2007). This package consists of three main programs, which were adapted to this soil study and operated at Wolfram Mathematica versão 5.2 enviroment.

a) itrimming.nb

Original image segmentation; it was replaced by CT-Analyser software which reduces significantly the processing time;

b) clabel.nb

Hoshen and Kopelman algorithm (1979) was implemented in this program to classify the set of pores, according the neighborhood rule used in the connectivity analysis (STAUFFER and AHARONY, 1994; IKEDA et al. 2000); the pore voxel is only considered connected to another voxel when there is face contact;

c) rwalk.nb

The random-walk within the set of pores is a lattice walk in a cubic lattice. The program output is the mean-square displacement (8) of walkers, $<r^2>$, in relation to τ (dimensionless integer time):

$$< r(\tau)^2 > = \frac{1}{n} \sum_{i=1}^{n} [((x_i(\tau) - (x_i(0))^2 + ((y_i(\tau) - (y_i(0))^2 + ((z_i(\tau) - (z_i(0))^2] \quad (8)$$

2.5.8 Visualization software: Data-Viewer e CTVox

The tomographic images which were obtained and calibrated at item 2.4.2 were inserted in Data-Viewer (Figure 10) and CT-Vox (Figure 11) software to perform qualitative observation of connectivity between porous and solid part. Both software are part of the program package developed by Skyscan (Belgium) and granted by Embrapa Instrumentation. The Data-Viewer

is appropriate for the visualization of axial, sagittal and coronal plane, whereas CT-Vox has the advantage to generate volumetric visualization of the object by intuitive manipulation of the object or/and camera.

Figure 10 - Data-Viewer interface and cutting plane

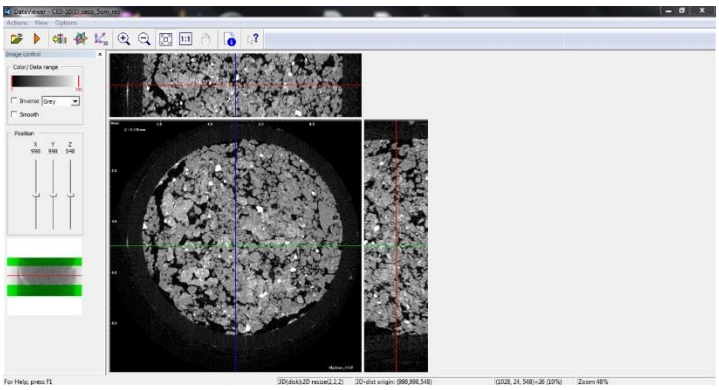

Source: Author (2015)

Figure 11 - CT-Vox interface and the object with volumetric rendering

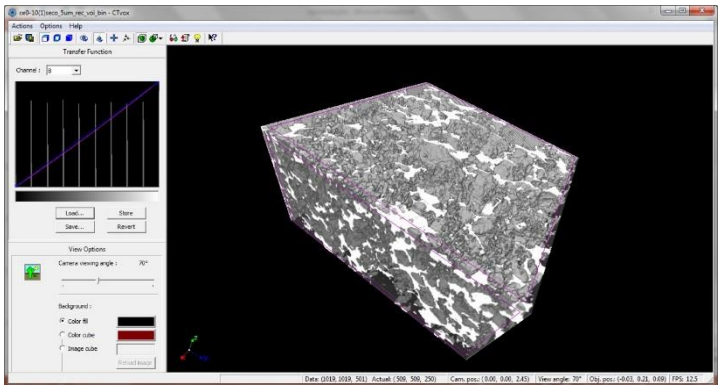

Source: Author (2015)

3. Results and discussion

3.1 Design of process

In accordance with this work study it was gathered a tool package aiming the acquisition of soil physical properties, both quantitative and qualitative (Figure 12 and 13). It was projected two flowchart representing two lines of the design process, based on three steps of operation and, whenever possible, it was considered the time, cost and accessibility.

Step 1 (Sample preparation): In the case of X-ray microtomography, the average time required for each sample is three days, from the sample extraction from the soil block up to the insertion of it in the equipment, with the acrylic tube previously prepared. Gamma-ray granulometric analyzer takes approximately 3 to 5 days, due to laborious preparation

procedure, as described at item 2.3.1. Both have variable cost, depending mainly on the distance between experimental area and preparation place.

Step 2 (Data/image acquisition): The acquisition time of microtomographic is around 2.5 hours. Although popularization of banchtop X-ray microtomography has improved the accessibility to the scientific community, the average price paid by the users ranges between U$50 to U$85 per hour; this price was investigated by the authors in 12 international and national laboratories. In the case of granulometric analyzer, the total analysis time is around 20 minutes and the average analysis price is U$ 2.00 per sample in Brazil. This equipment was built by Embrapa Instrumentation, where this research was developed, which means there was easy access.

Step 3 (Data/image processing): For the quantitative analysis it was used 4 softwares to process the previous acquired data. The total program execution time to process the acquired data, from the image reconstruction up to the results, varies from 180 to 240 minutes for each sample. In relation to software costs, Qualisolo, ImageJ, MASS and R belong to public domain and can be downloaded directly from Internet, such as free version of NRcon and CT-Analyser from the company website, nevertheless with some restrictions. The software accessibility was considered average by the fact that some of them are not open to public; manipulation of these software is without a doubt, very transparent at the user's manuals. On the other hand, qualitative analysis take about 540 to 600 minutes for each sample; in other words, the execution time is longer, as well as its computational cost is also high; Data-Viewer and CT-Vox free version could be found at Bruker's company page, with some restrictions, while Mathematica has cost U$ 1,150.00. Finally, Data-Viewer and CT-Vox software were considered to be of easy access, whereas Mathematica requires the user certain degree of programming knowledge.

Figure 12 - Quantitative design of the process

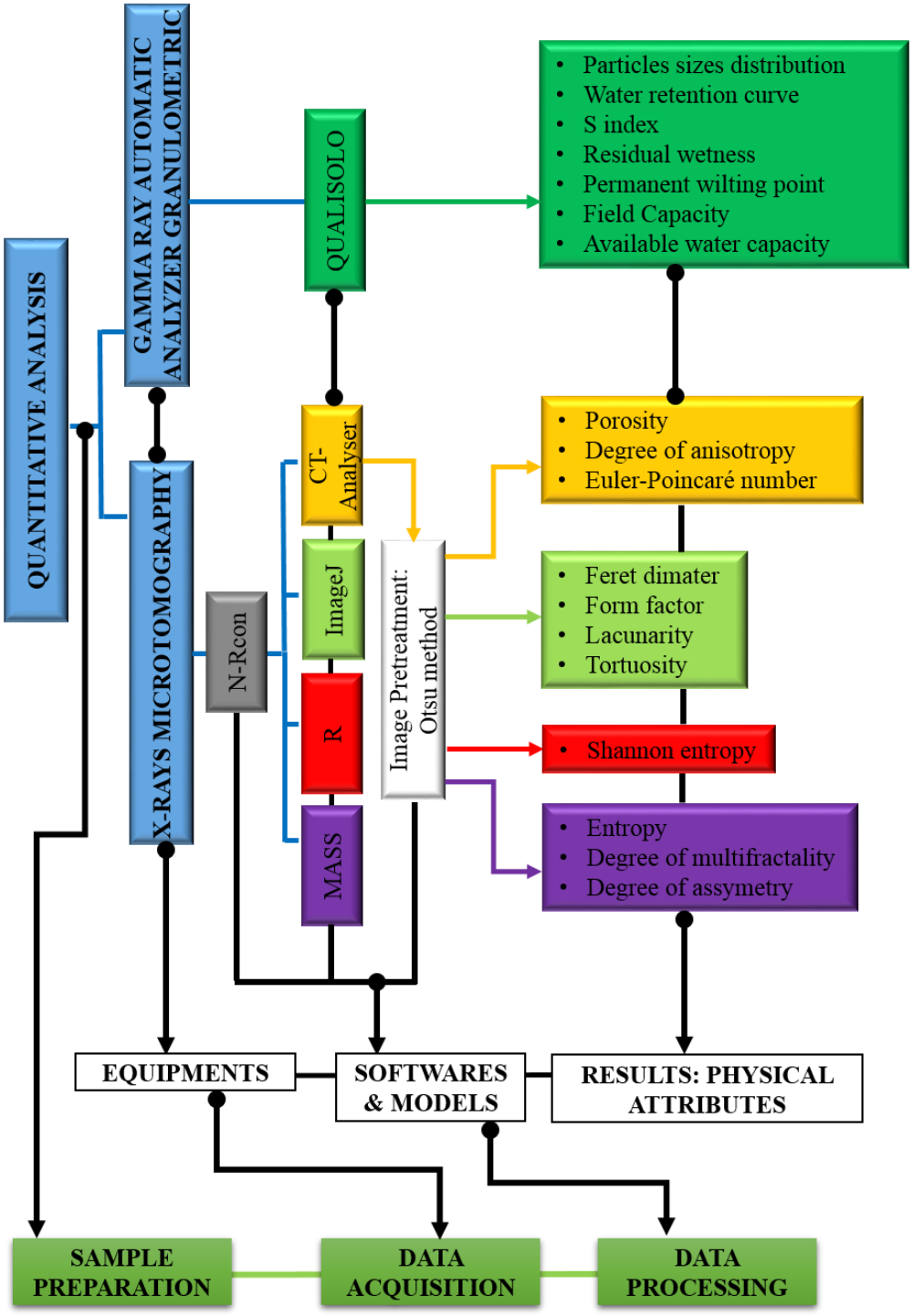

Source: Author (2016)

Figure 13 - Qualitative design of the process

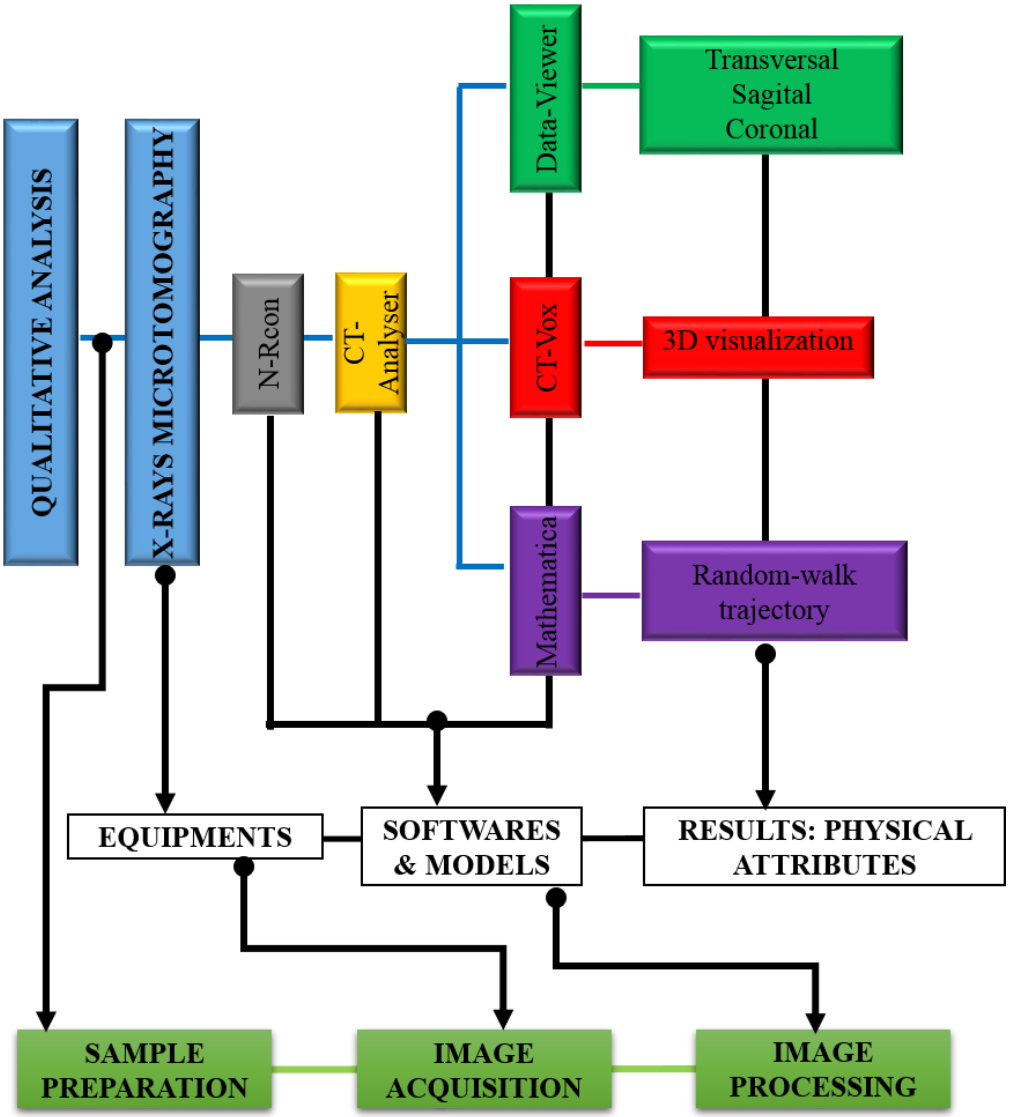

Source: Author (2016)

3.1.1 Correlation between physical attributes

Today, there are many methods and advanced tools to characterize and quantify physical attributes of the soil system; however, most of the time the results are analyzed separately; in other words, there is absence of a holistic look over the system dynamics. From the generated physical attributes, it was built a dendrogram. Since it is the first test, not all the acquired physical attribute at step 2 were studied in detail; however, they were considered as input data to obtain an overall panorama about possible existing correlations in the system.

3.1.1.1 Dendrogram

The dendrogram (Figure 14) in this study separated the results in two main observation groups at horizontal axis (value 0) according to equipment used: 1) Granulometric analyzer and 2) X-ray microtomography, with the exception of S index, which grouped with group 2). Subsequently, at 0.037 of vertical axis, group 2) was divided into 2 groups according to software functionality: 1) Qualitative and 2) Quantitative.

Figure 14 - Dendrogram test. The x axis number indicate distances between pair of object and the y axis means its final distance. Green boxes are physical attributes investigated with detail in this study and the white boxes are omitted attributes.

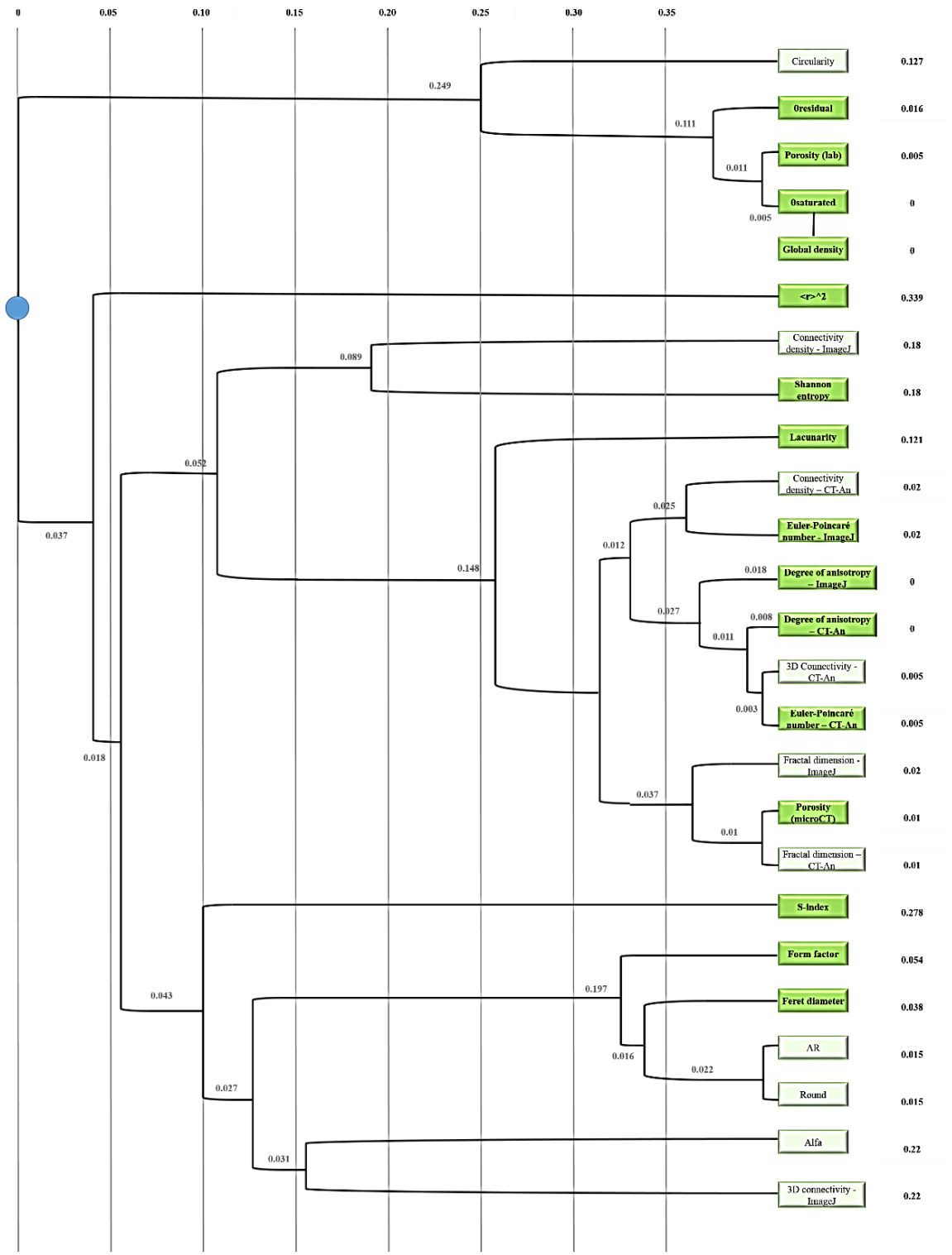

Source: Author (2016)

At the end of quantitative group, the observations or variables were grouped by their common characterizations at vertical axis. Briefly, they could be classified into 5 groups (Figure 15), showing the multiple physical interactions, which must be considered in soil studies.

Figure 15 - Brief classification of soil physical interaction groups. The unclassified variable and others are variables which were not inserted in this test.

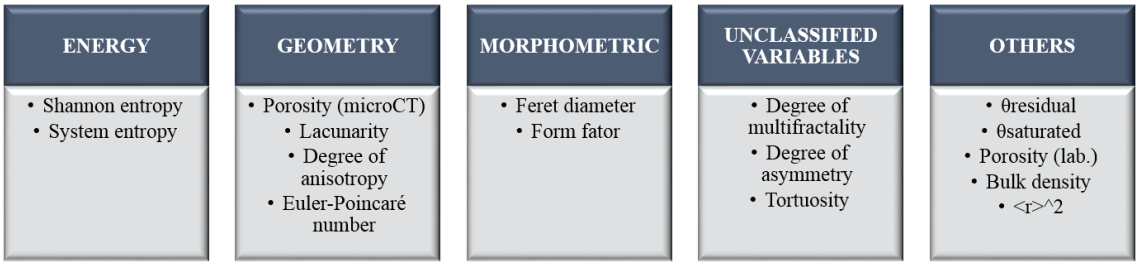

Source: Author (2016)

Even though this is the first dendrogram test applied to soil study in the physical scope, it is clear that the dendrogram contains vast amount of information, offering the possibility of deeper investigation and interpretation in future.

3.2 Tools demonstration

For a brief demonstration of the tools used in this work, it was initially considered samples prepared and inserted into the equipment. Then, in the second step of data/image acquisition were obtained: 1) granulometric distribution (Figure 16) and, 2) Tomographic image of 4.96 µm of spatial resolution (Figure 17).

Figure 16 - Sample granulometry

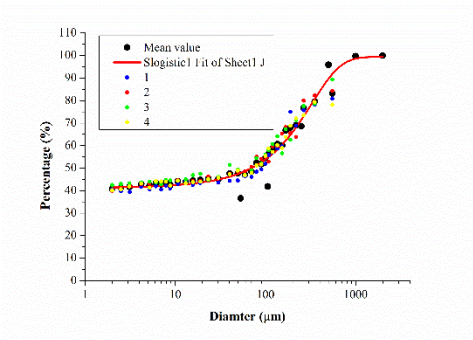

Source: Author (2015).

Figure 17 - Sample microtomographic

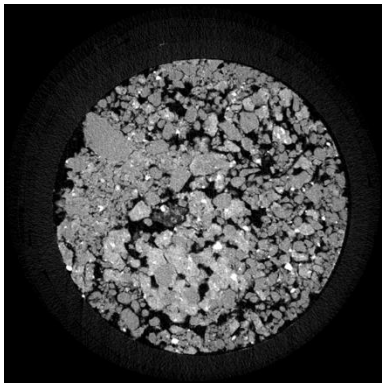

Source: Author (2015).

Subsequently, for the third step of data/image processing, it was obtained physical attributes according to Table 1 and Figures 18 to 20 the visualization part of plane and 3D simulation can be verified at figures 10 and 11.

Table 1. Final data processing result

Group classification	Physical attributes	Values	Unit
Energy	Shannon Entropy	13.68174	-
	System Entropy	Graphic analysis (Figure 18)	
Geometric	Porosity (microCT)	31.8990	%
	Lacunarity	0.0944	-
		Graphic analysis (Figure 19)	
	Degree of anisotropy	1.7545	-
	Euler-Poincaré number	-2671	-
Morphometric	Feret diameter	64.0135	μm
	Form factor	0.79293	-
Unclassified variable	Degree of multifractality	0.2893	-
	Degree of asymetry	0.9359	-
	Tortuosity	1,114	-
	S index	0.0362	
	θ_{pmp}	22	%
	θ_{cc}	26	%
	AWC	4	%
Others	$\theta_{residual}$	0.18	-
	$\theta_{saturated}$	0.45	-
	Porosity (lab)	55.3539	%
	Bulk density (lab)	1.23	g/cm^3
	<r>^2	302.5836	-
		Graphic analysis (Figure 20)	

Source: Author (2017)

Figure 18 - Entropy multifractal spectrum

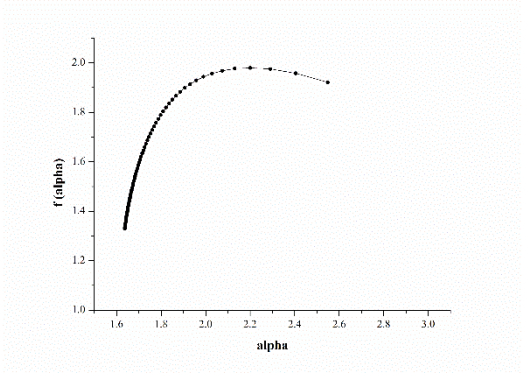

Source: Author (2016).

Figure 19: Lacunarity versus different Gliding box size

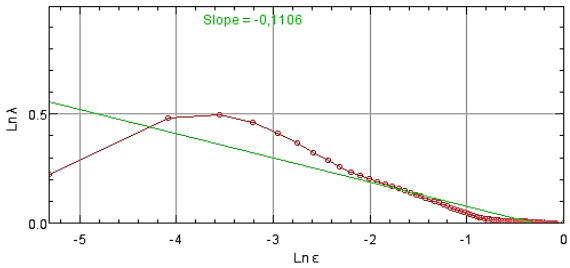

Source: Author (2016).

Figure 20: Random-walking of particles within the sample .

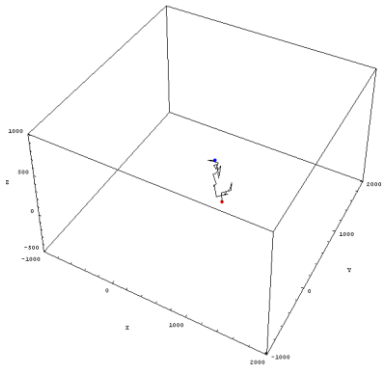

Source: Author (2016)

Finally, the data and image which were previously obtained, enabled the physical attributes clustering according to their characteristics, thus offering crossing information. Therefore, they provided an integrated view about interaction between physical attributes that occur within the soil.

4. Conclusion

The aim of the present work was achieved successfully, for it presented a tool package from the nonconventional techniques to obtain soil physical attribute at different scope; which is essential to comprehend and predict physical interaction of soil use in the environment. The flowcharts of the design processing allow users to select analysis line with criteria based on time, cost and accessibility; From the correlation between physical attributes, it was proved

that to perform a complete study of the soil, it must be considered group of attributes rather than used them separately. In addition, the dendrogram showed an excellent tool to determine similarity between the groups. Finally, we expect with the present work, to contribute to extend applications to soil use studies in an integrated way.

References

ALLAIN, C.; CLOITRE, M. Characterizing the lacunarity of random and deterministic fractal sets. **Physical review A**, v.44, n.6, p.3552, 1991.

ANDRADE, R. D. S.; STONE, L. F. Índice S como indicador da qualidade física de solos do cerrado brasileiro. **Revista Brasileira de Engenharia Agrícola e Ambiental**, v.13, n.4, p.382-388, 2009.

ARYA, L. M.; PARIS, J. F. A physicoempirical model to predict the soil moisture characteristic from particle-size distribution and bulk density data. **Soil Science Society of America Journal**, v.45, n.6, p.1023-1030, 1981.

BOTTINELLI, N. et al. Macropores generated during shrinkage in two paddy soils using X-ray micro-computed tomography. **Geoderma**, v.265, p.78-86, 2016.

CRESTANA, S.; MASCARENHAS, S.; POZZI-MUCELLI, R.S. Statical and dynamical three dimensional studies of water in soil using computed tomography scanning. **Soil Science**, v.140, p.326-332, 1985.

DEXTER, A. R. Soil physical quality: part I. theory, effects of soil texture, density, and organic matter, and effects on root growth. **Geoderma**, v.120, n.3, p.201-214, 2004.

EMPRESA BRASILEIRA DE PESQUISA AGROPECUÁRIA (EMBRAPA). **Sistema brasileiro de classificação de solos**. 3th ed. Rio de Janeiro: Centro Nacional de Pesquisa de Solos, Rio de Janeiro , 2013.

FERREIRA, T.; RASBAND, **W. ImageJ user guide. IJ1. 46r.** National Institutes of Health, Bethesda (NIH), MD. Available in: <http://rsb. info. nih. gov/ij/docs/guide/user-guide. pdf>. Accessed in: May 15, 2016.

GAUR, N.; MOHANTY, B. P. Evolution of physical controls for soil moisture in humid and subhumid watersheds. **Water Resources Research**, v.49, n.3, p.1244-1258, 2013.

HAINSWORTH, J. M.; AYLMORE, L. A. G. The use of computer-assisted tomography to determina spatial distribution of soil water content. **Australian Journal of Soil Research**. v.21, n.4, p.435-443, 1983.

HALSEY, T. C. et al. Fractal measures and their singularities: the characterization of strange sets. **Physical Review A**, v.33, n.2, p.1141, 1986.

HARRIGAN, T. P; MANN, R. W. Characterization of microstructural anisotropy in orthotropic materials using a second rank tensor. **Journal of Materials Science**, v.19, p.761-767, 1984.

HAUSSER, J.; STRIMMER, K. Package'entropy', Available in: < https://cran.r-project.org/web/packages/entropy/entropy.pdf>. Accessed in: May 15, 2016.

HOSHEN, J.; KLYMKO, P.; KOPELMAN, R. Percolation and cluster distribution. III. Algorithms for the site-bond problem. **Journal of Statistical Physics**, v.21, n.5, p.583-600, 1979.

IKEDA, S.; NAKANO, T.; NAKASHIMA, Y. Three-dimensional study on the interconnection and shape of crystals in a graphic granite by x-ray CT and image analysis. **Mineralogical Magazine**, v.64, n.5, p.945-959, 2000.

JARVIS, N.; LARSBO, M.; KOESTEL, J. Connectivity and percolation of structural pore networks in a cultivated silt loam soil quantified by X-ray tomography. **Geoderma**, v.287, n.1, p.71-79, 2017.

JORGE, L. D. C. et al. **Aplicação da técnica multifractal para caracterização de manejo de solo**. Rio de Janeiro: Embrapa Instrumentação Agropecuária, 2008. (Documentos).

KARPERIEN, A. **FracLac for ImageJ-FracLac Advanced User's Manual**. Australia: Charles Sturt University, 2007.

KATUWAL, S. et al. Linking air and water transport in intact soils to macropore characteristics inferred from X-ray computed tomography. **Geoderma**, v.237, p. 9-20, 2015.

LAFOND, J. A. et al. Multifractal properties of porosity as calculated from computed tomography (CT) images of a sandy soil, in relation to soil gas diffusion and linked soil physical properties. **European Journal of Soil Science**, v.63, n.6, p.861-873, 2012.

LEGLAND, D. **Manuel d'utilisation du plugin «Geodesic» pour ImageJ**. 2011. Available in: http://download2.nust.na/pub4/sourceforge/i/ij/ijtools/ijTools/ijGeodesics/ijGeodesics-2014.02.21/ijGeodesicsManuel.pdf>. Accessed in: Aug 20, 2016.

MANUAL for bruker-micro CT - CT analyser. v.1.13, 2013. Available in: <http://bruker-microct.com/next/CTan_UserManual.pdf>. Accessed in: June 12, 2016.

MARIA, I. C. D. et al. Sewage sludge application to agricultural land as soil physical conditioner. **Revista Brasileira de Ciência do Solo**, v.34, n.3, p.967-974, 2010.

MARINHO, M. A. et al. Depth distribution of soil organic carbon in an Oxisol under different land uses: Stratification indices and multifractal analysis. **Geoderma**, v.287, 2016. Available in:<https://www.researchgate.net/publication/308909011_Depth_distribution_of_soil_organic_carbon_in_an_Oxisol_under_different_land_uses_Stratification_indices_and_multifractal_analysis>. Accessed in: 30 June, 2016.

MARTÍNEZ, F. S. J.; CANIEGO, F. J.; GARCÍA-GUTIÉRREZ, C. Lacunarity of soil macropore space arrangement of CT images: Effect of soil management and depth. **Geoderma**, v.287, 2016.

MUNKHOLM, L. J. et al. Relationship between soil aggregate strength, shape and porosity for soils under different long-term management. **Geoderma**, v.268, p. 52-59, 2016.

NADERI-BOLDAJI, M; KELLER, T. Degree of soil compactness is highly correlated with the soil physical quality index S. **Soil and Tillage Research**, v.159, p.41-46, 2016.

NAIME, J. D. M; VAZ, C. **Estudo e implementação de modelo mais preciso para determinação da granulometria do solo por atenuação de raios gama**. São Carlos: Embrapa, 2007. (Boletim de Pesquisa e Desenvolvimento, 19).

NAIME, J. D. M.; SHINYA, V.; VAZ, C. **Programa para estimativa indireta da curva de retenção da água no solo**. São Carlos: Embrapa, 2004. (Comunicado Técnico, 60).

NAIME, J. M.; VAZ, C. M. P.; MACEDO, A. Automated soil particle size analyzer based on gamma-ray attenuation. **Computers and electronics in agriculture**, v.31, p.295-304, 2001.

NAKASHIMA, Y.; KAMIYA, S. Mathematica programs for the analysis of three-dimensional pore connectivity and anisotropic tortuosity of porous rocks using X-ray

computed tomography image data. **Journal of Nuclear Science and Technology**, v.44, p.1233-1247, 2007.

OTSU, N. A threshold selection method from gray-level histograms. **Automatica**, v.11, p.23-27, 1975.

PASSONI, S. et al. Software Image J to study soil pore distribution. **Ciência e Agrotecnologia**, v.38, n.2, p.122-128, 2014.

PEREIRA, M. F. L.; CRUVINEL, P. E. A model for soil computed tomography based on volumetric reconstruction: wiener filtering and parallel processing. **Computers and Electronics in Agriculture**, v.111, p.151-163, 2015.

PETROVIC, A. M.; SIEBERT, J. E.; RIEKE, P. E. Soil bulk density analysis in three dimensions by computed tomographic scanning. **Soil Science Society of America Journal**, v.46, n.3, p445-450, 1982.

PIRES, L. F. et al. Porosity distribution by computed tomography and its importance to characterize soil clod samples. **Applied Radiation and Isotopes**, v.92, p.37-45, 2014.

PLOTNICK, R. E. et al. Lacunarity analysis: a general technique for the analysis of spatial patterns. **Physical review E**, v.53, p.5461, 1996.

POSADAS, A. N. Multifractal characterization of soil pore systems. **Soil Science Society of America Journal**, v.67, n.5, p.1361-1369, 2003.

ROZENBAUM, O.; BRUAND, A; LE TRONG, E. Soil porosity resulting from the assemblage of silt grains with a clay phase: new perspectives related to utilization of X-ray synchrotron computed microtomography. **Comptes Rendus Geoscience**, v.344, p.516-525, 2012.

SANDIN, M. ET AL. Post-tillage evolution of structural pore space and saturated and near-saturated hydraulic conductivity in a clay loam soil. **Soil and Tillage Research**, v.165, p.161-168, 2017.

SHANTI, N. O. et al. X-ray micro-computed tomography and tortuosity calculations of percolating pore networks. **Acta Materialia**, v.71, p.126-135, 2014.

SKVORTSOVA, E. B. Changes in the geometric structure of pores and aggregates as indicators of the structural degradation of cultivated soils. **Eurasian Soil Science**, v.42, p.1254-1262, 2009.

SKYSCAN: Morphometric parameters measured by Skyscan™ CTanalyser software Available in: <http://bruker-microct.com/next/CTAn03.pdf>. Accessed in: June 11, 2016.

SOKAL, R. R. A statistical method for evaluating systematic relationships. **The University of Kansas Science Bulletin**, v.22, p.1409-1438, 1958.

STAUFFER, D.; AHARONY, A. **Introduction to percolation theory**. London: CRC press, 1994.

SZCZEPANIAK, A; MACEK, W. M. Asymmetric multifractal model for solar wind intermittent turbulence. **Nonlinear Processes in Geophysics**, v.15, n.4, p.615-620, 2008.

VARANDAS, J. M. M. **Avaliação da qualidade física do solo em um escala de microbacia**. 2011. 88 f. Tese (Doutorado) - Centro de Energia Nuclear na Agricultura da Universidade de São Paulo, 2011.

VAZ, C. M. P. et al. Validation of the Arya and Paris water retention model for Brazilian soils. **Soil Science Society of America Journal**, v.69, n.3, p.577-583, 2005.

VAZ, C. M. P. et al. Soil mechanical analysis through gamma ray attenuation. **Soil Technology**, v.5, p.319-325, 1992.

VAZ, C. M. P. Desempenho de 3 equipamentos da TDR para a medida da umidade e condutividade elétrica dos solos. In: CONGRESSO BRASILEIRO DE CIÊNCIA DO SOLO, 29., Ribeirão Preto. [**Anais...]** Ribeirão Preto: Sociedade Brasileira de Ciência do Solo, 2005.

VAZ, C. M. P. et al. New perspectives for the application of high-resolution benchtop X-ray microCT for quantifying void, solid and liquid phases in soils. In: TEIXEIRA, W.G. (Ed.). **Application of Soil Physics in Environmental Analyses**. Switzerland: Springer International Publishing, 2014.

VAZ, C. M. et al. Evaluation of an advanced benchtop micro-computed tomography system for quantifying porosities and pore-size distributions of two Brazilian Oxisols. **Soil Science Society of America Journal**, v.75, n.3, p.832-841, 2011.

VOGEL, H. J.; Kretzschmar, A. Topological characterization of pore space in soil: sample preparation and digital image-processing. **Geoderma**, v.73, n.1, p.23-38, 2002.

VOGEL, H. J. Topological characterization of porous media. In: MECKE, K.; STOYAN, D. (Ed.). **Morphology of condensed matter**. Berlin: Springer, 2015.

ZHANG, Z. B. et al. Characterizing preferential flow in cracked paddy soils using computed tomography and breakthrough curve. **Soil and Tillage Research**, v.146, p.53-65, 2015.

ZHAO, D. Quantification of soil aggregate microstructure on abandoned cropland during vegetative succession using synchrotron radiation-based micro-computed tomography. **Soil and Tillage Research**, v.165, p.239-246, 2017.

CHAPTER III

Characterization of soil architecture under different types of management through analytical tools

TSENG, C. L., ALVES, M. C., CRESTANA, S.

CHARACTERIZATION OF SOIL ARCHITECTURE UNDER DIFFERENT TYPES OF MANAGEMENT THROUGH ANALYTICAL TOOLS

Tseng C. L.[a], Alves, M. C.[b] and Crestana, S.[c]

[a]University of São Paulo, "São Carlos School of Engineering " 400 Avenida Trabalhador São-carlense, CEP: 13566-590 São Carlos, São Paulo, Brazil.

[b]Universidade Estadual Paulista, "Rural Engineering and Soil", 56 Avenida Brasil, Centro, CEP: 15385-000 Ilha Solteira, São Paulo, Brazil

[c]Embrapa Instrumentation, 1452, Rua XV de Novembro, CEP: 13560-970, São Carlos, São Paulo, Brazil.

ABSTRACT

Soil structure and architecture are essential carriers of soil functions and secure environmental quality. Therefore, adequate evaluation of management systems is essential to ensure the preservation and recuperation of soil architecture. The use of techniques such as X-ray microtomography and the automated soil particle size analyzer based on gamma-rays attenuation provides rapid quantification of soil physical properties and allows the evaluation of soil architecture, e.g., for the selection of appropriate actions to recuperate a degraded tropical soils. The aim of this study is to characterize and evaluate physical characteristics of soil under different types of management applying two techniques. Soil samples extracted from the UNESP experimental farm (Brazil) were separated into two different management groups according to the similarity of their textural class. The following results were obtained from the analysis: 1) Not only can Microtomography be used to extract the porosity, but a fraction of microporosity can be distinguished as well; 2) The form factor showed the soil geometric organization. This factor is relevant and valid for evaluating the degree of soil degradation; 3) The lacunarity values showed either fractal or random behavior of each type of management in that they reflect the degree of compaction, and are proportional to the total porosity (%). Finally, it can be concluded that the application of the concepts related to porosity, form factor, lacunarity and other geometric properties to soil management practices, provided new insights for better understanding the processes occurring within the soil including flow phenomena.

Keywords: Microtomography, management, porosity, form factor, lacunarity, tropical soil.

1. Introduction

Adequate soil management is essential to guarantee agricultural production and promote environmentally and socio-economically sustainable development around the world. Soon, to meet the demand, the preservation and recuperation of soil architecture will become an essential point for maintaining important soil functions securing environmental quality. However, one of the current challenges in the study of soil architecture is the lack of knowledge how to non-destructively and reliably evaluate physical parameters including soil structural status influenced by management practice and intensity.

The soil physical parameters are usually measured to obtain a better understanding or estimation of soil processes, such as tillage effects on soil structural quality (Reynolds et al., 2009). Using visual analysis, Carducci et al. (2016) assessed how an oxisol structure changed as a consequence of management, and they validated their findings by X-ray CT scanning of undisturbed soil samples. Pires et al. (2017) explored diverse tools to quantify pore system differences between conventional and no-till management systems. Likewise, Garbout et al. (2013) quantified tillage effects on topsoil structural quality and characterized the pore network using X-ray CT. Recently, Dal Ferro et al. (2014) used root image analysis to determine conventional and no-till system effects on soil structure and root growth dynamics. Naveed et al. (2016) quantified vertical stress transmission in an arable topsoil and compaction-induced soil structure applying X-ray CT. Zhao et al. (2017) visualized and determined the 3D aggregate microstructure with Synchrotron micro-computed tomography (SR-μCT) and image analysis.

From these applications of multiple techniques and methods existing for physical analysis, we selected several tools in this study that are non-invasive and manifest a pertinent option. Among these were the automated soil particle size analyzer (NAIME et al., 2001), the Arya and Paris (1981) model, which was validated for Brazilian soils by Vaz et al. (2005) and X-ray tomography, and digital images processing (PETROVIC et al., 1982, HAINSWORTH and AYLMORE, 1983, CRESTANA et al. 1985, PASSONI et al., 2014).

In Marchini et al. (2015), tomographic images were used to prove the evaluation of the recuperation process of a Brazilian oxisol with different types of management. Vaz et al. (2011) quantified the porosity and the pore size distribution of two Brazilian oxisols, resulting in important information for establishing appropriate scanning parameters for these soils. Beraldo et al. (2014) also applied a tomographic method to evaluate the porosity of three soil management systems, thereby verifying that their results corresponded to the macropore scale.

The work of Naveed et al. (2014) has demonstrated the use of tomographic X-rays to quantify the pore structure of natural and regenerated soil aggregates, as well as the association among aggregate OC, aggregate pore structure and mechanical properties derived from traditional techniques, such as tensile strength and specific rupture energy (SRE).

With respect to pore form or shape factors, Passoni et al. (2014) applied ImageJ software to characterize two Brazilian oxisols from the south-eastern region of Brazil. They successfully demonstrated the possibility of using this software to identify the characteristics of pores in tropical soils. Ma et al. (2015) calculated a form factor to quantify the pore structure based on Synchrotron micro-computed tomography (SR-μCT). Munkholm et al. (2016) confirmed that long-term management of the soil alters both its aggregate form and pore characteristics by using CT scanning and tensile strength measurements.

Although the lacunarity concept had been initially conceived to describe fractal properties, it can be extended to other natural spatial patterns without restrictions (PLOTNICK et al., 1996; ALLAIN and CLOITRE, 1991). In other words, the lacunarity curve corresponds to the degree of spatial heterogeneity and to the self-similar characteristics of the soil texture in practical terms. This concept applies regardless whether the soil texture is fractal or random. Additionally, the application of the lacunarity parameter in soil studies is considered promising for the quantification of intra-aggregate pores and confirms the hierarchical organization of pores described in Chun et al. (2008) and Muñoz et al. (2014). In that sense the work of Monreal et al. (2013) is particularly interesting, who applied the concept of lacunarity to investigate the behavior of spatial distribution of pedotaxa in Europe. In Roy and Perfect (2014), analytical and digital tools were used to investigate lacunarity and its influence on flow and transport processes within greyscale representations of soil aggregates. In another study, Martínez et al. (2016) analysed lacunarity in 3-D images of soil columns for characterizing their macropore space geometry. For the first time, all of the physical parameters above were used concomitantly to evaluate soil quality, whereas there exist only few studies that characterize tropical soils under different management.

The aim of this study is to evaluate the capability of automated soil particle size analysis and X-ray microtomography to derive physical characteristics of a Brazilian oxisol and its management-related degradation status.

2. Material and Methods:

2.1. Experimental Sites

The soil samples were obtained at the Fazenda de Ensino e Pesquisa da Universidade Estadual Paulista "Júlio de Mesquita Filho" (Unesp) (Teaching and Research Farm of the Paulista State University “Júlio de Mesquita Filho”), on the Ilha Solteira campus, in the city of Selvíria (Mato Grosso do Sul State - Brazil). This farm is located on the banks of the Paraná river (22o 22' S e 51o 22' W). In the 1960s, at the beginning of the construction of the Hydroelectric Power Station in Ilha Solteira (São Paulo State), an 8.6-m-thick soil layer was withdrawn from the original soil surface in order to prepare and construct the dam’s foundation. Since 1969, subsoil containing B horizon material has remained exposed to the surface and has shown serious stages of superficial compaction and a low presence of vegetation. The soil in the experimental area is a Brazilian oxisol. These soil samples were collected at 0-10 cm depth, in form of undisturbed block (30 cm x 30 cm x 10 cm) and were characterized by advanced stages of weathering, acidic pH, and is typical for equatorial and tropical regions (EMPRESA BRASILEIRA DE PESQUISA AGROPECUÁRIA, 2013).

2.2. Management Description

Upon their collection, soil samples were divided into two groups based on their granulometric and textural class; with respect to soil structural status, soil from native forest was considered to be a reference for comparison. In total, there were six types of management: Group I: 1) **NF** - Soil from Native Forest (control); 2) **RS** - Recuperated soil (green manure applied to soil over seven years from 1992 to 1999. Afterwards, soil was cultivated with *Brachiaria decumbens*); 3) **G** - Recuperating soil with *Astronium fraxinifolium* (Gonçalo-alves) + *Brachiaria decumbens* + sewage sludge; 4) **D** - Degraded soil (remaining soil from the construction of the Hydroelectric Power Plant); Group II: 5) **RP** - Recuperating pasture soil; 6) **DP** - Degraded pasture soil. All soil samples were collected from the superficial layer (0-10 cm). In this study, one sample was obtained from each management, a decision that was met owing to the fact that in this work the focus was on non-invasive analytical tools.

2.3. Equipment

Two analytical apparatuses were used to complete this study: i) Automated soil particle size analyzer and ii) Commercial X-ray microtomograph, model 1172 - Skyscan. With these devices physical parameters were derived for each management system.

2.3.1. Automated soil particle size analyzer

The automated soil particle size analyzer is an instrument developed by Embrapa - Instrumentation - São Carlos. It uses the attenuation of gamma rays and is based on the modified Beer-Lambert law to determine the distribution of particle sizes based on the water sedimentation process manifested in Stokes law (VAZ et al., 1992; NAIME et al., 2001).

For the soil sample pre-treatment, the soil samples were dried in stoves at 105^{o} C during 24 hours and sieved through 1.5 mm mesh to remove gravel and rest of plant roots, next, the mass attenuation coefficients were determined for all samples. The measurement is based on the relationship between cuvette and soil weights. Subsequently, 40 grams of soil were mixed with 10 ml of sodium hydroxide solution (NaOH), distilled water and placed in a Wagner type shaker. This dispersion was agitated for 16 hours to ensure that the solution was uniformly dissolved in the water. Finally, the solution was transferred to a cuvette and placed in the automated soil particle size analyzer for acquiring particle size distribution. For each soil management system, three measurements were accomplished with the aid of QUALISSOLO software. Thereafter the average value was calculated in Excel.

2.3.2 X-ray microtomography and image reconstruction

High resolution x-ray microtomography was used for acquiring and reconstructing tomographic images. Initially, the tomographic projections were obtained using an energy source with 100kV, a current of 100µA, and a filter of Al and Cu. The projections were then rotated for a total rotation of 360° in steps of 0.3°. The resolution was 5µm, as suggested by Vaz et al. (2011). Subsequently, the projections were reconstructed as bi-dimensional images with NRCon software (NRCon User Manual, 2011), with several parameters adjusted as needed.

2.4 Physical Analysis Methods and Software

2.4.1 Classical - Porosity (ϕ_c)

Initially, the Archimedes method was used to measure the density of the pre-selected samples. Equation (1) was then used accordingly to obtain the total porosity of the soil (ϕ_c), through the particle density (ρ_p), and the bulk density (ρ_b).

$$\phi_c = 1 - \left(\frac{\rho_b}{\rho_p}\right) \qquad (1)$$

2.4.2 CT-Analyser - Porosity (ϕ_t)

CT-Analyser is a software developed by Skyscan, provided by Embrapa - Instrumentation (Manual for Bruker-micro CT - CT Analyser, 2013).

First, the microtomographic image was binarized using the Otsu (1975) method, which consists of automatic selection of the optimum thresholds that minimize the between-class variances in the ROI (Region of Interest) of the images. Subsequently, the 2D porosity value was calculated by dividing the empty space by the total identified area, which was represented by equation (2) for each of the image slices. Finally, the integral of porosity of all 500 microtomographic layers was calculated as the equivalent of the 3D porosity (Eq. 3).

$$\phi_{t2D} = \frac{\text{Porous area}}{\text{Total area}} \qquad (2)$$

$$\phi_{t3D} = \int_1^{500} \frac{\text{Porous area}}{\text{Total area}}\, dS \qquad (3)$$

where dS is the differential of the area.

2.4.3 ImageJ - Form Factor

ImageJ is a public domain image processing program, which was developed by NIH (National Institutes of Health) and more than 500 plugins are available (SCHNEIDER et al., 2012).

The form factor provides information about the geometric structure organization. In other words, it is one of the indicators that is able to determine the degree of soil degradation. Skvortsova (2009) suggested a formula for the form factor (Eq. 4) to calculate the shape of the pores:

$$F = \left(\frac{4\pi S}{P^2} + \frac{D}{L}\right)/2 \qquad (4)$$

In this equation, S is the area, P is the perimeter; D and L are the transversal and longitudinal linear dimensions, respectively. All of these values were acquired from ImageJ' statistical image analysis.

Once the values of form factors are obtained, they are separated into five classes based on the shape of the pore, as can be seen in the Table 1 in Skvortsova (2009). Due to the large amount of information contained in a single microtomography and considering digital processing time, in this study, one layer of the middle section from 500 images was selected with severe care.

Table 1. Classification of pore-shape classes

Form factor interval	≤ 0.20	0.21-0.4	0.41-0.6	0.61-0.8	0.81-1
Pore Classification	Fissures	Elongated dissected	Isometric dissected	Isometric slightly dissected	Rounded

Source: Skvortsova (2009)

2.4.4 Image J - Lacunarity:

For the present study, the open plugin FracLac, developed by the University of Charles Sturt - Australia, was used under the ImageJ environment (KARPERIEN, 2007). This plugin was implemented to measure the lacunarity of the microtomographic image. The FracLac algorithm calculates the lacunarity using a measure of pixel intensity for different sizes of the "Gliding box" (ALLAIN and CLOITRE, 1991). FracLac uses the first moments Z(1) and Z(2) as defined by Plotnick et al. (1996), as a function of the mean of measurements (τ) and their standard deviation (σ), varying with the length of the box (b), and the width of the image (T) which is given in number of pixels, and the condition is always b ≤ T (5) and (6):

$$Z(1) = \tau \quad (5)$$

$$Z(2) = \sigma^2 + \tau^2 \quad (6)$$

By definition, the lacunarity equation (Λ(r)) is a straight correlation between functions Z (1) and Z (2), which is represented by equations (7) and (8):

$$\Lambda(r) = \frac{Z(2)}{Z(1)} \quad (7)$$

$$\Lambda(r) = \frac{\sigma^2}{\tau^2} + 1 \quad (8)$$

The ratio between σ and τ changes according to the varying size of the "Gliding box" (r), i.e. the lacunarity value depends on the scale of the "Gliding box" and on the image. Based on equation (7), a log -log plot of lacunarity versus size of the "Gliding box" on the x-axis is produced. As item 2.4.3, one representative microtomography was selected to calculate the lacunarity value.

3. Results and Discussion

3.1 Microtomographic calibration

Before analyzing the soil physical parameters, it is essential to calibrate the microtomographic images. By definition, there is a linear relationship between HU and the linear attenuation coefficient (CRESTANA, 1985). Thus, an X-ray microtomography calibration curve was established (model 1172 - Skyscan (Belgium)) for soil samples and diverse known materials obtained under a source energy of 100kV (Figure 1). Finally, the microtomographic images were obtained using the preselected specifications (Figures 2a - 2f).

Figure 1. Calibration curve of management types and different materials

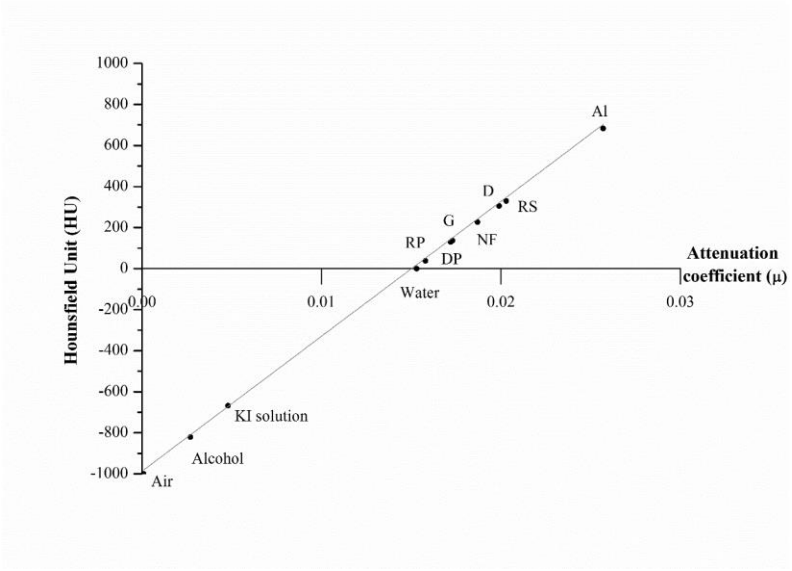

- **Al** – Aluminium
- **Alcohol**
- **Air**
- **D** – Degraded soil
- **DP** – Degrated pasture soil
- **G** – Recuperating soil
- **KI solution** – Postassium Iodide solution (1%)
- **NF** – Soil from native forest (Brazilian Savanna)
- **RP** – Recuperationg pasture soil
- **RS** – Recuperating soil
- **Water**

Equation	y = a + b*x		
Weight	No Weighting		
Residual Sum of Squares	19410.12419		
Pearson's r	0.99709		
Adj. R-Square	0.99354		
		Value	Standard Error
C	Intercept	-986.92985	26.2846
C	Slope	65747.98029	1675.95625

Source: Author (2014)

Figure 2. a) **NF** - Soil from native forest characterized by its heterogeneous formation; b) **RS** - Recuperated soil showing heterogeneous characteristics similar to NF; c) **G** - Recuperating soil which, even though it has big pores, still shows aspects closer to degraded soil f; d) **RP** - Recuperating pasture soil shows the initial stages of recuperation; e) **DP** - Degraded pasture soil characterized by agglomeration of aggregates typical of degraded soil; f) **D** - Degraded soil marked by homogeneity in its profile, which is a typical characteristic of high compaction.

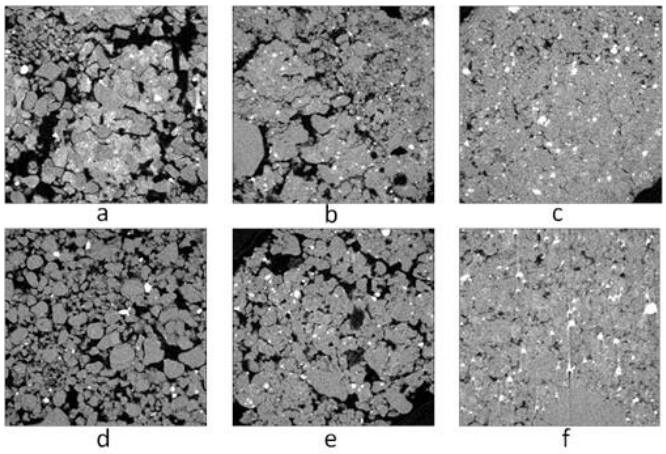

Source: Author (2014)

3.2 Particle size distribution

The automated soil particle size analyzer reduced the duration of the analysis to approximately 20 minutes. Hence, the equipment rapidly provides particle size distribution and textural class for each of the differently managed soils (Tables 2 and 3). The textural composition is a fundamental parameter that governs the soil behavior under different management.

Table 2. Granulometric percentage and textural class for group I management types

Granulometric (%)	Soil from Native Forest (NF)	Recuperated Soil (RS)	Recuperating Soil (G)	Degraded Soil (D)
Clay	40.08	41.23	37.35	44.92
Silt	7.67	6.42	6.74	5.51
Sand	52.25	52.35	55.91	49.57
Textural Class	Sandy Clay	Sandy Clay	Sandy Clay	Sandy Clay

Source: Author (2014)

Table 3. Granulometric percentage and textural class for group II management types

Granulometric (%)	Soil from Native Forest (NF)	Recuperating Pasture Soil (RP)	Degraded Pasture Soil (DP)
Clay	40.08	24.19	17.76
Silt	7.67	3.33	3.09
Sand	52.25	72.48	79.15
Textural Class	Sandy Clay	Sandy Clay Loam	Sandy Loam

Source: Author (2014)

3.3 Porosity – ϕ_c and ϕ_t

The pore size distribution is directly related to the water drainage and retention capacity of the soil as well as the aeration conditions. Nowadays, benchtop or cabinet-type scanners allow obtaining a resolution around 1 to 100µm with samples ranging from a few millimeters to a few centimeters in diameter (CNUDDE and BOONE, 2013; VAZ et al., 2011).

Due to time constraints and computational costs, microtomography was used here to detect pores with a diameter greater than 10 µm, which is the equivalent of the pre-selected resolution. This resolution was sufficient to detect macropores, mesopores and some micropores (Table 4). On the other hand, this spatial resolution is ideal for studying macropores, as verified by the evaluation of porosity under three systems of management by Beraldo, Scannavino Junior and Cruvinel (2014).

Table 4. Pore classification

Class	Subclass	Effective Diameter (μm)
Macropores	Coarse	> 5000
	Medium	2000-5000
	Fine	1000-2000
	Very fine	75-1000
Mesopores		35-75
Micropores		5-30
Ultramicropores		0.1-5
Cryptopores		<0.1

Source: Brewer (1964) and SSSA (2008)

This procedure highlights that, in this case, a comparison of the porosity percentages obtained with two different analytical methods of analysis for each of the different management systems became possible on a micrometric scale. This approach is different from the one introduced by Ambert-Sanchez et al. (2016), who applied conventional methods, along with industrial tomography with 0.6mm resolution for arid soil and for another unmanagement soil. Based on the porosity percentage obtained from this study, the percentage of micropores can be estimated by subtracting the total porosity obtained by the tomographic method (ϕ_t) from the lab-determined total porosity (ϕ_c), and all dimensions are reported as mean ± standard deviation (Tables 5 and 6).

Table 5. Porosity obtained by classical (ϕ_c) and microtomographic (ϕ_t) methods (%) for group I

Types of management	NF	RS	G	D
Total porosity (ϕ_c) in this study (%)	55.35	47.28	42.16	41.68
Standard Deviation	0.057	0.27	0.09	0.12
Total tomographic porosity / Macroporosity (ϕ_t) (%)	31.90	24.74	41.83	37.32
Standard Deviation	1,54	4,42	2,59	1,85
Microporosity ($\phi_c - \phi_t$) (%)	23.45	22.55	0.33	4.36
Standard Deviation	1.54	4.42	2.61	1.87

Source: Author (2015)

Table 6. Porosity obtained by classical (ϕ_c) and microtomographic (ϕ_t) methods (%) for group II

Types of management	NF	RP	DP
Total porosity (ϕ_c) in this study (%)	55.35	39.56	41.72
Standard Deviation	0.057	0.16	0.31
Total tomographic porosity/Macroporosity (ϕ_t) (%)	31.90	32.06	21.62
Standard Deviation	1,54	2.26	2.58
Microporosity ($\phi_c - \phi_t$) (%)	23.45	7.50	20.09
Standard Deviation	1.54	2.26	2.58

Source: Author (2015)

In this study, the analysis of different types of long-term soil management was noteworthy due to the unique character of tropical soils, as obvious from the studies of Marchini et al. (2015) and Bonini and Alves (2011), who investigated the same soils as in this study. Based on these procedures, each different group was analyzed as follows (Figure 3):

Figure 3. Total porosity (%) obtained by the classical method and by the tomographic method; **a)** Management group I and **b)** Management group II.

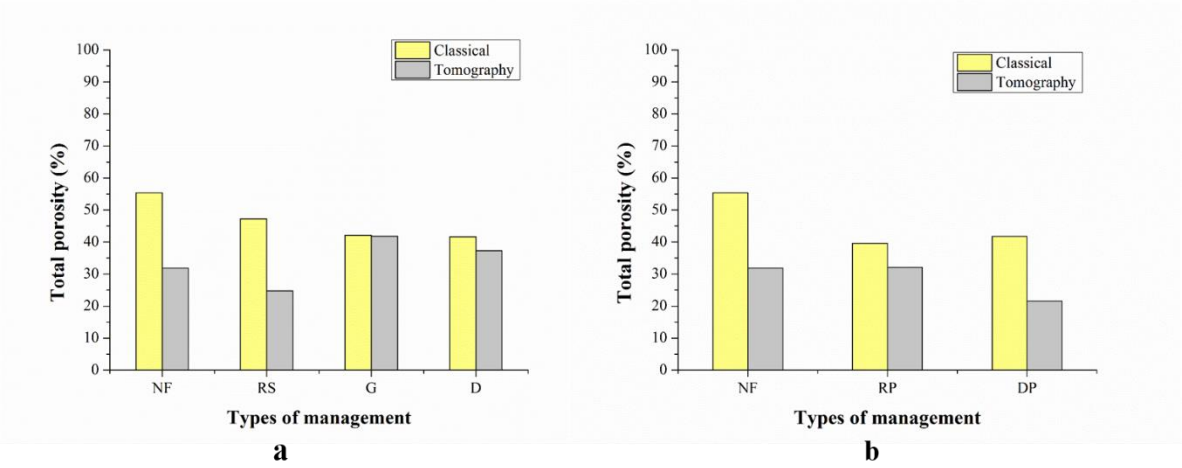

Source: Author (2015)

Group I (Figure 3a): Consistent with *in situ* field conditions and with Marchini et al. (2015), the total porosity percentage was obtained by the laboratory method. NF shows the high value of the measurement, followed by RS, and finally by G and D (similar values). These results have already been verified by the tomographic method. G shows the largest porosity, followed by D, NF, and RS; The soil G did not show any notable variation between the two methods, and this is due to the decompression effect caused by the native tree species Gonçalo-Alves (*Astronium fraxinifolium*), which favors the formation of large pores. Nonetheless, the physical quality remains similar to that of a degraded soil.

Group II (Figure 3b): A deviation of about 20% between the porosity value obtained in the classic method and that obtained through tomography was observed in DP, while for RP, this difference was around 8%. It can therefore be stated that DP contained more unidentified micropores than RP. In comparison with NF, the quantity of pores in RP was lower. However, the macroporosity of both soils showed that RP was close to NF, which leads to the conclusion that the soil structural recovery process was effective.

3.4 Form Factor

Following the classification by Skvortsova (2009), the stages of structure degradation in soil are as follows: granular structure, blocky structure, platy structure (predominantly in a horizontal direction), formation of compact soil (non-structured) and finally, a structure that acquires characteristics from its original material. Therefore, an evaluation of the porous

structure of different management groups was performed (Figure 4). As it was done for the previous item, all values were represented by mean ± standard deviation (Table 7 and 8).

Table 7. Form factor obtained by microtomography for group I

Types of Management	Soil from Native Forest (NF)	Recuperated Soil (RS)	Recuperating Soil (G)	Degraded Soil (D)
Mean	0.79	0.77	0.82	0.80
Standard Deviation	0.31	0.29	0.31	0.32

Source: Author (2015)

Table 8. Form factor obtained by microtomography for group II

Types of Management	Soil from Native Forest (NF)	Recuperating Pasture Soil (RP)	Degraded Pasture Soil (DP)
Mean	0.79	0.72	0.75
Standard Deviation	0.31	0.29	0.27

Source: Author (2015)

Group I (Figure 4a): G and D show advanced stages of degradation at the pore scale with a form factor between 0.61 and 1. This level is higher compared to RS and NF, which indicated that G and D lost their structural-geometric characteristics and, at the same time, acquired typical aspects from their original material. The average of the NF and RS pores was low, slightly isometric and dissected, thereby representing the quality of natural soil, while D and G have rounded pores, which indicates a greater uniformity and fragmentation and characterizes its stages of degradation.

Group II (Figure 4b): The average soil form factor in two pastures was as follows; the pores were slightly isometric and dissected. By separately analyzing the pore size histogram of pastures, it was observed that NF showed a higher degree of fragmentation by moving to a larger number of round pores, whereas RP found itself in a state prone to native forest with a reduced pore scale, thereby highlighting the positive impact of recuperation.

Therefore, the Skvortsova (2009) classification was relevant and valid for the tropical soil in this study; however, it is still necessary to conduct more experiments in order to validate and generalize this classification for tropical soil.

Figure 4. Form factor obtained by using of Skvortsova (2009) classification - **a)** Management group I and **b)** Management group II.

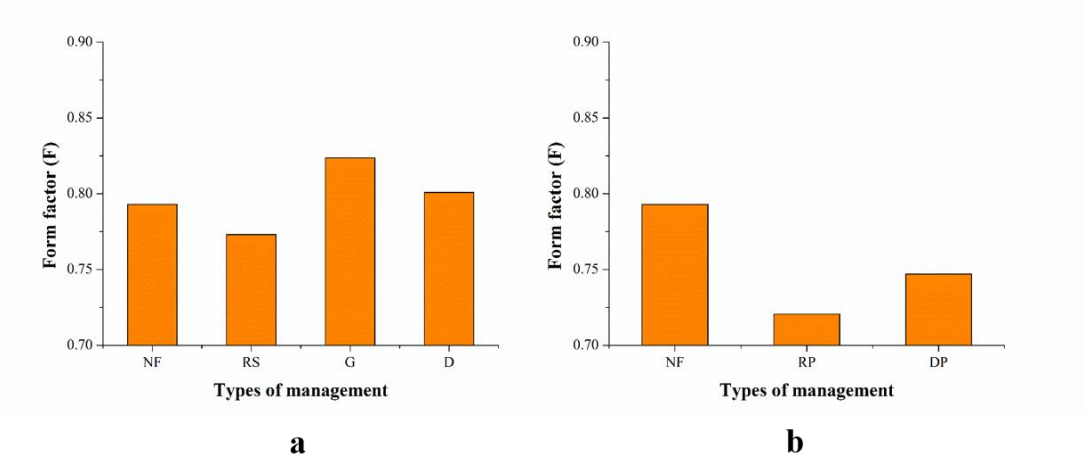

Source: Author (2015)

3.5 Lacunarity

The application of lacunarity in soil studies is a powerful tool to obtain important information about the physical properties of transport phenomena in soil. Roy and Perfect (2014) demonstrated lacunarity as a single number that takes into account the clustering of pixels in a pattern at different scales. In regards to the tomographic images of this study (Figure 5), it was observed that the curve tended to form a concavity (Figure 5a). This shape manifests the random behavior of soil structure that existed under this type of management. This result manifests the typical characteristic of a soil from native forest (NF). In contrast, the second curve of a degraded soil (D) showed an increasing degree of compaction while under management, the curve tended to straighten, which resembled fractal behavior (Figure 5b).

Figure 5. **a)** Lacunarity of soil from native forest (NF) characterized by the presence of concavity and **b)** Lacunarity of degraded soil (D) characterized by a reduction in concavity and by a straight appearance.

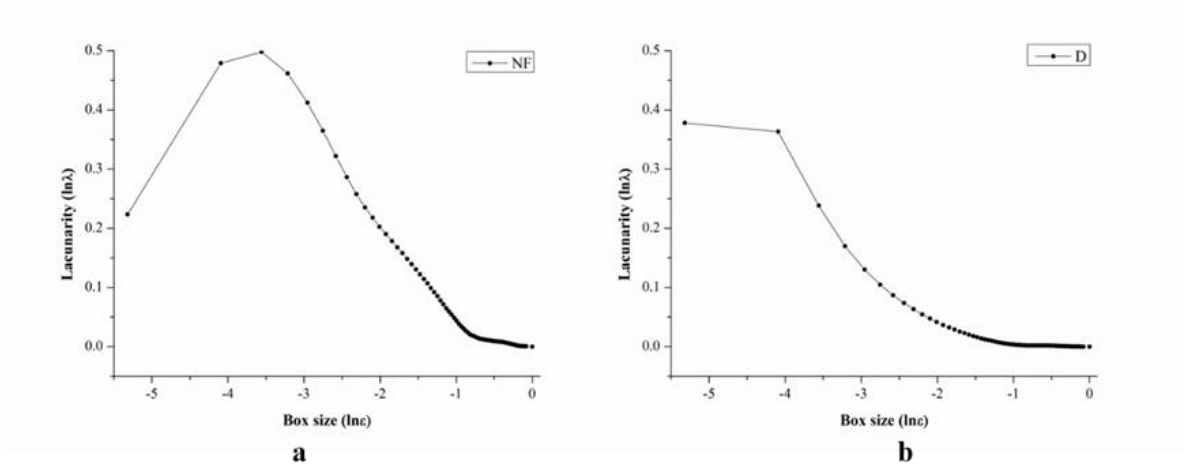

Source: Author (2015)

In fact, taking into account the results obtained by FractaLac, the relationship between occupied sets and lacunarity was inversely proportional. In other words, for the same box size, the lacunarity decayed when there was an increasing degree of compaction or a rupture in continuity.

Group I (Table 9)**:** When the compaction degree in managed soil increases, the average lacunarity decreases. Therefore, the managed soils are listed in decreasing order by their degree of compaction: D, G, NF, and RS.

Group II (Table 10)**:** The lacunarity in this group did not behave as expected, as DP showed the largest degree of lacunarity relative to the others. It can be assumed that this is the effect of the microtomographic resolution as this type of management has caused undetectable micropores (i.e, pores of fragmentation and standardization). More specifically, this result presents a clear sign of compaction and, therefore, creates a misperception.

Table 9. Lacunarity of Group I

Types of Management	Soil from Native Forest (NF)	Recuperated Soil (RS)	Recuperating Soil (G)	Degraded Soil (D)
Lacunarity	0.0944	0.1083	0.0524	0.0291

Source: Author (2015)

Table 10. Lacunarity of Group II

Types of Management	Soil from Native Forest (NF)	Recuperating Pasture Soil (RP)	Degraded Pasture Soil (DP)
Lacunarity	0.0944	0.0503	0.1358

Source: Author (2015)

3.6 Relationship between total porosity (%) and lacunarity

Conceptually, porosity is a parameter of reference in soil studies. However, despite its importance, further studies are necessary to obtain information on the degree of spatial heterogeneity (the distribution of pores in the soil). This study explored both the concepts of porosity and lacunarity (Figure 6) and verified that the two results were proportional to each other. In other words, the study proved that the association between the two concepts was consistent and is recommended for soil studies, especially in the future for relating structure to transport phenomena in the soil matrix.

Figure 6. The two graphs are similar as the soil's lacunarity value and total porosity are correlated.

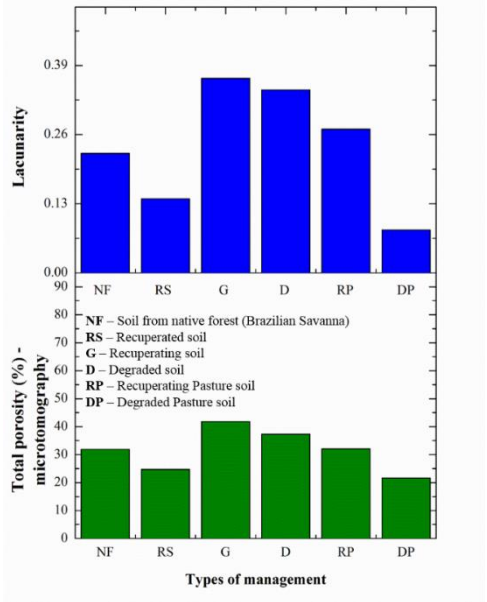

Source: Author (2015)

4. Conclusion

The methods used in this study were successful for analyzing and distinguishing the structural status and architecture of soil under different types of management. However, there are still limitations revealed by this study that should be taken into account and further addressed. For instance, microtomography was able to capture part of the micropores and

showed excellent opportunities to identify meso- and macropores entirely. Additionally, although the form factor was effective for pore class evaluation, it must be further validated in order to be generalized for tropical soils. Furthermore, the lacunarity parameter proved itself to be an important tool for estimating the soil structural status, i.e. each type of management carries a random or fractal character, which is, by the way, related to the suitable or degraded condition of the soil. In addition, lacunarity was related to the degree of discontinuity or continuity of the pores. However, it is not recommended to use lacunarity as the only quantifiable physical parameter. Aside from these restrictions, this study also showed that the lacunarity and the percentage of porosity matched. Finally, the combined use of the automated soil particle size analyzer and X-ray microtomograph allowed to characterize and evaluate physical characteristics of a Brazilian oxisol under different types of management. As a consequence the results presented are very promising in the sense that the approach employed here may help to foresee flow of water in soil with different structure.

5. Acknowledgements

We extend our thanks to CNPq and CAPES for financial support, to USP for its academic formation, to Embrapa, which made possible the use of its laboratories, developed technologies and technical support, and to Unesp for providing samples and technical support.

References

ALLAIN, C.; CLOITRE, M. Characterizing the lacunarity of random and deterministic fractal sets. **Physical Review A**, v. 44, n. 6, p. 3552-3558, 1991.

AMBERT-SANCHEZ, M. et al. Evaluating soil tillage practices using X-Ray computed tomography and conventional laboratory methods. **Transactions of the ASABE**, v. 59, n. 2, p. 455-463, 2016.

ARYA, L. M.; PARIS, J. F. A Physicoempirical model to predict the soil moisture characteristic from particle-size distribution and bulk density data. **Soil Science Society of America Journal**, v. 45, n. 6, p. 1023-1030, 1981

BERALDO, J. M. G.; SCANNAVINO JUNIOR, F. A.; CRUVINEL, P. E. Application of x-ray computed tomography in the evaluation of soil porosity in soil management systems. **Engenharia Agrícola**, v. 34, n. 6, p. 1162-1174, 2014.

BONINI, S. B.; ALVES, M. C. Recovery of soil physical properties by green manure, liming, gypsum and pasture and spontaneous native species[1]. **Revista Brasileira de Ciência do Solo**, v. 35, n. 4, p. 1397-1406, 2011.

BREWER, R. **Fabric and mineral analysis of soils**. New York: Wiley, 1964.

BRUKER MICROCT. **NRcon User Manual**. [S. l.]: Bruker microCT, 2011. Disponível em: <http://bruker-microct.com/next/NReconUserGuide.pdf >. Acesso em: Jun 28, 2016.

BRUKER. **CT-Analyser**. [S. l: s.n.]:, 2013. (Version 1.13). Disponível em: <http://bruker-microct.com/next/CTan_UserManual.pdf>. Acesso em: Jun 18, 2016.

CARDUCCI, C. E. et al. Visual analysis and X-ray computed tomography for assessing the spatial variability of soil structure in a cultivated Oxisol. **Soil and Tillage Research**, 2016. Article in press.

CHUN, H. C.; GIMÉNEZ, D.; YOON, S. W. Morphology, lacunarity and entropy of intra-aggregate pores: aggregate size and soil management effects. **Geoderma**, v. 146, n. 1, p. 83-93, 2008.

CNUDDE, V.; BOONE, M. N. High-resolution X-ray computed tomography in geosciences: a review of the current technology and applications. **Earth-Science Reviews**, v. 123, p. 1-17, 2013.

CRESTANA, S.; MASCARENHAS, S.; POZZI-MUCELLI, R. S. Static and dynamic three-dimensional studies of water in soil using computed tomographic scanning. **Soil Science**, v. 140, n. 5, p. 326-332, 1985.

DAL FERRO, N. Soil macro-and microstructure as affected by different tillage systems and their effects on maize root growth. **Soil and Tillage Research**, v. 140, p. 55-65, 2014.

EMPRESA BRASILEIRA DE PESQUISA AGROPECUÁRIA. **Sistema brasileiro de classificação de solos**. 3. ed., Rio de Janeiro: Centro Nacional de Pesquisa de Solos, 2013.

GARBOUT, A.; MUNKHOLM, L. J.; HANSEN, S. B. Tillage effects on topsoil structural quality assessed using X-ray CT, soil cores and visual soil evaluation. **Soil and Tillage Research**, v. 128, p. 104-109, 2013.

HAINSWORTH, J. M.; AYLMORE, L. A. G. The Use of computer-assisted tomography to determine spatial distribution of soil water content. **Australian Journal of Soil Research**, v. 21, n. 4, p. 435-443, 1983.

KARPERIEN, A. **FracLac for ImageJ:** using FracLac V 2.0 for ImageJ. [S. l.]: Charles Sturt University, 2007.

MA, R. Evaluation of soil aggregate microstructure and stability under wetting and drying cycles in two Ultisols using synchrotron-based X-ray micro-computed tomography. **Soil and Tillage Research**, v. 149, p. 1-11, 2015.

MARCHINI, D. C. Matéria orgânica, infiltração e imagens tomográficas de Latossolo em recuperação sob diferentes tipos de manejo. **Revista Brasileira de Engenharia Agrícola e Ambiental**, v. 19, p. 574-580, 2015.

MARTÍNEZ, F. S. J. Lacunarity of soil macropore space arrangement of CT images: Effect of soil management and depth. **Geoderma**, v. 287, p. 80-89, 2016.

MONREAL, J. C. Lacunarity of the spatial distributions of soil types in Europe. **Vadose Zone Journal**, v. 12, n. 3, p. 1-9, 2013.

MUNKHOLM, L. J. Relationship between soil aggregate strength, shape and porosity for soils under different long-term management. **Geoderma**, v. 268, p. 52-59, 2016.

MUNOZ, F. J.; SAN JOSE MARTÍNEZ, F.; CANIEGO, F. J. Fractal parameters of pore space from CT images of soils under contrasting management practices. **Fractals**, v. 22, n. 3, p. 1-9, 2014.

NAIME, J. M.; VAZ, C. M. P.; MACEDO, A. Automated soil particle size analyzer based on gamma-ray attenuation. **Computers and Electronics in Agriculture**, v. 31, n. 3, p. 295-304, 2001.

NAVEED, M. et al. Quantifying vertical stress transmission and compaction-induced soil structure using sensor mat and X-ray computed tomography. **Soil and Tillage Research**, 158, p. 110-122, 2016.

NAVEED, M. et al. Revealing soil structure and functional macroporosity along a clay gradient using X-ray computed tomography. **Soil Science Society of America Journal**, v. 77, n. 2, p. 403-411, 2013.

OTSU, N. A Threshold selection method from gray-level histograms. **Automatica**, v. 11, n. 285-296, p. 23-27, 1975.

PASSONI, S. et al. Software Image J to study soil pore distribution**. Ciência e Agrotecnologia**, v. 38, n. 2, p. 122-128, 2014.

PETROVIC, A. M.; SIEBERT, J. E.; RIEKE, P. E. Soil bulk density analysis in three dimensions by computed tomographic scanning. Soil Science Society of America Journal, v. 46, n. 3, p. 445-450, 1982.

PIRES, L. F. Soil structure changes induced by tillage systems. **Soil and Tillage Research**, v. 165, p. 66-79, 2017.

PLOTNICK, R. E. et al. Lacunarity analysis: a general technique for the analysis of spatial patterns. **Physical review E**, v. 53, n. 5, p. 5461-5468, 1996.

ROY, A.; PERFECT, E. Lacunarity analyses of multifractal and natural grayscale patterns. **Fractals**, v. 22, n. 3, p. 1440003-1-1440003-9, 2014.

SCHNEIDER, C. A.; RASBAND, W. S.; ELICEIRI, K. W. NIH Image to ImageJ: 25 years of image analysis. **Nat methods**, v. 9, n. 7, p. 671-675, 2012.

SKVORTSOVA, E. B. Changes in the geometric structure of pores and aggregates as indicators of the structural degradation of cultivated soils. **Eurasian Soil Science**, v. 42, n. 11, p. 1254-1262, 2009.

SOIL SCIENCE SOCIETY OF AMERICA. **Glossary of soil science terms**. Madison: [s.n.], 2008. Disponível em: <http://blogs.upm.es/techenglish/wp-content/uploads/sites/53/2015/05/Soil-Science-glossary.pdf>. Acesso em: 28 jun. 16.

VAZ, C. M. Evaluation of an advanced benchtop micro-computed tomography system for quantifying porosities and pore-size distributions of two Brazilian Oxisols. **Soil Science Society of America Journal**, v. 75, n. 3, p. 832-841, 2011.

VAZ, C. M. P., et al. Validation of the Arya and Paris water retention model for Brazilian soils. **Soil Science Society of America Journal**, v. 69, n. 3, p. 577-583, 2005.

VAZ, C. M. P.; OLIVEIRA, J. C. M.; REICHARDT, K. Soil mechanical analysis through gamma ray attenuation. **SMR**, v. 705, p. 319-325, 1992.

ZHAO, D. et al. Quantification of soil aggregate microstructure on abandoned cropland during vegetative succession using synchrotron radiation-based micro-computed tomography. **Soil and Tillage Research**, v. 165, p. 239-246, 2017.

CHAPTER IV

Quantifying physical and structural soil properties using X-ray microtomography

TSENG, C. L., ALVES, M. C., CRESTANA, S.

QUANTIFYING PHYSICAL AND STRUCTURAL SOIL PROPERTIES USING X-RAY MICROTOMOGRAPHY

Tseng, C. L.[a], Alves, M. C.[b] and Crestana, S.[c]

[a]University of São Paulo, "São Carlos School of Engineering " 400 Avenida Trabalhador São-carlense, CEP: 13566-590 São Carlos, São Paulo, Brazil.

[b]Universidade Estadual Paulista, "Rural Engineering and Soil", 56 Avenida Brasil, Centro, CEP: 15385-000 Ilha Solteira, São Paulo, Brazil

[c]Embrapa Instrumentation, 1452, Rua XV de Novembro, CEP: 13560-970, São Carlos, São Paulo, Brazil.

ABSTRACT

One of the current challenges in the study of recovering soil architecture is physically evaluating the internal soil structure in nonconventional ways. The aim of this study is to analyze the soil structures of two groups of recovering tropical soils and to simulate water movement pathways in three dimensions using nonconventional methods and physical soil parameters. The following results were obtained from the respective analysis: 1) the S Index was used as an indicator to effectively quantify the degree of management; 2) Qualisolo software was used to obtain the soil water retention curve (SWRC) of each management type; 3) the degree of anisotropy of the solid structure reflected the soil network; 4) the Euler-Poincaré number reflected the connectivity level of each management type; 5) the Shannon entropy indicated the degree of randomness of the soil; and 6) the results of the Arya and Paris model and the simulations of water movement pathways are similar. In conclusion, the results obtained reflect the internal soil structures and their corresponding characteristics. Thus, the results can be used to predict the influence of the soil architecture on the movement of water in the soil.

Keywords: Microtomography. S Index. Degree of anisotropy. Euler-Poincaré number. Shannon entropy. SWRC. 3D simulation. Tropical soil.

1. Introduction

The Brazilian cerrado (Savannah) biome is important for food and agricultural production due to its soil and climate. However, the cerrado soil has been intensively devastated by human activities in the past decade, and these activities have threatened the sustainable use of resources in the region. In this context, the recovery of degraded areas is important for ensuring the sustainable use of the soil. However, determining how to evaluate the physical architecture of the recovering tropical soil and preserving its internal structure remain challenges in the evaluation of this resource.

Among several minimally invasive and nonconventional techniques and methods, X-ray computerized tomography (XCT) has become a common method of studying the soil structure in recent decades. Petrovic et al. (1982), Hainsworth and Aylmore (1983) and Crestana et al. (1985) pioneered XCT methods for studies of soil density and measured the water content and water movement into the soil. Additionally, Appoloni et al. (1994) performed microscanning and microtomography using an X-ray tube.

Although XCT has become popular in recent decades, studies of tropical soils are uncommon in the literature. Nevertheless, given the rarity of related papers, some important tropical soil research using of XCT should be highlighted. Vaz et al. (2011) evaluated two Brazilian Oxisols and established the scanning parameters of the soil. Passoni et al. (2014) characterized the soil macroporosity of a Rhodic Ferralsol using a second-generation X-ray microtomograph. In addition, Beraldo et al. (2014) used microtomography to quantify the porosity in areas of no tillage, conventional tillage and native forest. Recently, Marchini et al. (2015) applied CT to study recovering Brazilian Oxisols under different types of management strategies. Furthermore, Marchini et al. (2015) qualitatively evaluated recovering tropical soil under different management strategies using microtomography.

Thus, to analyze the physical structure of the soil in a noninvasive manner and acquire a better understanding of the soil recovery process, the following physical parameters were selected to characterize the internal soil structure and quality during recovery: the S Index, soil water retention curve (SWRC), degree of anisotropy (DA), Euler-Poincaré number and Shannon entropy. In addition, this study provides a two-dimensional visualization of the soil and associated parameters and simulates water movement pathways in three dimensions. This approach can be used to visualize the recovery effects of different management strategies at the pore level and analyze the behavior of water in the soil after different treatments.

The S Index (soil physical quality) is obtained from the slope of the SWRC, which represents the relationship between the water content and the soil water potential. Several important physical soil properties can be estimated directly using S Index values (Dexter, 2004). Naderi-Boldaji et al. (2016) investigated the relationship between the S Index and soil compaction based on a single function. Additionally, many studies have used the S Index in some capacity; however, the S Index should not be used alone in studies of soil tropical due to the soil characteristics. In this study, we used Qualisolo software (NAIME et al., 2001), which was also used Arya and Paris (1981) to obtain the SWRC and S Index. This model was validated for Brazilian soil by Vaz et al. (2005). In addition to the SWRC, it provides the permanent wilting point (θ_{pmp}), field capacity (θ_{cc}) and available water capacity (AWC) for different study management groups.

The DA strongly reflected the orientation of the elements inside a determined volume (Odgaard, 1997); thus, it influences the flux characteristics in a porous medium (HERNÁNDEZ ZUBELDIA et al., 2015). Bottinelli et al. (2016) demonstrated the stability of the DA in the formation of macropores during shrinkage in rice-cultivated soils.

The Euler-Poincaré number is a fundamental parameter that describes the connectivity of spatial structures (VOGEL, 1997; VOGEl and ROTH, 2001). Recently, Martínez et al. (2015) used this parameter to study the geometry of aggregate soil; they concluded that this metric is capable of clearly reflecting the pattern of aggregates associated with different types of management. Additionally, Katuwal et al. (2015) used a case study to show that the parameter is inadequate when isolated connections are predominant.

The next selected physical parameter is Shannon entropy (2001), although this parameter is seldom included in soil analyses. Nevertheless, Gaur and Mohanty (2013) showed that Shannon entropy can be applied to understand the dominant physical control of spatiotemporal variability in soil moisture.

The application of the percolation theory in porous media involves the inclusion of random properties (BERKOWITZ and EWING, 1998). For example, a study of the fingering phenomenon used a modified invasion percolation model (ONODY et al., 1995). This study used an open source program published by Nakashima and Kamiya (2007) to simulate the transport properties inside the pores through three-dimensional microtomography, thereby providing a visualization of water pathways in the soil under dry conditions. Such studies are important in evaluating management strategies and soil quality under various conditions.

The objective of this study is to apply nonconventional methods to evaluate the physical soil structures of two groups of tropical soil in different recovery states and to simulate the

diffusion process of non-sorbing species (e.g., H_2O) in the pores to predict the water pathways in the soil.

2. Material and Methods

2.1. Experimental Sites

The soil samples were obtained at Fazenda de Ensino e Pesquisa da Universidade Estadual Paulista "Júlio de Mesquita Filho" (Unesp) (Teaching and Research Farm of Paulista State University “Júlio de Mesquita Filho”) at Ilha Solteira campus in the city of Selvíria (Mato Grosso do Sul State - Brazil). This area is located on the banks of the Paraná River (22° 22’ S and 51° 22’ W). Due to the construction of the hydroelectric power station at Ilha Solteira (São Paulo State) in 1969, subsoil containing the B horizon has remained exposed and exhibited severe superficial compaction and a low presence of vegetation. The soil in the experimental area is a dystrophic Red Latosol characterized by advanced stages of weathering (Embrapa Solos, 2013).

2.2. Management Description

The experiment implemented in this study included six management strategies, and they were divided into two groups according to their granulometric proximity. Group I include 1) Soil from the native forest (**NF**) (Brazilian Savannah); 2) Recuperated soil (**RS**) (green manure applied to soil over seven years from 1992 to 1999. Afterward, soil was cultivated with *Brachiaria decumbens*); 3) Recuperating soil with *Astronium fraxinifolium* (Gonçalo-alves) + *Brachiaria decumbens* + sewage sludge (**G**); and 4) Degraded soil (**D**) (remaining soil from the construction of the hydroelectric power plant). Group II includes 5) Recuperating pasture soil (**RP**) and 6) Degraded pasture soil (**DP**). All samples were collected from the superficial layer (0-10 cm).

2.3. Physical analysis

In this study, the sampling analysis was based on microtomography instead of a field sampling campaign.

2.3.1 X-ray microtomography and image reconstruction

The commercial, high-resolution X-ray microtomograph and NRCon software from Embrapa Instrumentation were used to acquire and reconstruct tomographic images,

respectively. The spatial resolution of images was 4.96 µm, and the reconstruction parameters were adjusted according to Vaz et al. (2011).

To perform the statistical calculations, 500 images of 1000 x 1000 pixels were appropriately treated for each management type. Initially, the images were binarized using the Otsu method (1975), which minimizes the sum of variances between image classes and the background. Second, CT-Analyser software was used to calculate the Euler-Poncaré number and the DA because both parameters are three-dimensional and do not have units. In addition, the same images were used in three-dimensional simulations. Except for the Shannon entropy, only one representative image was selected for each management type using the 'entropy' package in R (HAUSSER et al., 2012), a free software environment for statistical computing and graphics. This software was employed in this study due to the considerable amount of information contained in each image.

2.3.2 SWRC and the S index

The soil analysis in the laboratory was performed using three replicates of 40 grams for each management type, and samples were processed using an automatic particle size analyzer and Qualisolo software (NAIME et al., 2004). The SWRC and S index were estimated for each management type, and this software was previously validated for use in analyses of Brazilian soils (ANDRADE and STONE, 2009, VAZ et al., 2005). These variables were calculated in two steps, as described below. The average of three replicates for each management type was obtained from the results of these steps.

First, the SWRC (VAZ et al., 2005) was produced from the granulometry data provided by the particle size analyzer and the Arya and Paris model (1981). The model equation is described as follows:

$$\Psi_i = \frac{2\sigma}{\rho_w g R_i \sqrt{\frac{2\rho_p - \rho_s}{3\rho_s}\left(\frac{3w_i}{4\pi R_i^3 \rho_p}\right)^{1-\alpha}}} \quad (1)$$

where Ψ_i is soil matric potential, which is adjusted based on the inverse form of the van Genuchten equation (1980); α is scaling factor; ρ_w is the water density (kg m^{-3}); g is the acceleration of gravity ($m.s^{-2}$); R_i is the particle radius; ρ_p is the soil particle density (kg m^{-3}); ρ_s is the soil bulk density (kg m^{-3}); and w_i is the soil mass of the i^{th} fraction, which is calculated via fitting a sigmoidal model to cumulative particle size distribution data.

The same SWRC adjusted based on the van Genuchten equation (1980) was used to obtain the S index (DEXTER, 2004). The S index corresponds to the angular coefficient or slope of the tangent at the inflection point of the SWRC, as expressed by equation (2):

$$S = -n\,(\theta_s - \theta_r)\left[1 + \frac{1}{m}\right]^{-(1+m)} \qquad (2)$$

where S is the slope of the SWRC at its inflection point; n and m (1-1/n) are empirical parameters in the van Genuchten equation (1980); and θ_s and θ_r are the saturated and residual soil water contents (kg kg^{-1}), respectively. The S index reference values are shown in Table 1.

Table 1. S Index reference interval for root growth

S Index interval	≤ 0.020	>0.020 and = 0.035	> 0.035
Physical quality	Very poor	Poor	Good

Source: Dexter (2004)

2.3.3 Degree of Anisotropy

The mean intercept length (MIL) is a variable used to indicate how directionally dependent the pores are based on the eigenvalues used to calculate the DA. A series of vectors (w) originate from the center of the volume and are then divided by the number of times they intercept the porous or solid parts of the volume. To obtain the DA in 3D, the MIL distribution is described using an ellipsoid structure according to three axes in tensor form (HARRIGAN and MANN, 1984) (Figure 1).

Each tensor is derived from the DA and is a function of the eigenvalues. The expression of the DA calculated using the CT-Analyzer is given in equation (3):

$$\mathrm{DA} = \left(1 - \left[\frac{\mathrm{Min.eigenvalous}}{\mathrm{Max.eigenvalous}}\right]\right) \qquad (3)$$

where a value of 1 is considered completely anisotropic and 0 is isotropic (SKYSCAN, 2015).

Figure 1. An ellipsoid is statistically inserted in the 3D distribution of the MIL with the three orthogonal vectors between them, forming a tensor of 9 eigenvectors

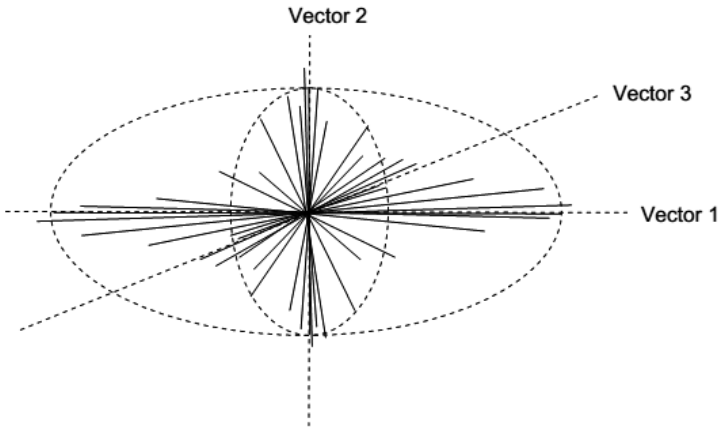

Source: Adapted from Skyscan (2015).

2.3.4 Euler-Poincaré Number

The Euler-Poincaré number (χ (X)) is a connectivity indicator of the structure in three dimensions. This metric is used to characterize the connections in a structure before it is separated into two parts. The basic topological properties of the Euler-Poincaré number of a 3D object X include the number of objects (pores) (β_0), the connectivity (β_1), and the number of enclosed cavities (β_2). Therefore, the 3D components used in the CT-Analyzer software are as follows (VOGEL, 2002; KATUWAL et al., 2015 and SKYSCAN, 2015):

$$\chi(X) = \beta_0 - \beta_1 + \beta_2. \quad (4)$$

According to Rozenbaum et al. (2012), the higher the Euler-Poincaré number is, the lower the connectivity; $\beta_0 > \beta_1$ in these cases. In the case of a negative value ($\beta_0 < \beta_1$), the connectivity of the porous structure will be higher than that of a positive value. Notably, β_2 value is not important for a network of natural pores because it is rare to find solid particles completely surrounded by porous spaces (VOGEL, 2002).

2.3.5 Shannon Entropy

To calculate the Shannon entropy, one image was preselected from the middle of each sample. Each image consisted of 1000 x 1000 pixels. Then, the expected value of information is determined based on each image (WU et al., 2013). This approach describes the disorder related to the management of the soil. The definition of entropy is given by Brunsell (2010) (5):

$$H(x) = -\sum_{i=1}^{n} p(x_i)\log(p(x_i)) \quad (5)$$

where p_i is the probability density function of variable x with bin i. The higher the value of H(x) is, the lower the entropy will be, and vice versa, i.e., the entropy reflects the degree of soil management randomness.

Thereby, the maximum likelihood (ML) estimator was used to calculate H(x) for each tomographic image. The ML principle is based on a set of random variables X_n, which is related to the probability distribution $P(x \mid \phi)$, where x is a vector in the sample and ϕ is a spatial parameter. The principle of ML is to select the value of ϕ that maximizes $P(x \mid \phi)$ based on observations. In other words, the ML estimator seeks to find the frequency of each level of grayscale that appears in the image and determine the H(x) value of the Shannon entropy of the system.

2.3.6 Visualization of the soil plane and three-dimensional simulation

This portion of the study was divided into two parts. In the first, the soil plane structure was analyzed using two-dimensional microtomography to visualize and assess each management type, as well as the potential effects on the present of water. DataViewer software, which is developed by Bruker microCT, was used to divide the image into three different planes: transverse (imaginary plane that divides object into superior and inferior parts), coronal (ventral and dorsal parts) and sagittal (right and left parts) planes.

In the second part, 3D pathways of water movement in the soil were simulated using Mathematica 5.2. This portion of the analysis consisted of three parts (Nakashima and Kamiya, 2012): 1) Itrimmin.nb - selects and segments the region of interest (ROI) of the tomography; 2) Clabel.nb – classifies the porous area of the image, which is essential for investigating the random movement (walk) of fluid molecules through the pores; and 3) Rwalk.nb - simulates the random diffusion of non-sorbing elements within the pores in three dimensions. The main output of Rwalk.nb is the mean square displacement, $<r^2>$, which is based on dimensionless integer time, τ, as demonstrated in equation (6), as well as plots of the displacement of the walkers along three axes in Cartesian coordinates (NAKASHIMA and KAMIYA, 2007):

$$< r(\tau)^2 > = \frac{1}{n} \sum_{i=1}^{n} [(x_i(\tau) - x_i(0))^2 + (y_i(\tau) - y_i(0))^2 + (z_i(\tau) - zx_i(0))^2]. \quad (6)$$

3. Results and Discussion

3.1 S Index and SWRC

The S index is considered an indicator of the quality of the soil structure; thus, the physical stage of soil degradation can be easily determined based on this index. However, the index should be carefully applied to tropical soils because the indicator was developed for soils in temperate climates (CARDUCCI et al., 2016 and DEXTER, 2004). To minimize potential interpretation errors, other physical and structural parameters should be used for each management strategy.

Group I (Table 2): NF exhibited the best S index value and represents a standard sample of natural soil conditions. In the laboratory, NF exhibited higher total porosity and lower soil bulk density compared to other management types; therefore, NF soil is of good physical quality. The S Index of RS is closest to that of NF among all samples; although, RS was not associated with good physical quality according to the reference values (Table 1). However, the results suggest that the effects of the recuperation process have been positive. The S Index of G is between those of RS and D; therefore, although G exhibited improvements in total porosity and soil bulk density, this management type is still similar to D, which is poor in terms of physical quality.

NF and RS exhibited similar SWRCs (Figure 2a). Thus, the RS structural quality was similar to that of natural conditions and positive from the perspective of land use. Moreover, management G was almost identical to D due to compaction characteristics; however, G is more likely to display long-term improvement.

Group II (Table 3): The soil quality of RP and DP remained poor; however, that of RP was slightly better than that of DP. Notably, the recovery techniques applied in the area had a positive effect on the quality, which should improve over time.

Likewise, the SWRC differences between NF and RP and DP (Figure 2b) suggest that the structural quality of NF is much better than that of RP and DP. These soil types are extremely compacted because of poor management in pasture areas.

Figure 2. SWRC the 0-10 cm layer. The inflection point and slop represent physically good or poor soil. The degradation sequence for the group I **(a)** is NF, RS, G and D, which are correspondents to their reality in field. Group II **(b)** sequence is NF, RP and DP, also are correspondents to the real situation.

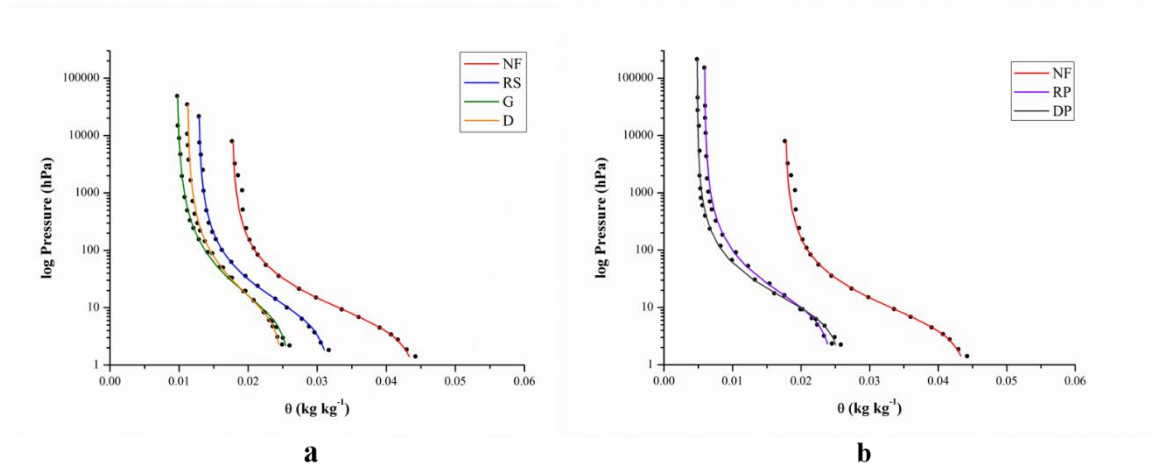

Source: Author (2015)

Table 2. S index for group I management types.

Types of management	Soil from Native Forest (NF)	Recuperated Soil (RS)	Recuperating Soil (G)	Degraded Soil (D)
S index	0.036	0.024	0.019	0.017
Bulk density (g cm^{-3})	1.23	1.45	1.58	1.61
Total porosity (%)	55.35	47.28	42.16	41.68

Source: Author (2015)

Table 3. S index for group II management types.

Types of management	Soil from Native Forest (NF)	Recuperating Pasture Soil (RP)	Degraded Pasture Soil (DP)
S index	0.036	0.024	0.029
Bulk density (g cm^{-3})	1.23	1.61	1.56
Total porosity (%)	55.35	39.56	41.72

Source: Author (2015)

3.2 Degree of Anisotropy

The DA indicates similar spatial characteristics in all four directions in the image. In other words, this physical parameter influences the flux behavior in the saturated soil (Hernández Zubeldia, 2015). The DA of a porous structure is associated with the anisotropic behavior of diffusion transport properties. When the value of DA is close to 1, the medium is fully anisotropic. When the value is 0, the medium is isotropic.

Group I (Figure 3a): The DA values of D and G are high, suggesting that they are more anisotropic than NF and RS. This result corresponds to observations in the field. Notably, RS and NF exhibit similar physical qualities, which lead to high quantities of water at the microscopic scale. Management G is highly compacted; therefore, its residual and saturated soil water contents (θ_r and θ_s) (Table 4) are low and degradation characteristics are similar to those of D. Due to presence of vegetation, large volumes of residual water can be stored in NF and RS. (Table 4).

Group II (Figure 3b): DP soil exhibits a lower DA value than RP and NF, i.e., it is more isotropic. However, its residual and saturated water contents (Table 5) are similar to those of RP. This similarity is related to the soil structure and arrangement. Notably, the small pores do not form a continuous network in this management type (Table 5).

Figure 3. Degree of anisotropy (DA). a) Group I - G and D are more anisotropic than NF and SR; b) Group II – RP is considerable close to NF, it is a positive signal about structure recovery process. DP still demonstrates difficulty on the flux transport.

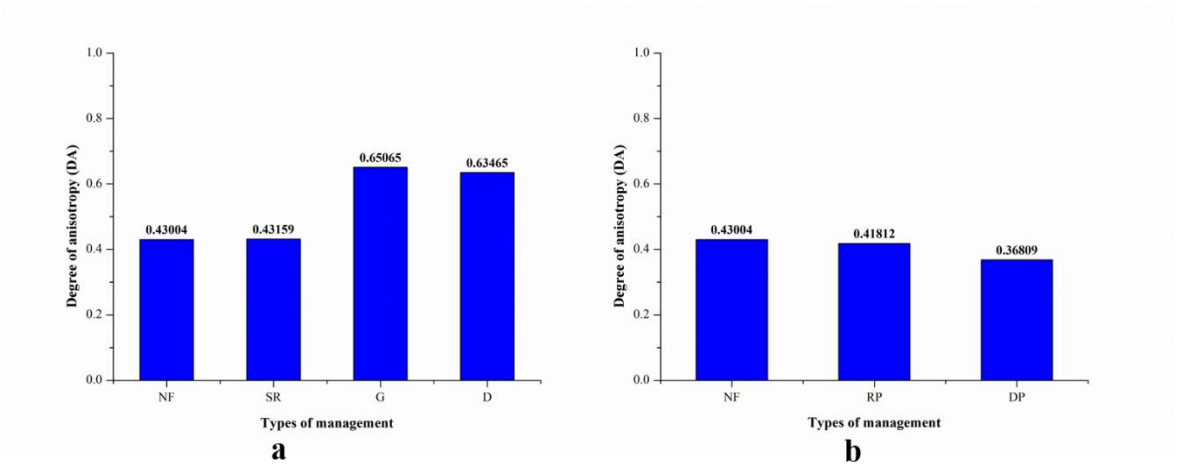

Source: Author (2016)

Table 4. Residual and saturated wetness (θ_r and θ_s) of group I

Type of management	Soil from Native Forest (NF)	Recuperated Soil (RS)	Recuperating Soil (G)	Degraded Soil (D)
θ_r	0.18	0.13	0.01	0.11
θ_s	0.45	0.32	0.27	0.25

Source: Author (2015)

Table 5. Residual and saturated wetness (θ_r and θ_s) of group II

Type of management	Soil from Native Forest (NF)	Recuperating Pasture Soil (RP)	Degraded Pasture Soil (DP)
θ_r	0.18	0.06	0.05
θ_s	0.45	0.25	0.26

Source: Author (2015)

3.3 Euler-Poincaré Number

The degree of soil compaction is inversely proportional to the Euler-Poincaré number. In other words, this parameter indicates the effect of the management strategy in terms of the level of connectivity.

Group I (Figure 4a): The results indicate that the solid structures of G and D are highly connected in comparison to those of NF and RS. This result is due to the effect of compaction. The NF and RS soils exhibit positive Euler-Poincaré numbers, i.e., they are more structured. . Conversely, G and D soil exhibit negative Euler-Poncaré numbers, which reflect a high number of non-continuous connections. The high connectivity in groups G and D is due to the effect of intensive manipulation in the area. Consequently, dense micropores exist in areas of large and continuous pores, as indicated by the results of porosity analysis.

Group II (Figure 4b): The DP soil is the poorest in terms of connectivity in comparison to NF. The DP group has a positive Euler-Poincaré number, which suggests that the pores are largely connected. The RP group has a negative Euler-Poincaré number, which suggests that the pores are characterized by some non-continuous areas; therefore, fluids can move through the pores in this group with little effort.

Figure 4. Euler-Poincaré number indicates solid structure connectivity, the positive value represents connected porous and the negative one means non-continuous structure. a) Group I connection hierarchy: RS (Soil recuperated); NF (Soil from native forest); D (Degraded soil) and G (Soil in recuperating). b) Group II connection hierarchy: DP (Degraded pasture) NF (Soil from native forest) and RP (Recuperating pasture).

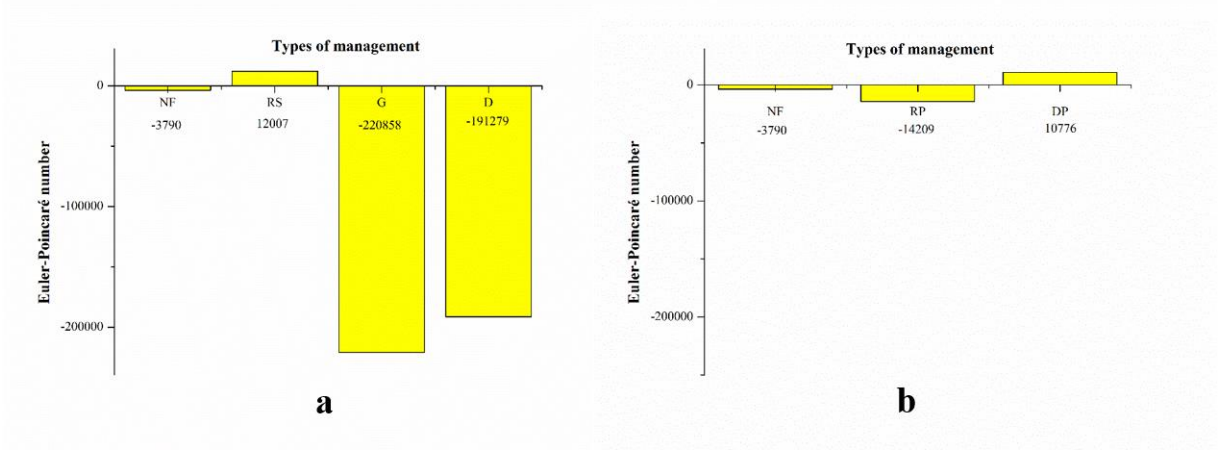

Source: Author (2016)

3.4 Shannon Entropy

Shannon entropy H(x) quantifies uncertainty or disorder. Thus, this metric can be used to characterize each management type. The empirical frequency of the grayscale level can reflect the relationship between porous and solid parts of a medium. Based on the frequency level, H(x) of the system can be obtained.

Group I (Figure 5a): The hierarchy of this group differs from that of other groups. D and RS were characterized by high values of entropy, i.e., low randomness compared to NF and G. This result is related to aggregate stability, which affects the system sensitivity in relation to the external environment; however, these relationships must be investigated in detail.

Group II (Figure 5b): NF exhibited the highest entropy compared to those of RP and DP. Thus, the NF system is more stable than other management types in this group.

Figure 5. Entropy caculated by estimador Maximum Likelihood (ML), where the higher the entropy, the lower is its randomness. a) Group I: NF (Soil from native forest); RS (Soil recuperated); G (Soil in recuperating) and D (Degraded soil); b) Group II: RP (Recuperating pasture) and DP (Degraded pasture).

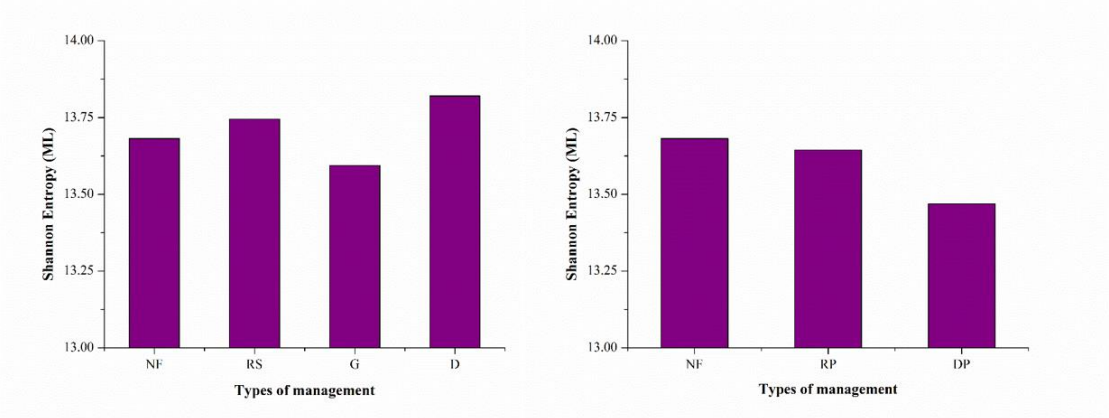

Source: Author (2016)

3.5. Soil Structure Visualization

Based on 500 tomographic images, a series of important management information was extracted along transverse, coronal and sagittal planes. In the transverse plane (Figure 6), NF (Figure 6a) was characterized by its heterogeneity, i.e., diverse distributions of aggregate and pore sizes, and RS (Figure 6b) exhibit similar characteristics. G (Figure 6c) was similar to degraded soil D (Figure 6d), and D was mainly homogenous, which is typical of high compaction. In RP (Figure 6e), the initial stages of recuperation are similar to those of NF, and DP (Figure 6f) is characterized by an agglomeration of aggregates typical of degraded soil D.

The coronal and sagittal planes (Figure 7 and 8) have similar characteristics; thus, they were analyzed together in this case. NF (Figures 7a and 8a) demonstrated a high connectivity between pores, which reflects a high exchange of gases and water. RS (Figures 7b and 8b) exhibited characteristics similar to those of NF; however, in terms of the porous connections and distribution of aggregates sizes, the properties of RS were inferior to those of NF. G (Figures 7c and 8c) and D (Figures 7d and 8d) clearly displayed aggregate compaction because both management types have relatively homogeneous aggregate arrangements. However, based on software analysis, some macropores were likely present. RP (Figures 7e and 8e) exhibited a high content of aggregates, but most aggregates were fragmented, which hampered water retention. Finally, DP (Figures 7f and 8f) exhibited physical characteristic

similar to those of D; however, more fragmented elements were observed in DP due to the remaining roots.

Figure 6. a) **NF** - Soil from native forest (Brazilian Savannah); b) **RS** - Recuperated soil; c) **G** - Recuperating soil still f; d) **D** - Degraded soil; e) **RP** - Recuperating pasture soil; f) **DP** - Degraded pasture soil.

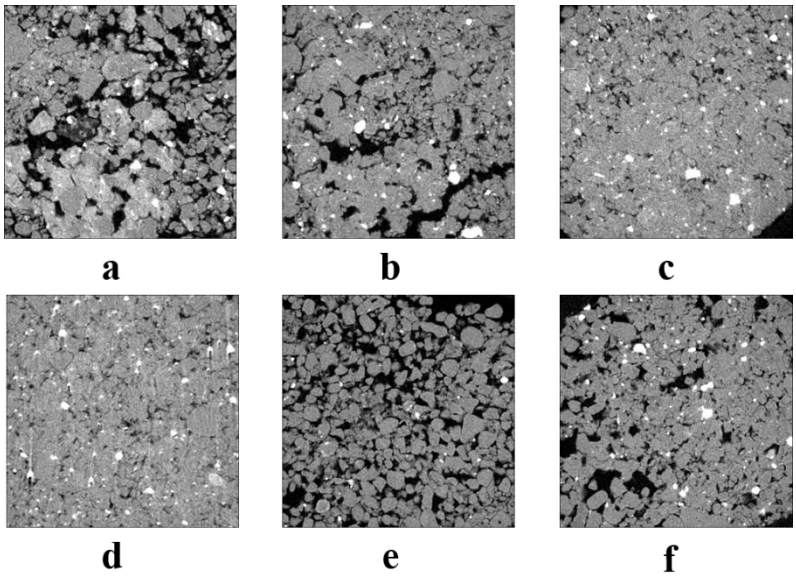

Source: Author (2015)

Figure 7. a) **NF** - Soil from native forest (Brazilian Savannah); b) **RS** - Recuperated soil; c) **G** - Recuperating soil still f; d) **D** - Degraded soil; e) **RP** - Recuperating pasture soil; f) **DP** - Degraded pasture soil.

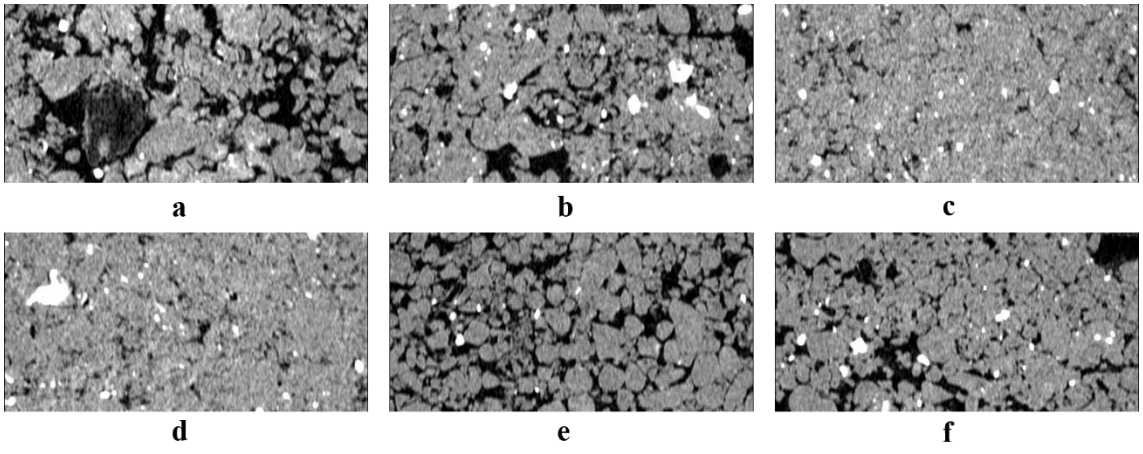

Source: Author (2015)

Figure 8. a) **NF** - Soil from native forest ; b) **RS** - Recuperated soil; c) **G** - Recuperating soil still f; d) **D** - Degraded soil; e) **RP** - Recuperating pasture soil; f) **DP** - Degraded pasture soil.

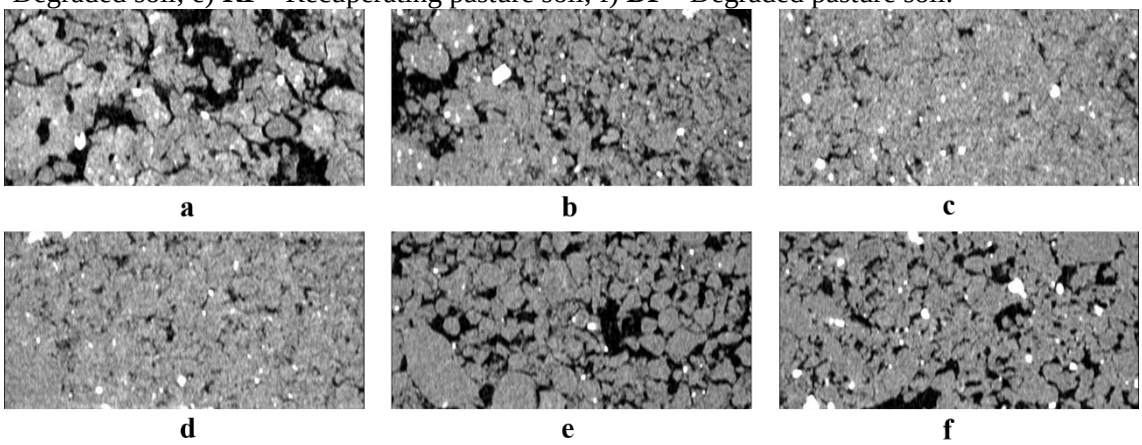

Source: Author (2015)

3.6 Water Movement Pathways in Three-Dimensional Simulations

The SWRCs were obtained using the Arya and Paris model and adjusted Van Genuchten (1980) equation (Table 6 and 7). In addition, the tomographic images were processed based on three different planes, the results were used in a 3D random walk model to simulate percolation in porous soil.

Group 1 (Figure 9)**:** Out of all the managed soils, the NF soil exhibited the highest total porosity. This result is an indication of the excellent drainage conditions and water storage in the soil. However, this soil does not have high connectivity, as indicated by the Euler-Poincaré number; therefore, it is a generally isotropic soil. The water paths through the pores are narrower and shorter than those of other soils (Figure 9a), and the available water capacity is small (Table 6).

The total porosity of RS soil is similar to that of NF, as are its drainage quality and available water capacity. However, based on the positive Euler-Poincaré, the connectivity of RS is much lower than that of NF and other types of managed soils. Although the DA of RS is close to that of NF, the percolation path is simplified by the pores (Figure 9b), thereby providing a higher water retention capacity than NF (Table 6).

According to the porosity results obtained by microtomography, the G soil exhibited the presence of remaining roots; therefore, these pores play a fundamental role in water drainage, although most pores are similar to those in degraded soil. The Euler-Poincaré number suggests the soil is characterized by high structural connectivity; consequently, the pore structure is likely anisotropic, reflecting the random nature of the pore percolation network

(Figure 9c). In addition, a large quantity of soil water is associated with this type of management (Table 6).

The high compaction of D is a direct reflection of its total porosity. However, D has a geometric structure and elevated connectivity between pores, which creates a high DA. The pore percolation network is a simple, long, and connected pathway due to its compact nature (Figure 9d); therefore, the D soil has a high water retention capacity (Table 6).

Table 6. Information about water in soil - Group I

Sample Type	NF	RS	G	D
θ_{pmp} (cm^3/ cm^3) %	22	19	16	19
θ_{cc} (cm^3/ cm^3) %	26	24	22	24
AWC (cm^3/ cm^3) %	4	5	6	5

θ_{pmp}: Permanent wilting point; θ_{cc}: Field Capacity; AWC:Available water capacity

Source: Author (2016)

Figure 9. Bird's-eye-view projected the trajectory of a single random walk through the percolated pore space with the boundary condition: The total time step is 400,000 with the initial (τ = 0) and final (τ = 400,000) positions. The start and end positions are marked by red and blue circles, respectively. **a)** NF (Soil from native forest); **b)** RS (Recuperated soil); **c)** G (Recuperating soil) and **d)** D (Degraded soil).

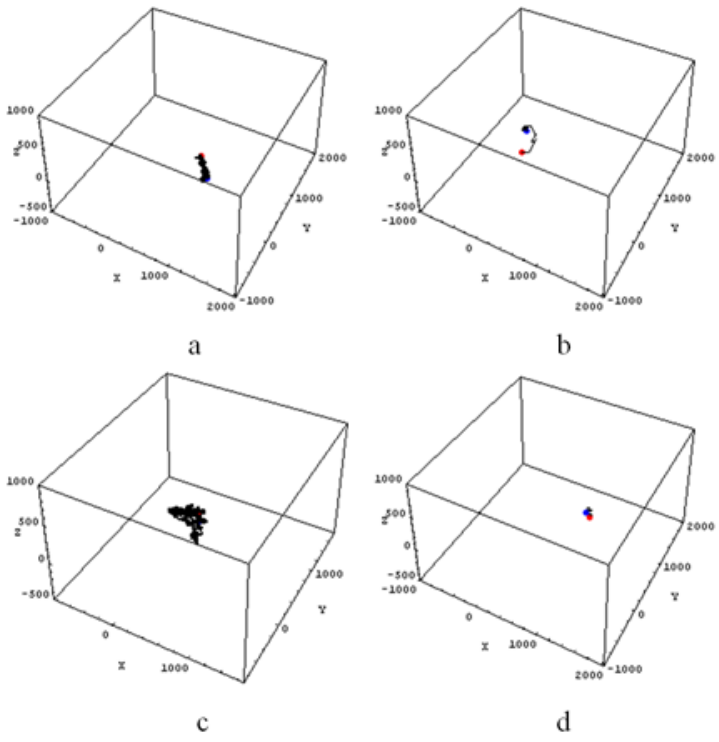

Source: Author (2016)

Group 2 (Figure 10)**:** In general, RP soil shows signs of the beginning of recuperation. It is clear that the negative connectivity of the RP soil is similar to the geometric characteristics of the NF soil. Similarly, the connectivity of the DA soil is similar to that of NF. Consequently, the RP soil displays random properties similar to those of NF along the three axes in the simulation (Figure 10a). However, RP soil has the capacity to deliver more water than NF due to its morphometric similarity to DP (Table 7).

The DP soil exhibited clear signs of compaction. Additionally, the Euler-Poincaré number of the soil is positive; thus, it lacks dense connections. This result corresponds to the high DA value, and the soil has isotropic characteristics, which lead to long and simplified percolation paths that facilitate the passage of water (Figure 10b). Therefore, the soil water availability is high (Table 7).

Table 7. Information about water in soil - Group II

Sample Type	NF	RP	DP
θ_{pmp} (cm^3/ cm^3) %	22	10	8
θ_{cc} (cm^3/ cm^3) %	26	16	13
AWC (cm^3/ cm^3) %	4	6	5

θ_{pmp}: Permanent wilting point ; θ_{cc}: Field Capacity; AWC: Available water capacity

Source: Author (2016)

Figure 10. Bird's-eye-view projected trajectory of a single random walk through the percolated pore space - **a)** RP (Recuperating pasture) and **b)** DP (Degraded pasture).

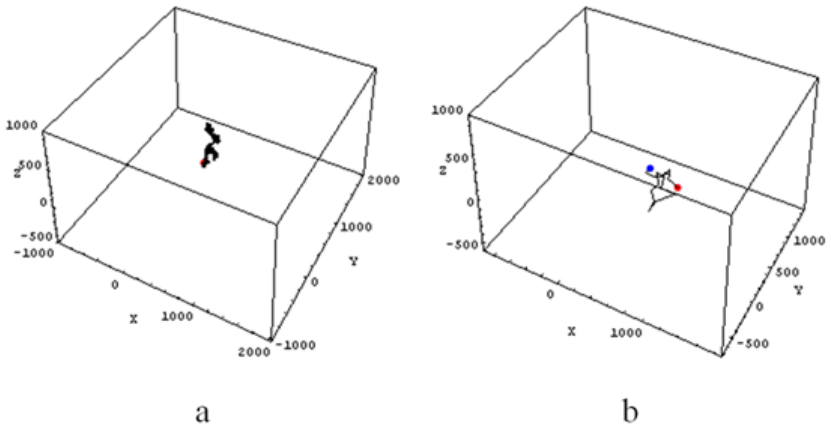

Source: Author (2016)

4. Conclusion

The aim of this study was to use non-conventional methods to evaluate the physical soil structure and simulate water movement pathways in three dimensions through X–ray microtomography. The S Index was used as an indicator to quantify the degree of management. However, to minimize the possible interpretation errors, other physical and structural parameters should be used based on the background of each management area. The Euler-Poincaré number indicates the connectivity of spaces and can be used to determine the percolation paths and DA of each type of management. The DA is an excellent indicator of spatial alignment within an image. The Shannon entropy reflects the management stability based on the relationship with the environment. The Arya and Paris model provided information on the water behavior in each type of managed soil, which was confirmed by the similarity between the physical parameters of this study in different soil planes and 3D simulations of water movement pathways. In conclusion, the physical and structural soil parameters and simulated water movement pathways effectively characterized the soil architecture of each sample. These results suggest the possibility of associating the soil structure with water movement in the soil and can be used to better understand soil-water synergy under different conditions.

5. Acknowledgements

We extend our thanks to CNPq and CAPES for financial support, to USP for its academic formation, to Embrapa, which made possible the use of its laboratories, developed technologies and technical support, and to Unesp for providing samples and technical support.

References

ARYA, L. M.; PARIS, J. F. A Physicoempirical model to predict the soil moisture characteristic from particle-size distribution and bulk density data. **Soil Science Society of America Journal**, v. 45, n. 6, p. 1023-1030, 1981.

BERALDO, J. M. G.; SCANNAVINO JUNIOR, F. A.; CRUVINEL, P. E. Application of x-ray computed tomography in the evaluation of soil porosity in soil management systems. **Engenharia Agrícola**, v. 34, n. 6, p. 1162-1174, 2014.

BERKOWITZ, B.; EWING, R. P. Percolation theory and network modeling applications in soil physics. **Surveys in Geophysics**, v. 19, n. 1, p. 23-72, 1998.

BOTTINELLI, N. et al. Macropores generated during shrinkage in two paddy soils using X-ray micro-computed tomography. **Geoderma**, v. 265, p. 78-86. 2016.

BRUKER. Morphometric parameters measured by Skyscan™ CTanalyser software. [S. l.: s.n.], 2015. Disponível em: <http://bruker-microct.com/next/CTAn03.pdf>. Acesso em: 28 jun. 2016.

BRUNSELL, N. A. A Multiscale information theory approach to assess spatial–temporal variability of daily precipitation. **Journal of Hydrology**, v. 385, n. 1, 165-172, 2010.

CARDUCCI, C. E. et al. Retenção de água do solo sob sistema conservacionista de manejo com diferentes doses de gesso. Revista de Ciências Agrárias, v. 58, n. 3, p. 284-291, 2016.

CRESTANA, S.; MASCARENHAS, S.; POZZI-MUCELLI, R. S. Static and dynamic three-dimensional studies of water in soil using computed tomographic scanning. **Soil Science**, v. 140, n. 5, p. 326-332, 1985.

DEXTER, A. R. Soil physical quality: part I. Theory, effects of soil texture, density, and organic matter, and effects on root growth. **Geoderma**, v. 120, n. 3, 201-214, 2004.

EMPRESA BRASILEIRA DE PESQUISA AGROPECUÁRIA. **Sistema brasileiro de classificação de solos**. 3. ed., Rio de Janeiro: Centro Nacional de Pesquisa de Solos, 2013.

GAUR, N.; MOHANTY, B. P. Evolution of physical controls for soil moisture in humid and subhumid watersheds. **Water Resources Research**, v. 49, n. 3, p. 1244-1258, 2013.

HAINSWORTH, J. M.; AYLMORE, L. A. G. The Use of computer-assisted tomography to determine spatial distribution of soil water content. **Australian Journal of Soil Research**, v. 21, n. 4, p. 435-443, 1983.

HARRIGAN, T. P.; MANN, R. W. Characterization of microstructural anisotropy in orthotropic materials using a second rank tensor. **Journal of Materials Science**, v. 19, n. 3, p. 761-767, 1984.

HAUSSER, J.; STRIMMER, K.; STRIMMER, M. K. **Package 'entropy'**. [S. l.: s.n.], 2012.

HERNÁNDEZ ZUBELDIA, E. et al. Cellular automata and X-ray microcomputed tomography images for generating artificial porous media. **International Journal of Geomechanics**, v. 16, n. 2, 2015.

JONGE, L. W. de; MOLDRUP, P.; SCHJØNNING, P. Soil infrastructure, interfaces & translocation processes in inner space ("soil-it-is"): towards a road map for the constraints and crossroads of soil architecture and biophysical processes. **Hydrology and Earth System Sciences**, v. 13, n. 8, p. 1485-1502, 2009.

KATUWAL, S. et al. Linking air and water transport in intact soils to macropore characteristics inferred from X-ray computed tomography. **Geoderma**, v. 237, p. 9-20, 2015.

MARCHINI, D. C. Matéria orgânica, infiltração e imagens tomográficas de Latossolo em recuperação sob diferentes tipos de manejo. **Revista Brasileira de Engenharia Agrícola e Ambiental**, v. 19, p. 574-580, 2015.

MARTÍNEZ, F. S. J. et al. Soil aggregate geometry: measurements and morphology. **Geoderma**, v. 237, 36-48. 2015.

NADERI-BOLDAJI, M.; KELLER, T. Degree of soil compaction is highly correlated with the soil physical quality index S. **Soil and Tillage Research**, v. 159, p. 41-46, 2016.

NAIME, J. D. M.; SHINYA, V.; VAZ, C. **Programa para estimativa indireta da curva de retenção da água no solo**. São Carlos, Embrapa Instrumentação Agropecuária: 2004. (Comunicado Técnico 60).

NAIME, J. M.; VAZ, C. M. P.; MACEDO, A. Automated soil particle size analyzer based on gamma-ray attenuation. **Computers and Electronics in Agriculture**, v. 31,n. 3, p. 295-304, 2001.

NAKASHIMA, Y.; KAMIYA, S. Mathematica programs for the analysis of three-dimensional pore connectivity and anisotropic tortuosity of porous rocks using X-ray computed tomography image data. **Journal of Nuclear Science and Technology**, v. 44, n. 9, p. 1233-1247, 2007.

NAKASHIMA, Y.; NAKANO, T. Steady-state local diffusive fluxes in porous geo-materials obtained by pore-scale simulations. **Transport in Porous Media**, v. 93, n. 3, p. 657-673, 2012.

ODGAARD, A. Three-dimensional methods for quantification of cancellous bone architecture. **Bone**, v. 20, n. 4, p. 315-328, 1997.

ONODY, R. N.; CRESTANA, S. Experimental studies of the fingering phenomena in two dimensions and simulation using a modified invasion percolation model. **Journal of Applied Physics**, v. 78, p. 2970-2976, 1995.

OTSU, N. A Threshold selection method from gray-level histograms. **Automatica**, v. 11, n. 285-296, p. 23-27, 1975.

PASSONI, S. et al. Software Image J to study soil pore distribution**. Ciência e Agrotecnologia**, v. 38, n. 2, p. 122-128, 2014.

PETROVIC, A. M.; SIEBERT, J. E.; RIEKE, P. E. Soil bulk density analysis in three dimensions by computed tomographic scanning. **Soil Science Society of America Journal**, v. 46, n. 3, p. 445-450, 1982.

ROZENBAUM, O.; BRUAND, A.; LE TRONG, E. Soil porosity resulting from the assemblage of silt grains with a clay phase: new perspectives related to utilization of X-ray synchrotron computed microtomography. **Comptes Rendus Geoscience**, v. 344, n. 10, p. 516-525, 2012.

SHANNON, C. E. A Mathematical theory of communication. **ACM SIGMOBILE Mobile Computing and Communications Review**, v. 5, n. 1, p. 3-55, 2001.

VAN GENUCHTEN, M. T. A Closed-form equation for predicting the hydraulic conductivity of unsaturated soils. **Soil Science Society of America Journal**, v. 44, n. 5, p. 892-898, 1980.

VAZ, C. M. P. et al. Evaluation of an advanced benchtop micro-computed tomography system for quantifying porosities and pore-size distributions of two Brazilian Oxisols. **Soil Science Society of America Journal**, 75, 832-841, 2011.

VAZ, C. M. P. et al. Validation of the Arya and Paris water retention model for Brazilian soils. **Soil Science Society of America Journal**, v. 69, n. 3, p. 577-583, 2005.

VOGEL, H. J. Morphological determination of pore connectivity as a function of pore size using serial sections. **European Journal of Soil Science**, v. 48, n. 3, p. 365-377, 1997.

VOGEL, H. J.; ROTH, K. Quantitative morphology and network representation of soil pore structure. **Advances in Water Resources**, v. 24, n. 3, p. 233-242, 2001.

VOGEL, H.-J. Topological characterization of porous media. In: MECKE, K; STOYAN, D. **Morphology of condensed matter:** physics and geometry of spatially complex systems. Springer: Berlin Heidelberg, 2002. p. 75-92.

WU, Y. et al. Local Shannon entropy measure with statistical tests for image randomness. **Information Sciences**, v. 222, p. 323-342, 2013.

CHAPTER V

The application of multifractal analysis in microtomography for evaluating recovery techniques at a Brazilian oxisol

TSENG, C. L., POSADAS, A. N. D., CRESTANA, S.

THE APPLICATION OF MULTIFRACTAL ANALYSIS IN MICROTOMOGRAPHY FOR EVALUATING RECOVERY TECHNIQUES AT A BRAZILIAN OXISOL

Tseng, C. L.[a]*, Posadas, A. N. D.[b] and Crestana, S.[c]

[a]University of São Paulo, "São Carlos School of Engineering " 400 Avenida Trabalhador São-carlense, CEP: 13566-590 São Carlos, São Paulo, Brazil.

bInternational Potato Centerniversidade Estadual Paulista, "Avenida La Molina 1895, La Molina, Apartado Postal 1558, Lima, Peru

[c]Embrapa Instrumentation, 1452, Rua XV de Novembro, CEP: 13560-970, São Carlos, São Paulo, Brazil.

ABSTRACT

The soil in the environment is an open and complex system, which is the basis of food production and support to life. Current management and use of this resource are in critical condition for a sustainable development. Thereby, besides the development of recovery technique, it is fundamental the presence of the evaluation methods that are nonconventional and minimally invasive. The aim of this work is to apply multifractal analysis to high-resolution tomography of a soil which was submitted to six different management in three layers. The analysis showed an excellent tool to distinguish the managements and the effect of recovery technique adopted. The recovery reached up to layer 0-10 cm according to Marchini (2015), which were used conventional evaluation technique.

Keywords: Multifractal analysis, x-ray microtomography, entropy, degree of multifractality, degree of asimetry.

1. Introduction

The soil is an open and complex system starting from the molecular interaction level up to natural phenomenon at global scale (JENNY, 1994, HEUVELINK and WEBSTER, 2001 AND PACHEPSKY AND HILL, 2017). However, the current state of this resource in the world is at risk and worsening (FAO, 2015). Consequently, it puts some stress in the food production and food security. Among the solutions highlighted by The Intergovernmental Technical Panel on Soils (ITPS) is to minimize the soil degradation and recover those which are degraded (FAO, 2015).

For this, it is necessary to have a technique that is able to describe the soil porous structure and distinguish the adopted management in a minimally invasive way, such as the application of multifractal model to x-ray microtomography. The multifractal model concept (MANDELBROT, 1982) is derived from the system fractal geometry through scaling, i.e. the relation between a certain box size and the number of object contained it (Power law with D as its exponent, the D means fractal dimension) . The multifractal analysis allows to detect internal variation of system by solving a local density through a multifractal form (HALSEY et al., 1986; CHHABRA et al., 1989; CHHABRA and JENSEN, 1989); The high-resolution x-ray microtomography (μCT) is an excelente tool to observe soil internal structure non-conventionaly, which is widely used today in soil research (TAINA et al., 2008; PIRES et al., 2010; CNUDDE and BOONE, 2013).

The application of multifractal model to characterize and describe heterogeneous porous media, is a very active research area, even in different subject. According to Perfect and Kay (1995), there are three categories of application in the soil Science: i) physical properties description; ii) modelling of physical process in the soil; iii) quantification of soil spatial variability.

It is highlighted some important works in the categories i) and ii) in the last decade: Posadas et al. (2003) characterized internal structure of three soil groups through spectrum shape and symmetry; Miranda et al. (2006) determined particles distribution of a saprolite material; Posadas et al. (2009) quantified water fingering phenomenon in soil by magnetic resonance image (MRI), identified preferential flow in the soil; Paz Ferreiro et al. (2010) used multifractal analysis to quantify acquired porosity from the mercury injection and nitrogen adsorption.

With technological advances and populazation of X-ray microtomograph in the past years, the application of multifractal method to high-resolution images for a further investigation of

physical interactions that occur within the soil was made possible. It is highlighted some works such as Martínez et al. (2010), which tested the method to investigate macroporosity using a set of tomography images. Torre et al. (2016) studied structure complexity of an arable sandy loam, applying multifractal analysis to original gray image and compared the 2D and 3D result; Wang et al. (2016) used microtomography to analyze porous distribution of a reconstructed soil during an ecological restoration of an open-cast coal-mine.

Therefore, through multifractal spectrum, it is possible to characterize soil heterogeneity, as mentioned above. None the less, there are other interesting informations that can also be extracted from the spectrum, such as the system entropy, degree of multifractality and degree of asymmetry; these are important parameters to be explored. The entropy calculated in this study provides global (average) information of the system (VOSS, 1988); the degree of multifractality and asymmetry (POSADAS et al., 2005; SZCZEPANIAL and MACEK, 2008, HU and WANG, 2009) were used to evaluate results from the recovery techniques applied in the management (MARCHINI et al., 2015).

The aim of this study is to evaluate the recovery techniques applied in the degraded soil (MARCHINI et al., 2015), by using mutifractal analysis in high-resolution tomography, providing the multifractal espectrum, system entropy and degree of multifractality and asymmetry for each management in two different plane and three depth.

2. Material and method

2.1 Study area

The soil samples used in this study were collected in Selvíria city (Mato Grosso do Sul State) – Brazil, located at right bank of Paraná river (22° 22' S e 51° 22' W). The region's climate is Aw as reported by Köppen, the annual rainfall average is 1370mm. The average temperature is 23.5ºC, 75% is the relative humidity of the air. The soil is a distrophic red latossol, its class textural is a sandy clay loam and, characterized by advanced stages of weathering (EMBRAPA, 2006), the native vegetation is Cerrado .

The implantation of hydroelectric plant of Ilha Solteira (São Paulo State - Brazil) in the 1960s, it was removed 8.6m of soil layer for the construction; since then the soil has been exposed. The area recovery experiment started in 1992: The preparation of the area was conducted with subsoiling at 40cm depth and then plowing and harrowing.

The studied managements were: 1) Soil from native forest of Cerrado (NF); 2) Recuperated soil (RS); 3) Soil in recuperation with *Astronium fraxinifolium* (Gonçalo-alves) +

Brachiaria decumbens + sludge (G); 4) Degraded soil (D); 5) Recuperating pasture (RP) and 6) Degraded pasture (DP). For the soil multifractal analysis were collected non-deformed samples using acrylic tube of 8mm x 15mm (internal diameter x height) in three depths: 0-10; 10-20; 20-30cm.

2.2 Tomographic images

The non-deformed soil were scanned using X-ray microtomography, model 1172 – Skyscan (Bruker), then, it was acquired 1000 tomographic projections with 4.96 μm of spatial resolution. After that, it was used NRcon software to reconstruct the microtomographic and 500 images were selected from the central part of the sample; all the adopted parameters for image acquisition and reconstruction were adjusted according to Vaz et al. (2011). Once the microtomographics were obtained, again 5 images were selected from the axial plane (XY) and coronal plane (XZ) by using software Data-Viewer. In order to make the image pretreatment, using ImageJ software to binarize images (OTSU, 1975) and finally, the images were saved in a number table (txt.) pixel by pixel.

Figure 1 - Soil microtomographic at 0-10cm depth, axial plane, 1000 x 1000 pixel, 8 bits: (1) Soil from native forest of Cerrado (NF); (2) Recuperated soil (RS); (3) Soil in recuperation with *Astronium fraxinifolium* (Gonçalo-alves) + *Brachiaria decumbens* + sludge (G); (4) Degraded soil (D); (5) Recuperating pasture (RP) and (6) Degraded pasture (DP).

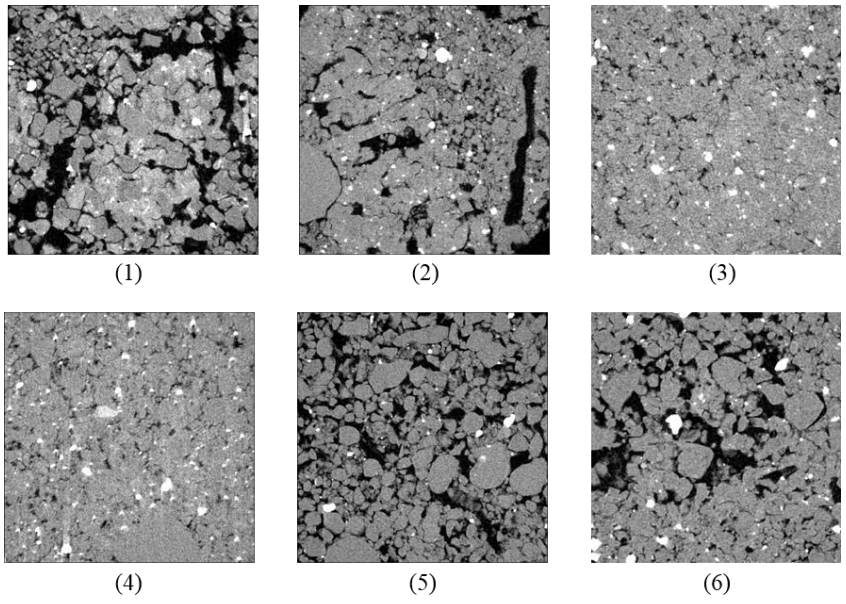

Source: Author (2015).

Figure 2 - Soil microtomographic at 0-10cm depth, coronal plane, 1000 x 1000 pixel, 8 bits: (1) Soil from native forest of Cerrado (NF); (2) Recuperated soil (RS); (3) Soil in recuperation with *Astronium fraxinifolium* (Gonçalo-alves) + *Brachiaria decumbens* + sludge (G); (4) Degraded soil (D); (5) Recuperating pasture (RP) and (6) Degraded pasture (DP).

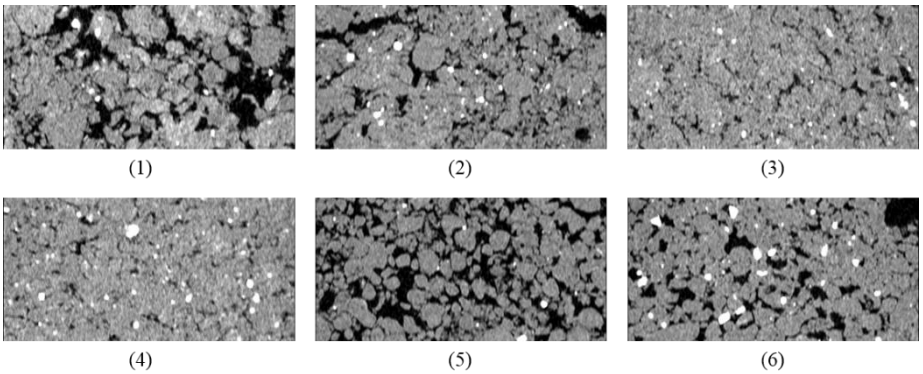

Source: Author (2015).

2.3 Multifractal technique

2.3.1 Theoretical basis

The fundamental equation that describes the fractal theory is given by relation between number and the object sizes (FEDER, 1988) (Equation 1):

$$N(l) \sim l^{-D} \quad (1),$$

where N(*l*) is the object number, *l* is scaling and *D* is the fractal dimension, i.e., power law between scaling and fractal dimension; in practice the "Box-counting" methods is widely used to calculate N(*l*).

However, N(*l*) is unable to solve region problem with high or low mass density. Then, for better characterization of local densities of a complex system, it can be used multifractal method (VICSEK, 1992), which provides continuo spectrum of exponent, i.e., fractal dimension of a state or system, described by equations (2a and 2b) (CHHABRA et al., 1989; HU and WANG, 2007; POSADAS, et al., 2003).

$$p_i(l) \sim l^{\alpha_i} \quad (2a)$$

$$N_\alpha(l) \sim l^{-f(\alpha)} \quad (2b),$$

where p_i means the probability of measurement at the i-nth box; α is Lipschitz-Holder exponent that characterizes the scaling in spatial location; N_α is the box number with size *l* of the same probability. The multifractal spectrum f(α) can be defined as fractal dimension of a set of boxes with exponent α. According to Posadas et al. (2003) f(α) can still be express as subset of fractal dimension:

$$f(\alpha) = -\lim_{l \to 0} [\log N_\alpha(l) / \log l] \quad (3)$$

From this, the general fractal dimension (D_q) is described through scaling distribution moments p_i as (POSADAS et al., 2003; CHHABRA et al., 1989):

$$\sum_{i=1}^{N(l)} p_i^q = l^{\tau(q)} \qquad (4a)$$

$$\tau(q) = \frac{(q-1)}{D_q} \qquad (4b),$$

where q is momentum order ($-\infty < q < \infty$), D_q is general fractal dimension and τ_q is the correlation of q-nth momentum order exponent. By Legendre transformation, the equation (4b) can be rewrite as $f(\alpha)$ and τ_q (CHHABRA et al., 1989; POSADAS et al., 2003; HU and WANG, 2009):

$$f(\alpha(q)) = q\alpha(q) - \tau(q) \qquad (5a)$$

$$\alpha(q) = d\tau(q)/dq \qquad (5b).$$

The spectrum $f(\alpha)$ becomes a downwards concave function when q = 0 and, therefore $f(\alpha)$ and D_q presente similar informations (JORGE et al., 2008). When q assumes values 0, 1 and 2, D_0 becomes the capacity dimension, which quantifies the system entropy (macro state system); D_1 is the entropy dimension related to the information entropy, i.e., Shannon entropy (SHANNON and WEAVER, 1949) and D_2 is the correlation dimension, which quantifies measurement in a given box size *l*.

From the relation between D and q, it could still be deduce the degree of multifractality, as well as the degree of asymmetry (HALSEY et al.,1986; SZCZPANIAK and MACEK, 2008):

$$\Delta = \alpha_{max} - \alpha_{min} = D_{-\infty} - D_{\infty} \qquad (6)$$

$$A = \frac{\alpha_0 - \alpha_{min}}{\alpha_{max} - \alpha_0} \qquad (7),$$

when $f(\alpha_0) = 1$, the singular spectrum will be maximum (OTT, 2002; SZCZEPANIAK and MACEK, 2008).

2.3.2 Use of MASS software (Multifractal Analysis & Scaling System)

This software which is not public domain, was developed by Centro Internacional de La Papa (CIP) and uses Box-Counting method (POSADAS, et al., 2001). For the multifractal technique application, it was used images converted in a number matrix of 2.2, only at number 0 (black) and 255 (white); When identifying matrix size in the program input, it was established *q* increment varying from -10.00 to 10.00; Subsequently, it is was selected and standardized the appropriate *q* scaling range (l) for image in the software interface; for this study, the *l* values were: 40, 50, 100, 125, 200, 250 and 300 and, finally, it was necessary to

do the linearity analysis using software, generating as a result the multifractal spectrum in function of f(q) and α(q).

3. Results and discussion

3.1 Multifractal spectrum

The multifractal spectrum analysis provides the characterization of soil system, i.e., the spatial distribution of soil porous structure (POSADAS et al., 2003; TORRE et al., 2016). There were various parameters generated from the plane spectrum, such as Δf and Δα, which are fundamental to describe the curvature behavior (Figure 3), in other words, they represent the spatial distribution of soil porous structure. The parameter Δf shows the higher and lower system scaling value, while Δα indicates the set complexity. The next step was to analyze the multifractal spectrum of the six managements in the axial and coronal planes at three different depths and in parallel, comparing them with works done realized by Marchini et al. (2015).

Figure 3 - Multifractal spectrum example and the parameters derived from it

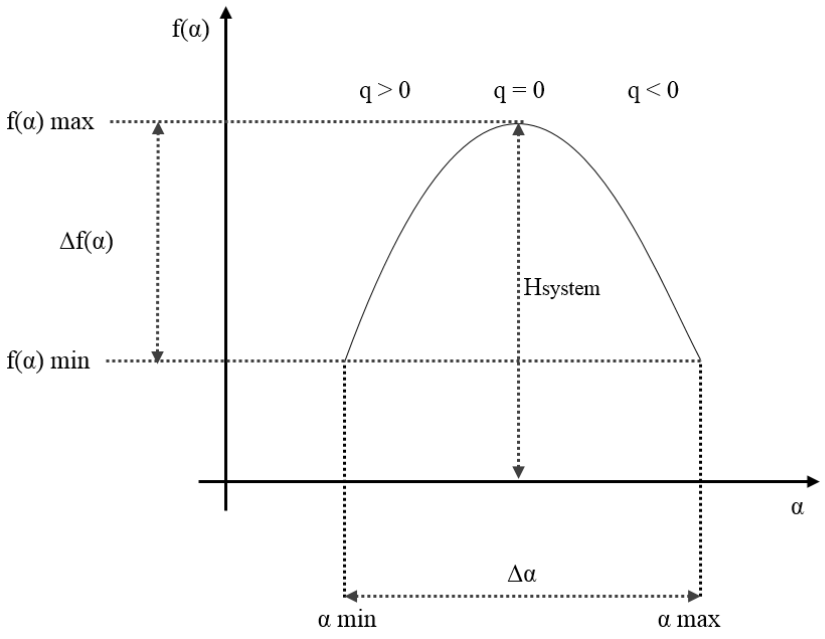

Source: Author (2016)

3.1.1 Axial Plane

When observing at the spectrum symmetry in the first instant (Figure 4), it could be verified that managements NF (1), RS (1), RP(5) and DP(6) present more “flat” shape in comparison with G(3) and D(4), i.e., they are more heterogeneous system than the last two, for the higher the spectrum width, the higher will be the involved scaling variety and vice versa (POSADAS et al., 2003; MARTÍNEZ et al., 2010). Consequently, these results showed that management G (3) and D (4) tend to be random system, whereas the rest of management tend to be multifractal due to their scaling variety. In other words, porous distribution in different sizes.

With respect to management depth, in general, they all tend to be more homogeneous in other depth. However, it was worth emphasizing the management RS (2) and G (3), which were those that better answered to the recovery techniques (MARCHINI et al., 2015). By graphic RS (2) it can be presumed that recovery technique reached layer 10-20 cm, in fact, it was better than NF (1); For G (3) the technique was efficient at 0-10 cm, as proved by multifractal methods and by Marchini et al. (2015), due to the addition of sludge and *Brachiaria decumbens* in this surface, increasing the organic matter content. On the other hand, in layer 10-20 cm, the result got worse, i.e., there was a strong fractal support in this layer. Although at 20-30 cm depth showed similar curvature to that of superficial layer, which must be better investigated in another plane due to Gonçalo-alves root penetration. Management RP (5) showed a more homogeneous aspect than DP (6); these unexpected result, should be attributed to the fact that DP (6) has higher clay content in comparison with RP (5), thereby turning it system more complex (POSADAS et al., 2001).

Figure 4 - Managements multifractal spectrums at axial plane in different depth: (1) Soil from native forest of Cerrado (NF); (2) Recuperated soil (RS); (3) Soil in recuperation with *Astronium fraxinifolium* (Gonçalo-alves) + *Brachiaria decumbens* + sludge (G); (4) Degraded soil (D); (5) Recuperating pasture (RP) and (6) Degraded pasture (DP).

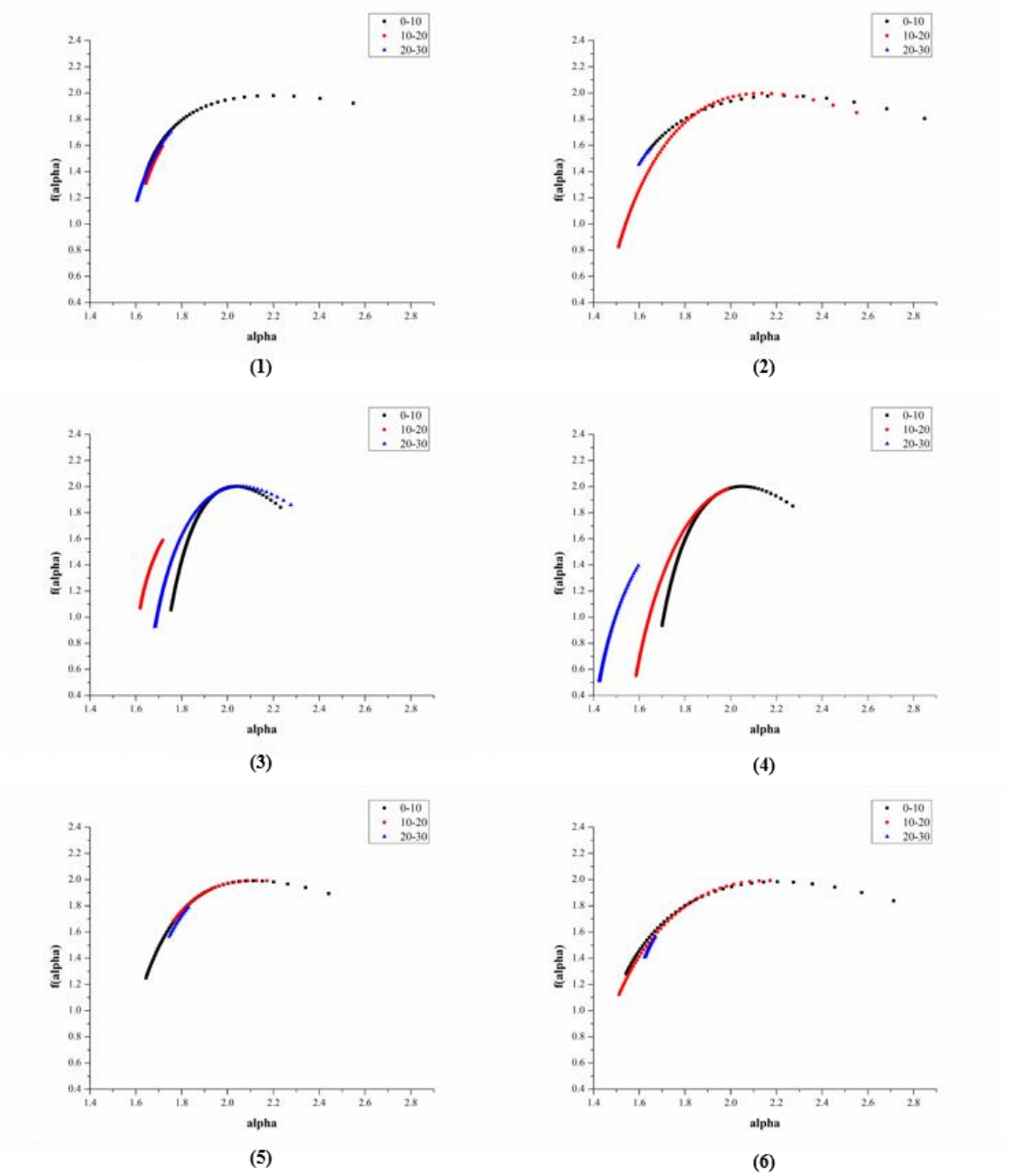

Source: Author (2016)

3.1.2 Coronal Plane

All managements in this plane have spectrum with lower f(α) value and are predominant to the left side of the spectrum; this fact should be attributed to the superficial compaction effect (at axial plane) or root presence in the soil structure, according to Lipiec et al. (1998), it

is common to detected the absence of continuous structure in this plane. As proved by Posadas et al. (2003), the low value of α represents the absence of massive structure and pores cluster.

Therefore, the difference between the three depths is the key to evaluate this plane (Figure 5). In the case of NF (1), the two superficial layers are very close due to their similarities in pores spatial distribution (MARCHINI et al., 2015), none the less, the 0-10 cm layer is slightly less massive than the 10-20 cm; at 20-30 cm, the low f(α) value was certainly caused by native vegetation root; In RS (2), all layers are characterized by lows scaling value, i.e., the distribution of pores sizes is close for the three depth detected by tomographic; G (3) is highlighted by its similarity with NF (1) at 20-30 cm. In this case it must take into the consideration the decompressed action of Gonçalo-Alves roots; However, the distribution of different class of pores is extremely poor in the two superficial layers. D (4) is very poor its distribution of different pores sizes and it is very compacted at 20-30 cm; In RP (5), the recovery technique still doesn't present clear improvement in the two first layers. However, at 20-30cm, it showed a higher Δα among all layers of this management, in other words, the applied technique should have reached this depth in the first moment; DP (6) is extremely compacted at 0-10cm, yet, in other layers, it has similar aspects only differentiated by the degree of compactation.

Figure 5 - Managements multifractal spectrums at coronal plane in different depth: (1) Soil from native forest of Cerrado (NF); (2) Recuperated soil (RS); (3) Soil in recuperation with *Astronium fraxinifolium* (Gonçalo-alves) + *Brachiaria decumbens* + sludge (G); (4) Degraded soil (D); (5) Recuperating pasture (RP) and (6) Degraded pasture (DP).

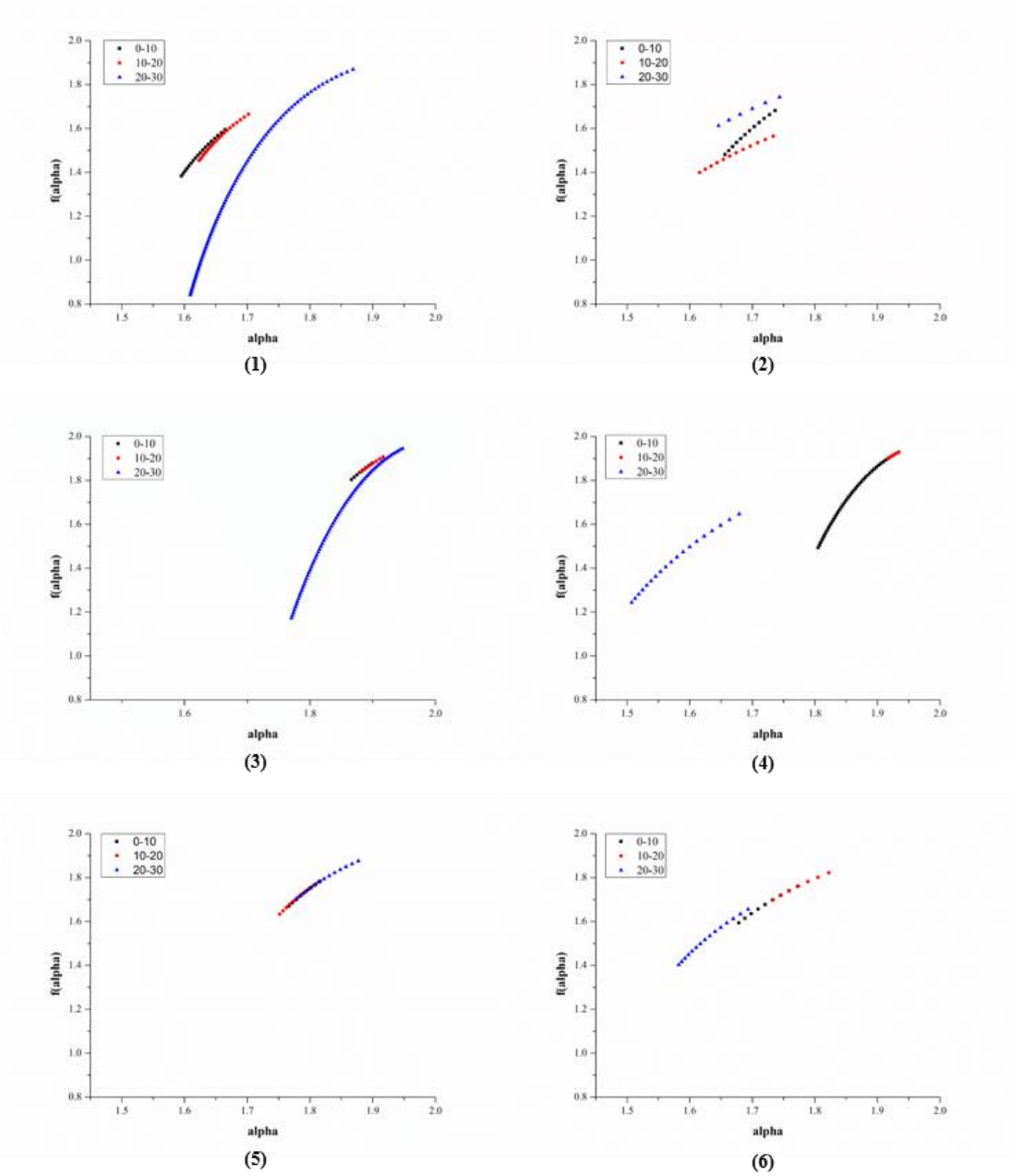

Source: Author (2016)

3.2 Entropy of system

As an open system, the soil naturally organizes itself and dissipates entropy to the environment. Consequently, a degraded soil is the one that imports the entropy of its circumstance to reach a stable condition. From the multifractal spectrum it was possible to quantify the entropy of system for each management (Figure 3), considering $f(\alpha_{max})$ as global

(average) entropy of the system, which allows the evaluation of efficiency and evolution of recovery techniques applied to management in different plans and depth.

3.2.1 Axial Plane

The entropy (Table 1) clearly showed the system order, being NF less entropic among all management at 0-20 cm; In contrast, D was the most entropic. In other words, this management has changed greatly. Then, the result is coherent with one of the recovery techniques objectives: to induce interventions in soil aiming entropy dissipation to the environment, i.e., through the anthropogenic activities, which alter soil's physical, chemical and biological properties for the improvement of its structuring and aggregation at a shortest time compared to natural ways.

At 0-10 cm (Table 1), the nature of surfaces is considered as determinant factor in the infiltration process, mainly when there is vegetation coverings. It was verified that RS entropy is equal to NF, in other words, the applied technique was effective; G however in spite of its vegetation coverings (Gonçalo-Alves e *Brachiaria decumbens*) and sludge, in term of entropy, remains the same as D, in such a way, both management have close constant infiltration rate (Marchini et al., 2015). The DP entropy being higher than RP, is certainly related to the textural content of each one, as multifractal technique is sensible to detection of particle size distribution (POSADAS et al., 2001).

At 10-20 cm (Table 1) NF remains the least entropic, however, there was a small drop in G value. Presumably, it is a remnant effect of soil preparation or vegetation, leaving a great amount of microstructure in this depth, whereas to the rest of the other managements their entropy has increased; in other words, this depth is the area where has tolerated higher horizontal compaction.

At 20-30 cm (Table 1) NF entropy has increased; this deviation should be related to the amount of activities and weight that soil carries in this layer. It is worth highlighting that RS has had a significant drop, which should be attributed to dispersed roots quantity in this depth, leaving the massive structure and less entropic; G keeps the same value at 0-10 cm; the changes occurred in D, RP and DP are insignificant.

Table 1. Entropy of six managements in axial plane

Entropy	NF	RS	G	D	RP	DP
0-10	1.9794	1.979	2.001	2.001	1.9904	1.9826
10-20	1.5952	1.9964	1.9774	2.0008	1.9928	1.9928
20-30	1.7032	1.5732	2.001	1.99	1.9934	1.9924

Source: Author (2016)

3.2.2 Coronal Plane

At 0-10 cm (Table 2) the open system tendency is to keep the entropy low, as showed NF; after that, RS showed efficiency of the recovery technique at vertical axis; G remains close to D with high entropy value, in other words, the constant infiltration rate continues to be lower, the G system still needs to lose more entropy to the environment; RP presented to be a little worse than DP, therefore, the applied technique in this case was not vertically successful.

At 10-20 cm (Table 2), RS indicates the lower entropy value among all managements, then, in term of entropy, the recovery of this management only reached up to this depth; G and D remain similar, it also reflects their infiltration rate are close (MARCHINI et al., 2015); for RP, there was not significant alteration; There was a small increase in the DP, showing where the higher compactation in this management took place.

At 20-30 cm (Table 2), with the exception of D and DP, all the others had their entropy increased, in other words, there was a tendency to a more complex system, reducing the chance of the system to return closer to their initial state of NF.

Table 2. Entropy of six managements in coronal plane

Entropy	NF	RS	G	D	RP	DP
0-10	1.5954	1.6816	1.8778	1.9288	1.7834	1.7606
10-20	1.665	1.5654	1.907	1.928	1.7794	1.822
20-30	1.8686	1.7428	1.9452	1.6464	1.8756	1.656

Source: Author (2016)

3.3 Degree of multifractality (Δ)

The degree of multifractality is a heterogeneity indicator of a surface or object. It is an indirect measurement that reflects the size, shape and connections between porous space and soil solid part at different scales; In this way, soil is considered as to be a multifractal material. The width of spectrum (Δα) indicates the degree of multifractality (HU and WANG, 2007),

the larger is Δ, the stronger will be its multifractality, in other words, the structure is more heterogeneous and complex. Thus, through the quantification of multifractal spectrum, it is possible to confirm how much the recovery techniques are effectives.

3.3.1 Axial Plane

At 0-10 cm (Table 3), the results showed that RS soil approaches a NF, in other words, it is a very positive response, proven that the technique was effective in the recovery process; G remains a poor structure in the first layer, however, it is expected that the restructuration process is not so fast; RP showed an intermediate value between NF and D, this is a sign of its structural recovery. The DP value was above NF but this should be attributed to the amount of roots of remnant pasture in this management, which strongly alter its structure.

At 10-20 cm (Table 3), it can be noticed, except NF and RP, that all the other managements had their values reduced, i.e., the soil homogeneity at this depth has increased; the managements RS and G had high values, responding well to soil recovery; DP kept similar characteristics at the surface.

At 20-30 cm (Table 3), RS was close to NF; G and RP presented the lowest value, i.e., the technique effect has not reached this phase; D and DP are the most highest, however, it must be attributed to fissure presence within the soil at this depth.

Tabela 3. Degree of multifractality of six managements at axial plane

Degree of multifractality (Δ)	**NF**	**RS**	**G**	**D**	**RP**	**DP**
0-10	0.28943	0.27938	0.16936	0.21586	0.24664	0.34002
10-20	0.25762	0.35542	0.29718	0.29952	0.1675	0.3555
20-30	0.30024	0.30976	0.2334	0.46318	0.17276	0.3115

Source: Author (2016)

3.3.2 Coronal Plane

At 0-10 cm (Table 4), RS came closer to NF; G is also closer to D, the RP multifractality is still low, therefore, its structure remains poor; DP is close to RS, however, this is again attributed to pasture roots, it doesn't really mean a better condition to crop.

At 10-20 cm (Table 4), except for RS, G and RP, the managements had an increase in their degree of multifractality. This means that vertically the structure of these managements showed improvement. The others management had their values reduced in comparison with the first layer, i.e., the structural distribution became more homogeneous.

At 20-30 cm (Table 4), the managements had an increase (except RP), specially G and DP. The causes that led those results can be the presence of Gonçalo-Alves tree roots and crack, respectively.

Tabela 4. Degree of multifractality of six managements at coronal plane

Degree of multifractality (Δ)	**NF**	**RS**	**G**	**D**	**RP**	**DP**
0-10	0.2765	0.239	0.07066	0.11614	0.15288	0.22886
10-20	0.26314	0.24684	0.0725	0.05102	0.16252	0.19616
20-30	0.27146	0.26082	0.13458	0.35046	0.14388	0.30432

Source: Author (2016)

3.4 Degree of asymmetry (A)

The degree of asymmetry is an important indicator to the multifractal analysis, as it shows the fluctuation degree of different fractal exponents; in the case of soil, it means the weight of the division between porous and solid part. When the spectrum declines to left side, it means a high fractal exponent and fluctuation in the measurement; when is to the right side, the fractal exponent and fluctuation are low. Physically, when A = 1, the spectrum is symmetric; with A > 1, the spectrum left side represents the porous part and A < 1, the right side is the solid part (SZCZEPANIAK and MACEK 2008; HU and WANG, 2009; MACEK and WAWRZASZEK, 2011).

3.4.1 Axial Plane

At 0-10 cm (Table 5), all managements showed positive values; the recovery techniques had satisfactory responses. RS and NF again showed higher values in relation to other managements, in other words, there a predominant of porous space, it is structurally massive; G is slightly better than D, both spectrum indicate pores presence, however, they are inferior than the other management. RP and DP are at medium position in overall ranking.

At 10-20 cm (Table 5), it was verified that porous part continues prevailing for RS management, whereas the rest declines to solid part. It is emphasized that G presented the most negative value, showing the degrading state of the management; RP and DP are equals in this depth.

At 20-30 cm (Table 5), all management presented negative number, except G, as a consequence of penetration of tree root, which act as descompactation agent.

Table 5. Degree of asymmetry of six managements at axial plane

Degree of asymmetry (A)	NF	RS	G	D	RP	DP
0-10	0.9360	1.0266	0.68892	0.62456	0.70423	0.76668
10-20	-0.65816	0.66122	-0.81322	-0.16048	0	0
20-30	-0.73847	-0.92308	0.590836	-0.77842	-0.04808	-0.92

Source: Author (2016)

3.4.2 Coronal Plane

The degree of multifractality is negative for all management and depth (Table 6). However, this should not be interpreted as intense compactation of management, but as a predominance of solid structure in this plane. Due yo this fact, it is necessary to take into consideration: 1) vertical pressure due to the soil weight and 2) the structural geometric distribution through other physical parameters, such as density, porosity, aggregates distribution among others, for better interpretation the obtained results.

Table 6. Degree of asymmetry of six managements at coronal plane

Degree of asymmetry	NF	RS	G	D	RP	DP
0-10	-0.88532	-0.83815	-0.85419	-0.3992	-0.84857	-0.81289
10-20	-0.86567	-0.77217	-0.75538	-0.83754	-0.82136	-0.80194
20-30	-0.48718	-0.84082	-0.26922	-0.75202	-0.67655	-0.81885

Source: Author (2016)

4. Conclusions

a) The main objective of this study was reached, as multifractal technique applied in microtomographic of high-resolution showed itself as an excellent tool to distinguish the managements, as well as the effects of adopted recovery techniques;
b) At axial plane, RS and G responded positively to the recovery techniques at 0-10 cm depth, as for RS the effect reached up to10-20 cm;
c) At coronal plane, the trees roots of management G reached the layer 20-30 cm, although it is still necessary the structural distribution. In general, the management RP did not respond well to the at two planes and not even to the depths;

d) It is important to consider the soil as an open system for multifractal analysis.
e) The soil entropic recovery is highly dependent of 1) vegetation covering and roots distribution; 2) degree of superficial compactation and 3) textural class;
f) The recovery techniques were efficient at 0-10 cm, in other words, they clearly alter the entropy. The effectiveness of the techniques declines according to the depth;
g) The recovery effects are different between axial and coronal planes; The degree of multifractality was effective for structural heterogeneity quantification of managements;
h) The degree of asymmetry was efficient to classify the management at axial plan, however, for the coronal plane, it is necessary to have the aid of other physical parameters in order to acquire a better interpretation of results.

5. Acknowledgements

We extend our thanks to CNPq and CAPES for financial support, to USP for its academic formation, to Embrapa, which made possible the use of its laboratories, developed technologies and technical support, to Centro Internacional de La Papa (CIP) for granting MASS software use and, to Unesp for providing samples and technical support.

Reference

CHHABRA, A. B. et al. Direct determination of the f (α) singularity spectrum and its application to fully developed turbulence. **Physical Review A**, v.40, n.9, p.5284, 1989.

CHHABRA, A.; Jensen, R. V. Direct determination of the f (α) singularity spectrum. **Physical Review Letters**, v.62, n.12, p.1327, 1989.

CNUDDE, V.; BOONE, M. N. High-resolution X-ray computed tomography in geosciences: a review of the current technology and applications. **Earth-Science Reviews**, v.123, p.1-17, 2013.

EMPRESA BRASILEIRA DE PESQUISA AGROPECUÁRIA (EMBRAPA). **Sistema brasileiro de classificação de solos**. 3th ed. Rio de Janeiro: Centro Nacional de Pesquisa de Solos, Rio de Janeiro, 2013.

FEDER, J. **Fractals**. New York: Plenum Press, 1988.

FOOD AND AGRICULTURE ORGANIZATION OF THE UNITED NATION (FAO). **Status of the world's soil resources**. Rome: Food and Agriculture Organization of the United Nations, 2015.

HALSEY, T. C. et al. Fractal measures and their singularities: the characterization of strange sets. **Physical Review A**, v.33, n.2, p.1141, 1986.

HEUVELINK, G. B. M.; WEBSTER, R. Modelling soil variation: past, present, and future. **Geoderma**, v.100, n.3, p.269-301, 2001.

HU, M. G.; WANG, J. F. Multifractal Analysis of Global Total Column Ozone Image. In: SIMONS, T.; PSIHOYIOS, G.; TSITOURAS, CH. (Ed.). **Numerical analysis and applied mathematics**: International Conference on Numerical Analysis and Applied Mathematics 2009: Volume 1. Melville: American Institute of Physics, 2009. P. 390-393. (AIP Conference Proceedings, 1168)

JENNY, H. **Factors of soil formation**: a system of quantitative pedology. New York: Dover Publications, 1994.

JORGE, L. A. de C. et al. **Aplicação da técnica multifractal para caracterização de manejo de solo**. São Carlos: Embrapa, 2008. (Documentos, 41) Available in: <https://www.embrapa.br/en/busca-de-publicacoes/-/publicacao/31887/aplicacao-da-tecnica-multifractal-para-caracterizacao-de-manejo-de-solo>. Accessed in: 15, jan, 2017.

LIPIEC, J.; HATANO, R.; SŁOWIŃSKA-JURKIEWICZ, A. The fractal dimension of pore distribution patterns in variously-compacted soil. **Soil and Tillage Research**, v.47, n.1, p.61-66, 1998.

MACEK, W. M.; WAWRZASZEK, A. Multifractal structure of small and large scales fluctuations of interplanetary magnetic fields. **Planetary and Space Science**, v.59, n.7, p.569-574, 2011.

MANDELBROT, B.B. **The Fractal Geometry of Nature**. New York: W. H. Freeman and Company, 1982.

MARCHINI, D. C. et al. Matéria orgânica, infiltração e imagens tomográficas de Latossolo em recuperação sob diferentes tipos de manejo. **Revista Brasileira de Engenharia Agrícola e Ambiental**, v.19, p.574-580, 2015.

MARTÍNEZ, F. S. J. et al. Multifractal analysis of discretized X-ray CT images for the characterization of soil macropore structures. **Geoderma**, v.156, n.1, p.32-42, 2010.

MIRANDA, J. G. V. et al. Multifractal characterization of saprolite particle-size distributions after topsoil removal. **Geoderma**, v.134, n.3, p.373-385, 2006.

OTSU, N. A threshold selection method from gray-level histograms. **IEEE Transaction Sytems, man, and Cybernetics**, v.9, n.1, p.62-66, 1979.

OTT, E. **Chaos in dynamical systems**. New York: Cambridge University Press, 2002.

PACHEPSKY, Y.; HILL, R. L. Scale and scaling in soils. **Geoderma**, v.287, p.4-30, 2017.

PAZ FERREIRO, J.; MIRANDA, J. G. V.; VIDAL VÁZQUEZ, E. Multifractal analysis of soil porosity based on mercury injection and nitrogen adsorption. **Vadose Zone Journal**, v.9, n.2, p.325-335, 2010.

PERFECT, E.; KAY, B. D. Applications of fractals in soil and tillage research: a review. **Soil and Tillage Research**, v.36, n.1, p.1-20, 1995.

PIRES, L. F. et al. Twenty-five years of computed tomography in soil physics: a literature review of the Brazilian contribution. **Soil and Tillage Research**, v.110, n.2, p.197-210, 2010.

POSADAS, A. et al. Characterizing water fingering phenomena in soils using magnetic resonance imaging and multifractal theory. **Nonlinear processes in geophysics**, v.16, n.1, p.159-168, 2009.

POSADAS, A. N. D. et al. Multifractal characterization of the spatial distribution of ulexite in a Bolivian salt flat. **International Journal of Remote Sensing**, v.26, n.3, p.615-627, 2005.

POSADAS, A. N. et al. Multifractal characterization of soil particle-size distributions. **Soil Science Society of America Journal**, v.65, n.5, p.1361-1367, 2005.

POSADAS, A. N. Multifractal characterization of soil pore systems. **Soil Science Society of America Journal**, v.67, n.5, p.1361-1369, 2003.

SHANNON, C. E.; WEAVER, W. **The mathematical theory of information**. [S.l.: s.n.], 1949.

SZCZEPANIAK, A.; MACEK, W. M. Asymmetric multifractal model for solar wind intermittent turbulence. **Nonlinear Processes in Geophysics**, v.15, n.4, p.615-620, 2008.

TAINA, I. A.; HECK, R. J.; ELLIOT, T. R. Application of X-ray computed tomography to soil science: a literature review. **Canadian Journal of Soil Science**, v.88, n.1, p.1-19, 2008.

TORRE, I. G.; LOSADA, J. C.; TARQUIS, A. M. Multiscaling properties of soil images. **Biosystems Engineering**, 2016. Article in press

VAZ, C. M. et al. Evaluation of an advanced benchtop micro-computed tomography system for quantifying porosities and pore-size distributions of two Brazilian Oxisols. **Soil Science Society of America Journal**, v. 75, n.3 p.832-841, 2011.

VICSEK, T. Fractal growth phenomena: v. 2. Singapore: World Sientific, 1992.

VILLAS-BOAS, P. R.; CRESTANA, S.; POSADAS, A. Modelagem e simulação. Brasília: Embrapa, 2014. Available in: <http://ainfo.cnptia.embrapa.br/digital/bitstream/item/137686/1/Conceitos-e-aplicacoes-baixa.pdf>. Accessed in: 15, jan, 2017.

VOSS, R. F. Fractals in nature: from characterization to simulation. In: BARNSLEY, M.F. **The science of fractal images**. New York: Springer-Verlag, 1988. p. 21-70.

WANG, J. et al. Using computed tomography (CT) images and multi-fractal theory to quantify the pore distribution of reconstructed soils during ecological restoration in opencast coal-mine. **Ecological Engineering**, v.92, p.148-157, 2016.

CHAPTER VI

Characterization of water dynamics process under drying cycle in a Brazilian soil using microtomography digital processing

TSENG, C. L., VAZ, C. M. P., CRESTANA, S.

CHARACTERIZATION OF WATER DYNAMICS PROCESS UNDER DRYING CYCLE IN A BRAZILIAN SOIL USING MICROTOMOGRAPHY DIGITAL PROCESSING

Tseng, C. L.[a]*, Vaz, C. M. P.[b] and Crestana, S.[b]

[a]University of São Paulo, "São Carlos School of Engineering " 400 Avenida Trabalhador São-carlense, CEP: 13566-590 São Carlos, São Paulo, Brazil.

[b]Embrapa Instrumentation, 1452, Rua XV de Novembro, CEP: 13560-970, São Carlos, São Paulo, Brazil.

ABSTRACT

The study about water dynamic into the soil over time is essential in Soil Physics. The X-ray microtomograph and digital image processing are considered powerful tools to investigate phenomena related to soil water dynamics, due to the capacity to preserve the integrity of the soil architecture. This study aims to quantify soil physical geometrical and morphological parameters related to fluid movement of a Brazilian tropical soil along the time. The use of 1% solution potassium iodine (KI) in the soil solution showed excellent image contrast; the unsharp filter and Otsu method improved image quality. Among the evaluated parameters, the Shannon entropy has introduced the amount of information contained within the microtomography. The air filled porosity has indicated oscillatory behavior of the soil-fluid interface at micrometric scale. The lacunarity has shown random behavior of percolation cluster and its effect soil evaporation. The Euler-Poincaré number has highlighted the increase of connectivity between pore spaces over a period of time. The degree of anisotropy has proved to be a strong indicator of preferential flux direction, represented by a damped harmonic oscillator equation. The 2D tortuosity has found slightly sinuous path on plan xy. It was observed a correlation between tortuosity (3D) with Euler-Poincaré number. At the same time random-walk simulation demonstrates a restrict diffusion process into the soil. The present study provides original results and new perspective about the fluid dynamics into the soil at micrometric scale.

Keywords: Microtomography. Porosity. Lacunarity. Euler-Poincaré number. Degree of anisotropy. Tortuosity. Fluid dynamic.

1. Introduction

The study of fluid movement has always been a major issue in the Soil Physics, since it is fundamental for hydrological processes studies in different scales. Such processes are infiltration, redistribution, drainage, evaporation, evapotranspiration and solute transport (LIN, 2010; KUTÍLEK; NIELSEN, 1994). In this way, the more we know about functional architecture of soil three phases (solid, liquid and gaseous) more adequate will be its use.

In the last decade, tools such as X-ray microtomograph have increased in popularity in soil and other porous media studies (VAZ et al. 2014). This fact allowed a lot of research related to soil functional architecture, involving from quantification of hydraulic proprieties, using X-ray tomography technique with digital image processing, (GERKE et al. 2012; KOESTEL; LARSBO, 2014; TRACY et al. 2015) and including fluid simulation models (ONODY; POSADAS, 1995; NAKASHIMA; KAMIYA, 2007; LANDRY; KARPYN; AYALA et al. 2014; POT et al., 2015; ZHANG; CRAWFORD; YOUNG et al. 2016).

In literature, it is possible to find several studies, which refer to quantification of water movement into the soil. Vaz et al (2014) have done a differentiation of the three phases of water in soil, by using an X-ray microtomograph. Yang et al. (2015) visualized water wetting in a porous material through synchrotron microtomograph.

As a result, X-ray microtomography technique has also provided researches that trace water movement into the soil at different scales (CRESTANA et al., 1985; KOESTEL; LARSBO 2014; TSENG et al. 2014), such as: compacted structure morphology (Janzen et al. 2013), macropores and water and gas transport into the soil (KATUWAL et al. 2015); water flux characterization by capillary wetting (GÈRAUD et al. 2003); quantification of trapped gases in capillary fringe (MOHAMMADIAN; GEISTLINGER; VOGEL et al., 2015); water and air distribution into the soil pore system (POT et al. 2015); use of Lattice Boltzmann model to simulate water flux in a non-saturated soil (ZHANG et al., 2016); Lèvy flight as result of a normalized random-walk for particles (MORAES, 2013) and random-walk simulation using a discretized lattice walk in a porous media (NAKASHIMA; KAMIYA, 2007).

Despite of large amount of research already conducted to the present moment by using X-ray microtomograph, the measurement of fluid movement into the soil has proved to be a challenge for the Soil Physics community. The main limitations are related to the access to high resolution systems as synchrotron facilities, which allows varying resolutions and energies (PETH, 2010), the high cost of image processing commercial software and adequate

geometrical and morphological parameters to better characterize and model dynamic soil processes.

Therefore, the aim of this study is to provide quantification of physical parameters related to fluid movement geometry and morphology of a Brazilian tropical soil over a period of time.

2. Material and Methods

2.1 Sample description

The soil sample was collected at the experimental farm of the Universidade Estadual Paulista (UNESP), Ilha Solteira campus, São Paulo State, Brazil, classified as a dystrophic Red Latosol (EMPRESA BRASILEIRA DE PESQUISA AGROPECUÁRIA, 2013), with 40.08% of clay, 7.67% of silt and 52.25% of sand.

2.2 Description and installation of the experiment

2.2.1 Equipment and image acquisition

For this experiment it was used an X-ray microtomograph Skyscan - 1172 model, which was made available by Embrapa Instrumentation. Initially, it was acquired tomographic projections (Figure 1a), which were reconstructed in stacks of two-dimensional images with 5.48 μm of spatial resolution through software NRcon – Skyscan (Figure 1b), according to Vaz et al. (2011). The reconstruction tomographic parameters were: ring artifact of 10, smoothing filter of 5, beam hardening correction of 60% and scales converted to Hounsfield Unit (HU). Finally, it was selected a region of interest (ROI) in the set of images for analysis (Figure 1c).

Figure 1: Tomographic projection of a soil sample (a); reconstructed two-dimensional image (b); and region of interest (ROI) of a ross-sectional image (c).

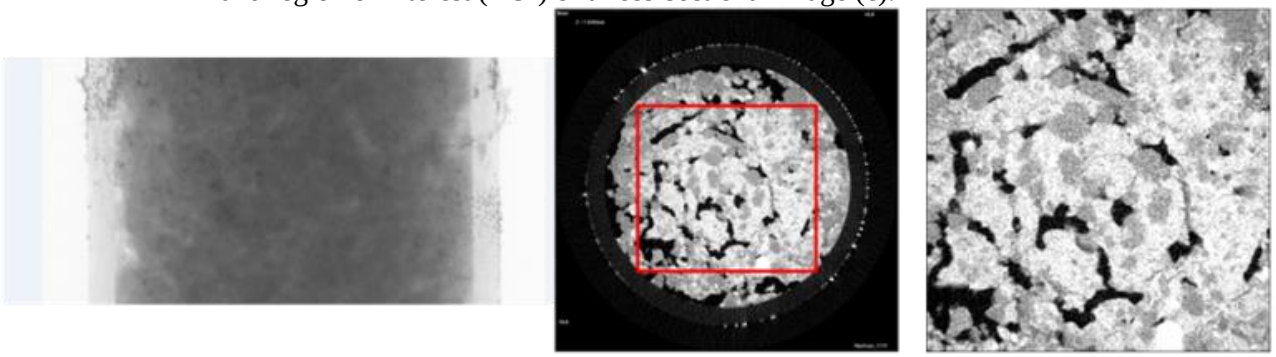

Source: Author (2015)

2.2.2 Experimental assembly

An undisturbed soil sample (8mm diameter x 12mm high) was collected in an acrylic tube, oven dried at 105°C during 48 hours and placed on the microtomograph stage for scanning (Figure 2). The soil sample was saturated with a 1% solution KI (potassium iodine) and kept for a week to ensure best solution redistribution. After that the solution supply was closed and image acquired at times 0, 7, 26, 48, 72, 85, 134 and 370 hours. During the acquisition the top part of the sample was sealed to avoid evaporation.

Figure 2: Experiment installed inside the x-ray microtomograph

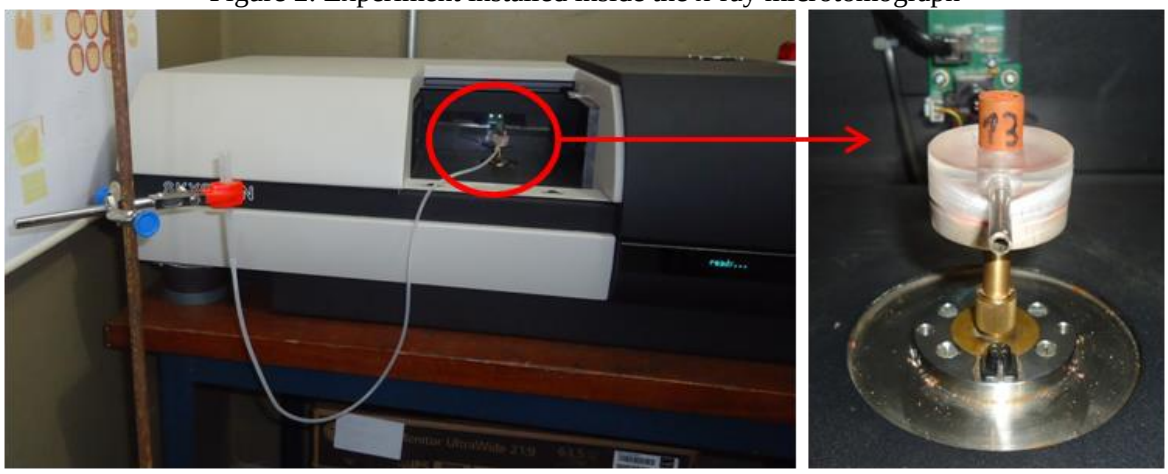

Source: Author (2015)

2.3 Preprocessing and image segmentation

In order to differentiate and quantify the different phases of the soil at tomography, besides using appropriate reconstruction parameter, it was essential to select adequate filter method to promote better differentiation of distinctive phases of the soil. Therefore, for this study, the first step of preprocessing was used unsharp mask filter (ImageJ), which consists of subtracting a blurry image by the original one, resulting in a better contrast of the original image; in the other words it sharpened image edges reducing noises (GONZALEZ ; WOODS, 2010).

The second preprocessing step was image segmentation to extract the set of relevant data for analysis. For completing this step, it was used the Otsu (1975) method which minimizes the sum of variances between image classes and its background. This method is widely used in soil analyses, mainly applied in the porous media's drying processes (LÉONARD et al., 2003, 2004, 2005). Wang et al. (2011) showed Otsu method is the most recommend one for images with difficult peak differentiation on histogram (Figure 3).

Figure 3: Histogram of a microtomographic image of the soil sample at time 18 hours after the solution supply was closed

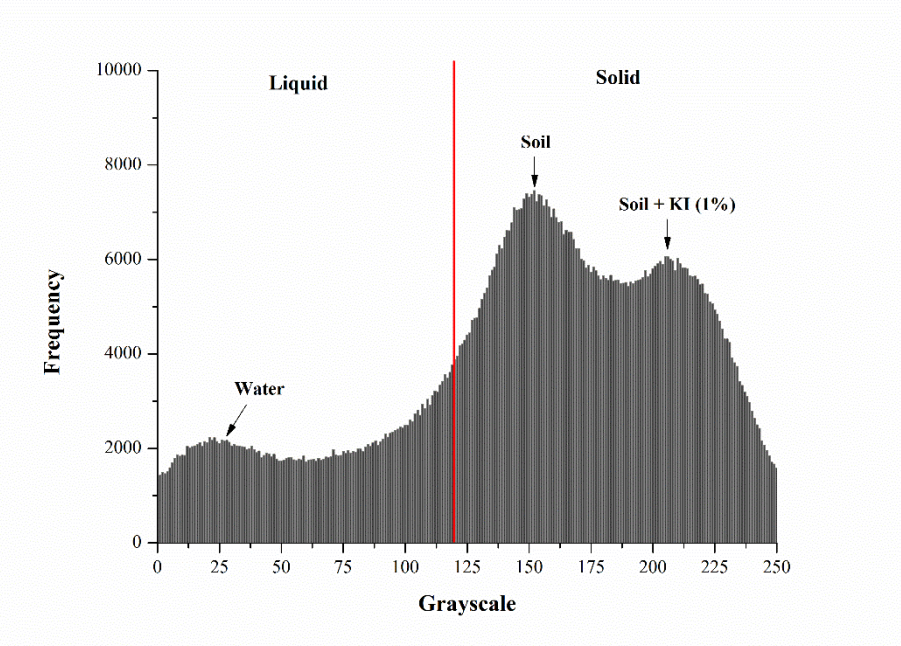

Source: Author (2015)

2.4 Analysis methods

2.4.1 Shannon entropy

According to the laws of thermodynamics, the entropy is the measurement of randomness degree of a certain system and, by definition, the more disorganized, the highest will be the value of entropy. Thus, the information entropy states that the amount of information contained in a message, is related to the frequency of bits group, which are transmitted. In other words, entropy is given as a statistic concept that measures the uncertainty associate to random variable (SHANNON, 1948), quantifying the expected value of the information in a message (WU et al., 2013). In this way, once message information is established, its entropy degree will be reduced. The equation is given by:

$$H(X) = -\sum_{k=1}^{K} p(x\chi_k)\mathrm{Log}_2\left(p(x_k)\right) \geq 0 \qquad (1)$$

where H is information measure, $p(x_k)$ is the probability distribution of a variable x with k bin (BRUNSELL, 2010).

For this study, it was selected a representative tomographic image of each timeline and, this image was transformed into a text file pixel by pixel according to its gray scale. Once the file is obtained, it is used an estimator developed in the interface R (HAUSSER; STRIMMER, 2009), which is simple and widely used in the Shannon entropy estimate. Then, a particularly estimator of entropy, the maximum likelihood estimator (H^{ML}) is difined a categorical random

variable with size p and associated cell probabilities $\theta_1, \ldots \theta_p$ with $\theta_k > 0$ and $\sum_k \theta_k = 1$. is represent by next equation:

$$H^{ML} = -\sum_{k=1}^{p} \theta_k^{ML} \log(\theta_k^{ML}) \quad (2)$$

where, the ML frequency estimates is:

$$\theta_k^{ML} = \frac{y_k}{n} \quad (3)$$

with $n = \sum_{k=1}^{p} y_k$, as the total number of counts.

2.4.2 Soil water retention curve (SWRC)

The Arya and Paris (ARYA; PARIS, 1981) model was used in this study to estimate the soil water retention curve of Brazilian soil, using the soil particle distribution, bulk density and total porosity (ARYA; PARIS, 1981; NAIME; SHINYA; VAZ, 2004; VAZ et al., 2005). The SWRC is essential to evaluate water percolation inside of soil. The model is based in two concepts: i) The capillarity equation that is related the matric potential (ψ_i) with pores radius, given by the equation (4); ii) The second one calculates water content from the particles sizes distribution (VAZ et al., 2003). The scaling value (α) is adjusted with the Van Genuchten (1980) equation in its inverse form, as given by equation (5).

$$\psi_i = \frac{2\sigma}{\rho_w g R_i \sqrt{\frac{2(\rho_p - \rho_s)}{3\rho_s} \left(\frac{3w_i}{4\pi R_i^3 \rho_p}\right)^{1-\alpha}}} \quad (4)$$

$$\alpha = 1 - \frac{Log\left[\frac{3}{2e}\left(\frac{2\sigma}{\rho_w \psi_i g R_i}\right)^2\right]}{Log\,(n_i)} \quad (5)$$

where, σ (N m^{-1}) is the surface water tension in the air-water interface; g (m s^{-2}) is the acceleration of gravity ; ρ_w (kg m^{-3}) is the water density ; ρ_p (kg m^{-3}) is soil particle density; ρ_s is soil bulk density ; R_i is soil particle radius ; w_i (kg kg^{-1}) is the soil mass of the i^{th} fraction calculated with a sigmoidal model fitted to the cumulative particle-size distribution data ; n_i is the number of particles of size class i and e is the void ratio (ARYA and PARIS, 1981).

2.4.3 Soil porosity

In general, soil porosity is estimated by invasive or indirect methods, which often modify internal soil structure. For this study, it was chosen the tomographic method in order to characterize the porosity without interfering with soil physical integrity. The Otsu method

was used to evaluate image porosity for the image threshold and, next step the two-dimensional porosity value was calculated from equation (6) to each image set. Finally, it was applied an integration calculus over all portions equivalent to 3D porosity, from equation (7) (CT-Analyser)

$$\phi_{2D} = \text{Porous area}/\text{Total area} \quad (6)$$

$$\phi_{3D} = \int \text{Porous area}/\text{Total volume} \quad (7)$$

The effective diameter of the soil pore system is totally irregular, which is different from capillary tubes, idealized by retention curve model. Due to its proximity with reality, we have used the Feret diameter for this study. According to Feret diameter definition, it is necessary to find the average distance between two parallel lines, which are tangential to the object.

$$D_{average} = \frac{D_x + D_y}{2} \quad (8)$$

where, D_x and D_y represent minimum and maximum object diameter.

2.4.4 Lacunarity

The concept of lacunarity was originally introduced in fractals studies, which can be used to other natural spatial patterns without restriction (PLOTNICK, et al. 1996; ALLAN; CLOITRE, 1991). Luo and Lin (2008) suggest that lacunarity reflects the macropore distribution and the spatial pattern of flow and transport.

For this study it was used FracLac plugin, which is an extension of ImageJ processing software, which uses "gliding box" algorithm to obtain lacunarity (ALLAIN; CLOITRE, 1991) with average of pixels intensity. This algorithm rewrites the first instants Z(1) and Z(2), which was defined by Plotnick et al. (1996) as function of the average (μ) and standard deviation (σ), as well as box length (b) over image width (T) at pixels, always with $b \leq T$ (9) and (10):

$$Z(1) = \mu \quad \text{and} \quad (9)$$

$$Z(2) = \sigma^2 + \mu^2 \quad (10)$$

Therefore, lacunarity results in:

$$\Lambda(r) = \sigma^2/\mu^2 + 1 \quad (11)$$

The ration between σ and μ changes according to the gliding box size (KARPERIEN, 2007; VALOUS et al., 2010). At last, from the equation onwards it is possible to plot a log-log lacunarity graphic versus different sizes of gliding box values (PLOTNICK et al., 1996).

2.4.5 Euler-Poincaré number

The Euler-Poincaré caracteristic or Euler-Poincaré number represents the connectivity of a porous space in 3-D (VOGEL; KRETZSCHMAR, 1996). The topological basic proprieties of Euler-Poincaré number are composed of: separate objects number (β_0), as to say, porous; connectivity number (β_1); and finally, closed cavity (β_2). In conclusion, the three-dimensional components used in CT-Analyzer software are given by Vogel (2002), Katuwal et al. (2015) and Bruker (2015):

$$\chi(X) = \beta 0 - \beta 1 + \beta 2 \qquad (12)$$

In agreement with Rozenbaum, Bruand and Le Trong (2012), the Euler-Poincaré number is inversely proportional to the connectivity value (i.e. $\beta_0 > \beta_1$). When the Euler-Poincaré number is negative, this means the greater will be connectivity of a porous structure (i.e. $\beta_0 < \beta_1$). Actually, β_2 is not very important for a natural porous network, considering that solid particles are complete enclosed by porous spaces (VOGEL, 2002).

2.4.6 Degree of anisotropy (DA)

Degree of anisotropy is a measure that quantifies how much the porous are directly dependent. It is obtained from Harrigan and Mann (1984):

$$\mathrm{DA} = \left(1 - \left[\frac{\text{Minimum eigenvalue}}{\text{Maximum eigenvalue}}\right]\right) \qquad (13)$$

Where, number 1 represents totally anisotropic and 0 is isotropic (SKYKCAN, 2015). The Mean Intercept Length (MIL) is a selfvalue analysis to estimate DA value. MIL was constituted by a series of vectors, which starts from the central volume and cross it entirely. After that, these vectors were divided by number of times that intercepted porous or solid parts of the entire volume. At the end, MIL is described as an ellipsoid in three axes in the form of tensor and as the result of the DA value.

2.4.7 Tortuosity in two and three-dimensions

Tortuosity is a parameter that measures porous sinuosity degree, which is important for the comprehension of fluid preferential direction (gas and liquid) into the soil. In literature, there are various mathematical definitions about tortuosity based on medium the geometrical structure, the conductivity, diffusivity and permeability relations (SHANTI et al., 2014). It is important to highlight that the tortuosity concept in porous media is a basic attribute to understand and describe fluid behavior, since it involves the three phases of the soil (solid, liquid and gas). Thus, the interaction between fluid and pore system can be divided into two

types: diffusive (gas and solute) and convective-dispersive (water and air) (Figure 4), according to

Figure 4: Transport parameters in gas and liquid phases

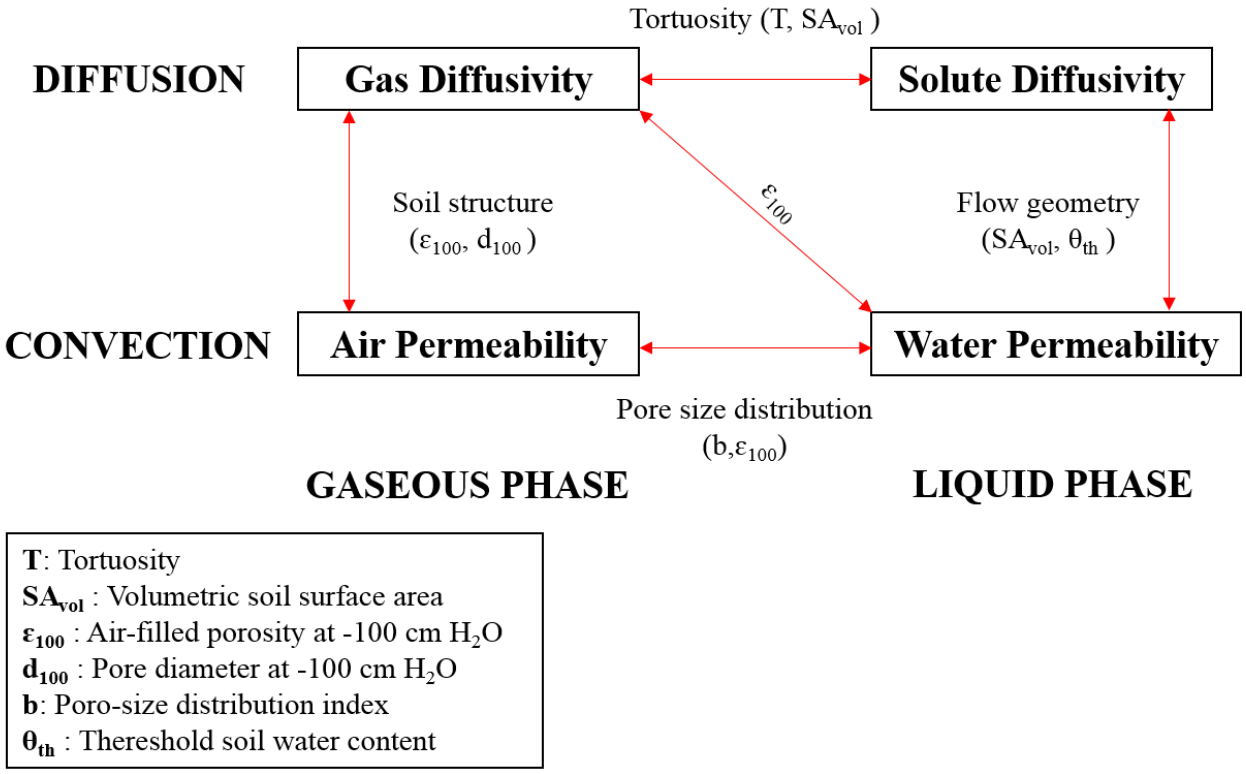

Source: Adapted from Moldrup et al. (2001)

Due to the complex fluid interaction into the soil, the focus on the present study is to approach only the diffusion part, by using software and algorithm that existent in other research areas, in order to investigate the soil tortuosity in two and three-dimensions.

Tortuosity has been calculated by two different methods in two and three-dimensions, respectively: i) the relation between geodesic and Euclidian (GER) distances and ii) Diffusion parameter (DP).

a) GER method: ijGeodesics plugin (ImageJ) allows to calculate geodesic distance, in other words, the longest distance between two points of object (i.e. porous canal length) from a binary image. This value allows calculating tortuosity based on the ratio between geodesic and Euclidian distances (i.e. the narrowest distance between two points) pixel by pixel (LEGLAND, 2011; SHANTI et al., 2014);

$$\text{Tortuosity} = \frac{\text{Geodesic distance}}{\text{Euclidian distance}} \qquad (14)$$

b) DP method: It was used “random-walk simulation” algorithm developed by Nakashima and Kamiya (2007). This algorithm package consists of three main programs, which were adapted to this soil study, all of which developed at Mathamatica version 5.2 environment.

1) Itrimming.nb: Segmentation of original image. It was replaced by CT-Analyser software, which can significantly reduce processing time;
2) Clabel.nb: Hoshen e Kopelman (1976) algorithm was implemented into this program to classify the set of porous according to the usual adjacent rule, which is commonly used in connectivity analysis (STAUFFER; AHARONY, 1994; IKEDA; NAKANO; NAKASHIMA, 2000). Porous voxel is only considered linked to other porous when having face contact;
3) Rwalk.nb: Random-walking into the set of porous through lattice walk of a simple cubic lattice (Figure 5). The program output is walkers mean-square displacement [15] (i.e. $<r^2>$) in function of τ (dimensionless integer time):

$$< r(\tau)^2 > = \frac{1}{n} \sum_{i=1}^{n} [((x_i(\tau) - (x_i(0))^2 + ((y_i(\tau) - (y_i(0))^2 + ((z_i(\tau) - (z_i(0))^2] \quad (15)$$

Figure 5: Random walk at a 3D system

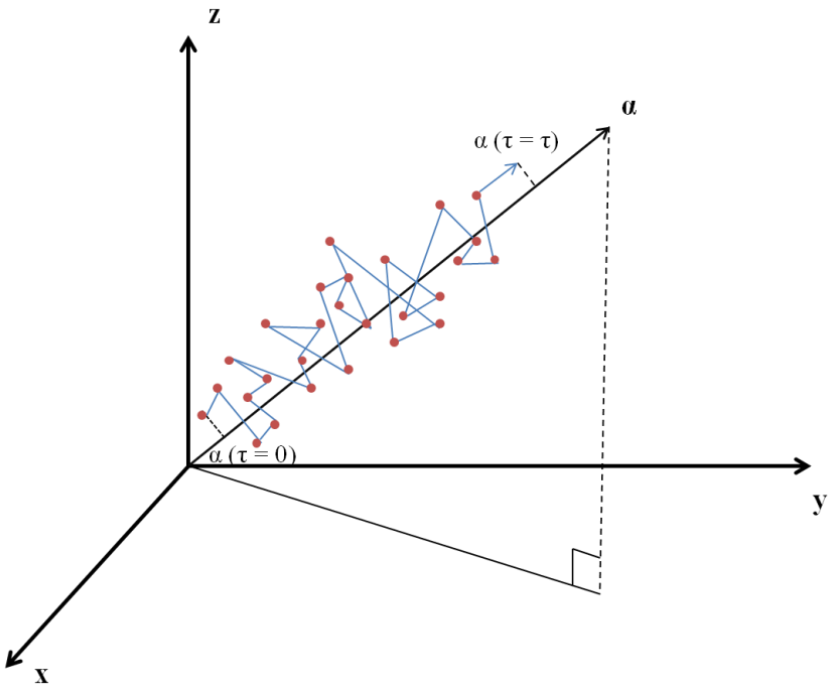

Source: Adapted from Nakashima et al. (2008)

Furthermore, the diffusion coefficient D of non-sorbent species in a three-dimensional isotropically porous media can be represent by:

$$D(t) = \frac{1}{6}\frac{d\langle r^2\rangle}{dt} \quad (16)$$

Thus, pore structure tortuosity can be defined as:

$$\text{Tortuosity} = \frac{D_0}{D(t)} = \frac{a^2}{\frac{d\langle r(\tau)\rangle^2}{d\tau}} \quad \text{as t and } \tau \to \infty \quad (17)$$

Where $\mathbf{D_0}$ is the initial diffusion coefficient and **a** represents the cubic lattice constant (i.e. CT voxel cubic size).

3. Results and discussion

3.1 Image quality

3.1.1 Tracer

The water movement into the soil was evaluated in different ways. The high-resolution X-ray microtomography and digital image processing allowed to detect and quantify the three phases (i.e. solid, liquid, gas). However, due to a series of factors related to technology available today, the image contrast (i.e. phase's difference) still need improvements. Consequently, artificial doping became necessary for studies of water into the soil, more specifically the interface contrast, e.g. potassium iodide (KI), calcium iodide (CaI) and sodium iodide (NaI) (PERRET et al., 1999). In general, KI is the most widely used dopant to improve contrast of the liquid interface, and solute transport into the soil macropores as well (KOESTEL; LARSBO, 2014). Therefore, the present study applied a 1% KI solution (VAZ et al., 2014) in a Brazilian savanna soil (Cerrado) (Figure 6) according to the histogram presented in Figure 7. Hence, KI (1%) is enough to produce good contrast (Figure 6a) and it allowed to detect water saturation with time (Figure 6b and c).

Figure 6: Visualization of a fixed region in the tomographic images showing variation over time. KI (1%) addition into the sample, drying process (dark blue) was accompanied by pore emergence (purple and black). The presence of residual moisture in soil is clearly observed over time: a) 0 hour; b) 26 hours and c) 370 hours.

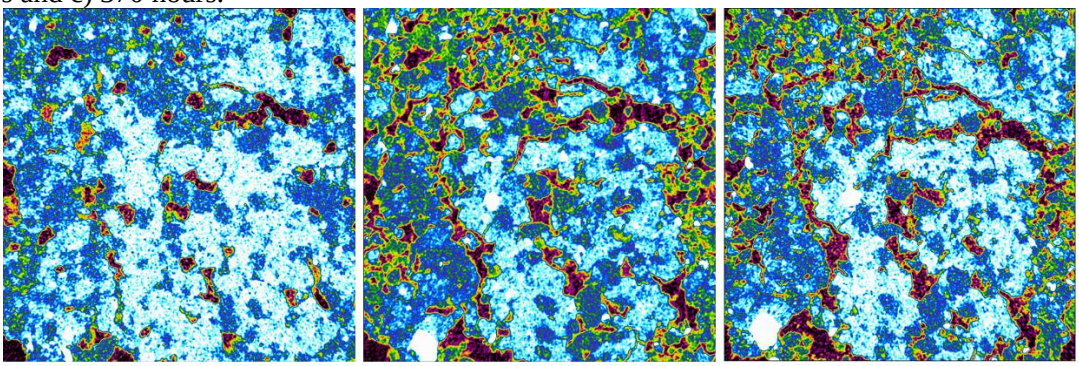

a **b** **c**

Source: Author (2016)

Figure 7: Soil microtomographic images normalized histogram at different saturation conditions. a) half-width difference among KI (1%), dry soil and KI (3%) b) The average difference between the two times

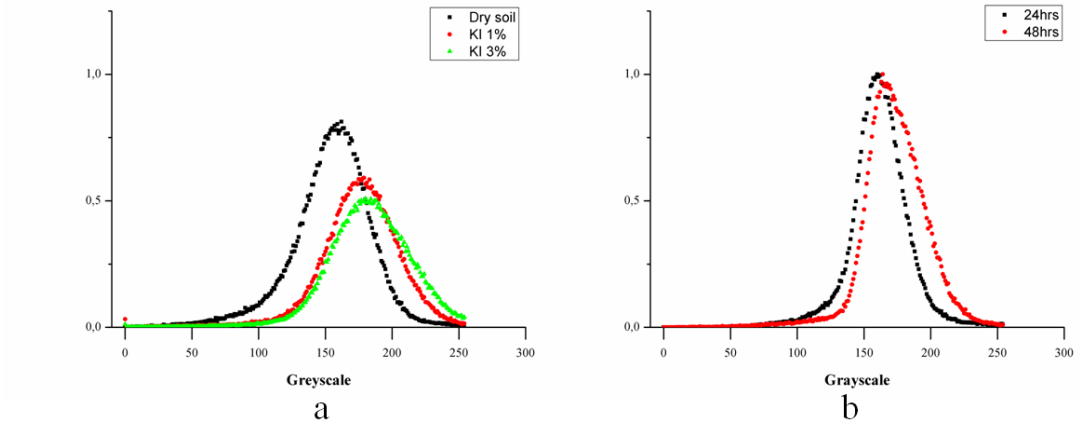

Source: Author (2016)

3.1.2 Digital image preprocessing

The main objective of the computed tomography technique is to provide a representation of the internal structure of an object in different planes (axial, coronal and sagittal). Nevertheless, considering the instrumental and computational limitations, in general, the reconstructed images carry artifacts, which compromise image quality and separation of the three soil phases. Thus, is essential to apply a pre-preprocessing procedure in digital images before conducting any analysis procedure.

Digital image preprocessing in this study consisted of two steps: 1) Filter and 2) Segmentation, which will be covered in details in the next topics.

3.1.2.1 Filter

The aim of applying filter consists of transformation technics to correct and highlight specific image characteristics. This study focuses on distinction of different soil phases. In this regard, it was selected eight types of available filter by ImageJ (FERREIRA; RASBAND, 2012). Within all options of filter (Figure 8), unsharp mask showed the appropriete result, highlighting the edges of it phase (Figure 8), the selection criteria was based on the nearest filter and original image histogram. Although this filter requires more theoretical backgrounds, in practice it enhances sharpness without noises, in comparison to other Fourier methods (SHEPPARD et al., 2004).

Figure 8: Image filtering using a) Convolution; b) Gaussian blur; c) Median; d) Mean; e) Minimum; f) Maximum; g) Unsharp mask and f) Variance.

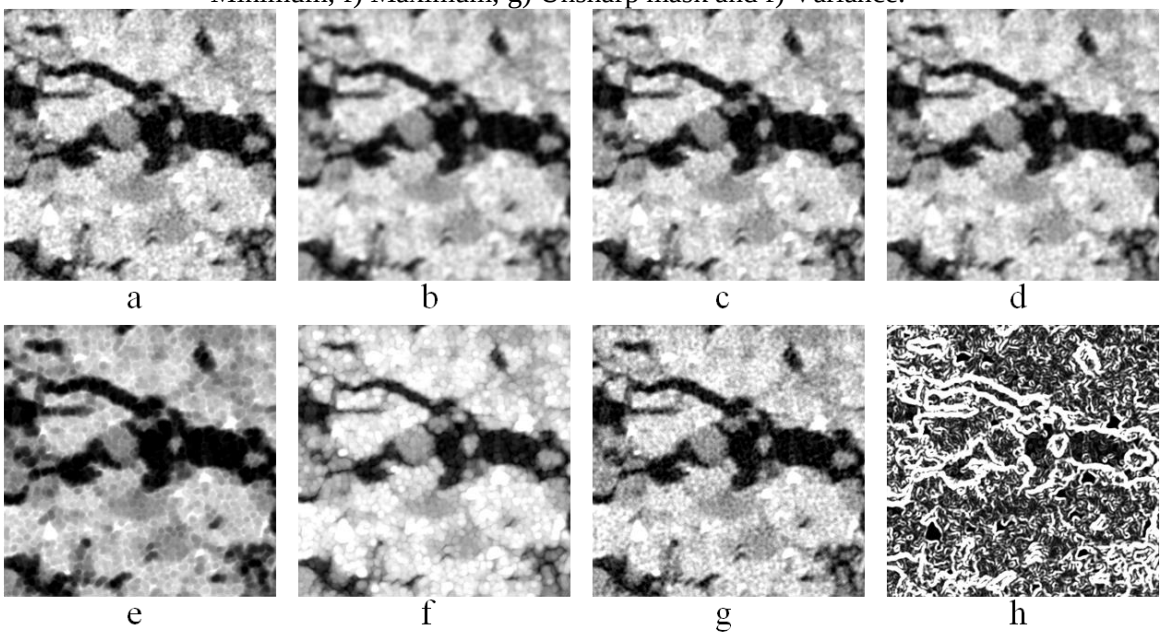

Source: Author (2016)

As filtering parameter, it was adopted σ equal to 1 (Gaussian smoothing) and unsharp mask equal to 0.6 as experimental references for this study. This former parameter influences image contrast and filtering power respectively (Figure 9).

Figure 9: Image grayscale histograms (a) for the original image (b) and after applying the unsharp mask filter (c).

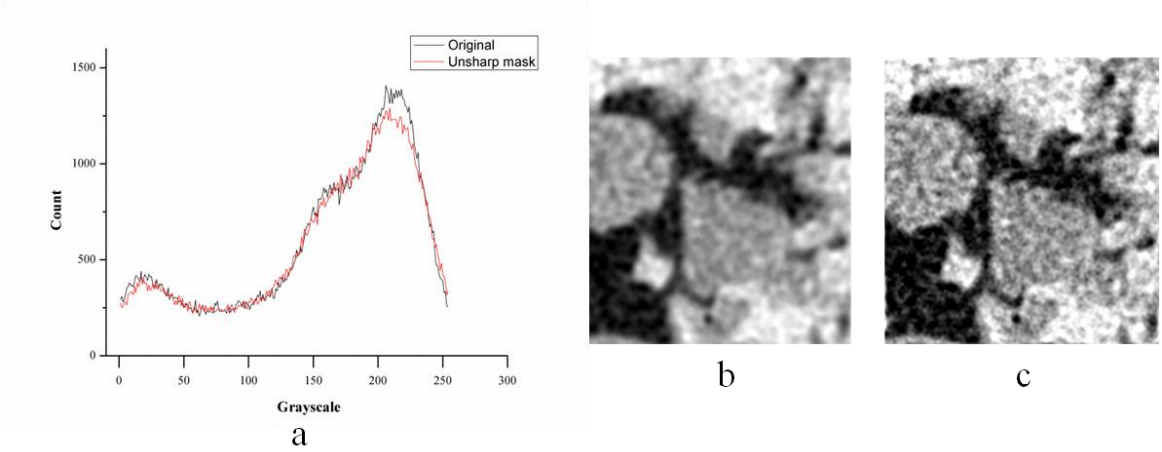

Source: Author (2016)

After image filtering, the soil's phases edges are now highlighted in histogram and, consequently, the image quality was improved.

3.1.2.2 Segmentation

Defining the limits between the different phases (threshold) is an important step in the segmentation process (GONZALEZ; WOODS, 2008). Otsu (1975) method, which was selected for this study, proved to be an excellent method to characterize fluid diffusive process into the soil (Figure 10) (Table 1). Vasquez et al. (2015) obtained good results with this method, using a new automatic framework to characterize the propagation of wetting front on microtomographic images.

Figure 10: Binarized soil microtomographic images using Otsu (b), Li (c); d) Mean (d), e) Percentile (e), Yen (f), and Triangle (g) methods; and the original grayscale image (a).

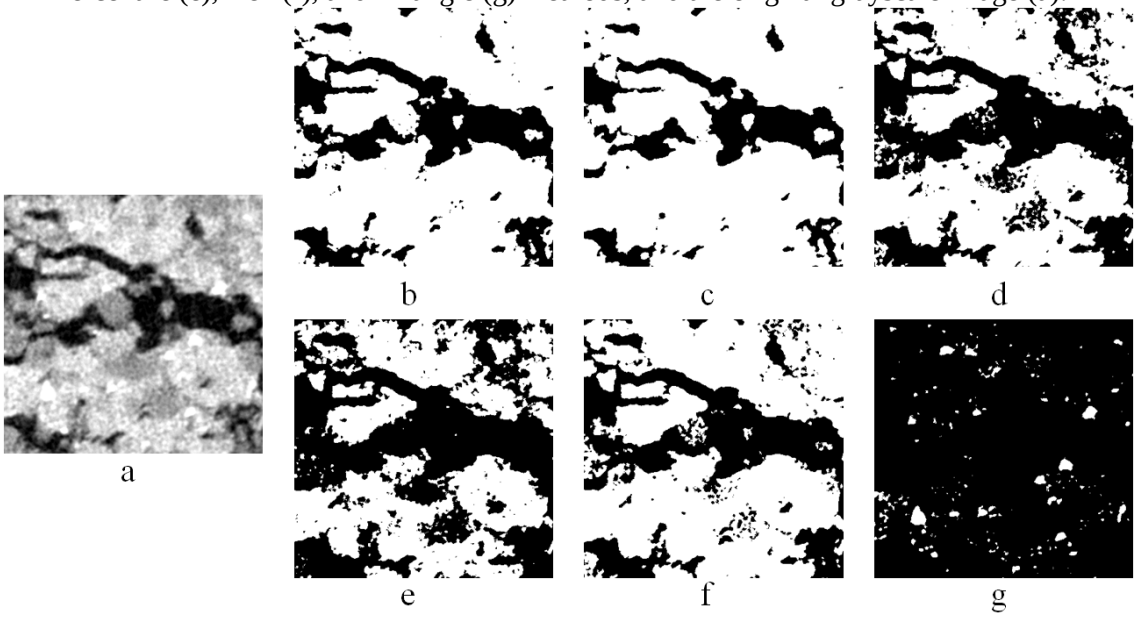

Source: Author (2016)

Table 1: Segmentation methods and porosity (%)

Methos	Porosity (%)
Manual	30.26
Otsu	29.88
Li	21.82
Mean	43.05
Percentile	49.74
Yen	34.12
Triangle	97.08

Source: Author (2016)

3.2 Physical parameters analysis

The present study generated a range of result related to dynamic process of fluid into the soil. Thus, in next topic this result will be discuss, from tomographic calibration curve to bird's-eye-view trajectory of soil's percolated porous.

3.2.1 Shannon Entropy

As stated by Shannon (1948) the entropy definition, the amount of information contained in a message, the more the information, the less entropy and vice versa. Therefore, the dynamic of the bit set representative of each phase is verified according to its entropy change.

It was verified in the first instant (Figure 11) a slight increase in the entropy value, i.e. a small decline in information quantities. Due to solution supply interruption and, at the same time adsorbed liquid was still seeking the new state of equilibrium within its media during 7 hours, i.e. filling the smallest porous for a period of 7 hours. However, around 26 hours after the supply interruption, it was marked a fast decrease of entropy. This means that there is an increase of information amount during this period of experiment, i.e. an intense process of evaporation in this stage. This phenomenon was observed by other parameters in this study. After this stage, the entropy stabilized into a constant value, which does not have relevant changes, due to the probability of each representative bits become similar. Therefore after this stage, the process can be differentiated only by its organization form, which will be better described in next topic.

Figure 11: ML entropy as a function of time.

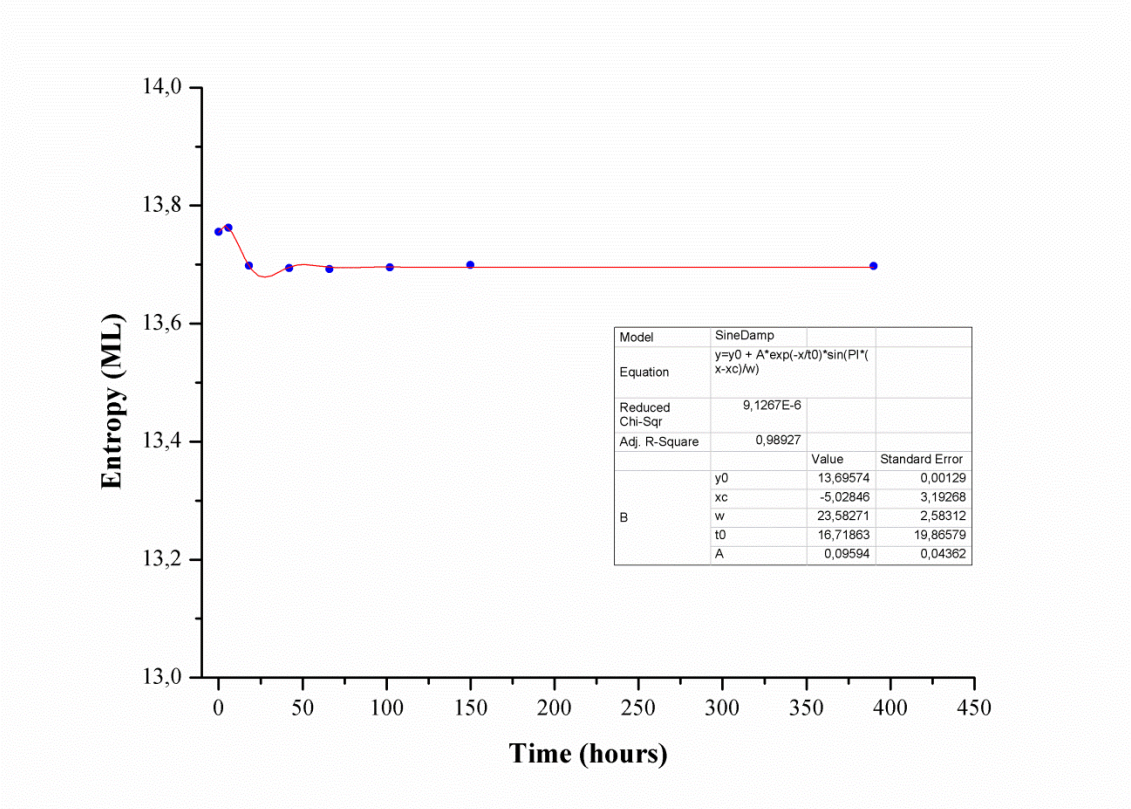

Source: Author (2016)

3.2.2 Soil water retention curve

The physical-hydrological propriety characterization may be done by different ways, among which the soil water retention curve. This relation reflects porous sizes distribution and, it was influenced mainly by factors like soil structure and organic material contents of the soil

In agreement with Pachepsky and Rawls et al. (1991), for the high potential (> - 10 KPa), i.e., the water amount retained in the soil is strongly affected by its structural stability, e.g. density and porosity; while for low potential (< - 1500 KPa), the properties like texture, organic matter content and mineralogy became predominant at water retention. Thus, for this study, water retention curve represents a tropical soil from Cerrado (Figure 12).

Figure 12: Soil water retention curve of clayey tropical soil from Cerrado. From the curve also was obtained other parameters: θ_{pmp} (permanent wilting point) (cm^3/ cm^3) is 22%; θ_{cc} (field capacity) (cm^3/ cm^3) is 26% and available water (WD) equal 4%.

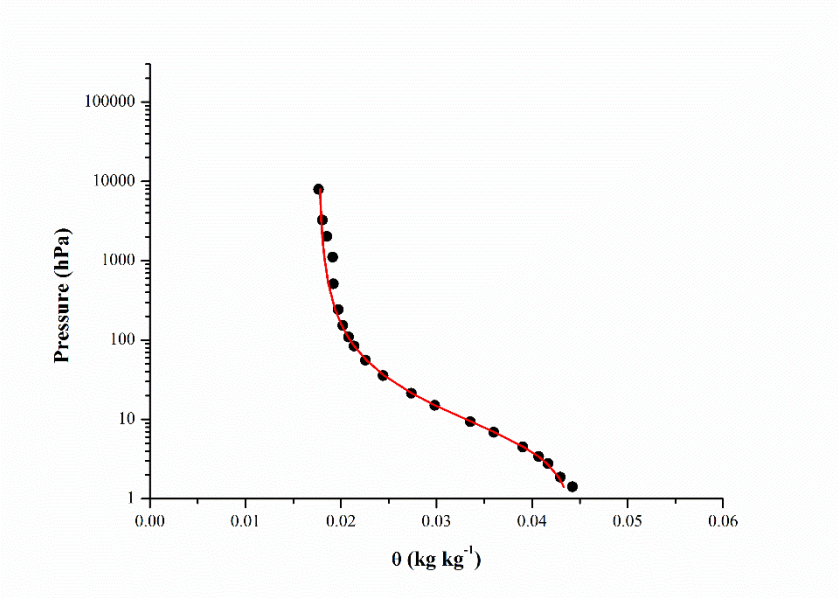

Source: Author (2016)

Currently, X-ray tomography application to evaluate the soil porous structure has become increasingly accessible. Consequently, other way to investigate physical-hydrological properties was opened. Rab et al. (2014) showed macropores quantification through microtomography in accordance with water retention curve in a loamy soil under pasture. It should also be considered that the water behavior into the soil is a dynamic process, therefore, water retention curve obtained is as reference to investigate inter-relation between physical-hydrological parameter of soils over time, allowing a better visualization of the general framework of water movement into the soil.

3.2.3 Soil porosity

The porosity quantification and porous size distribution are essential to understand the water movement into the soil. The porosity is the representative fraction of the soil where the air and solution dynamic process occur (HILLEL, 2007). Based on the soil water retention curve it is evident that there is good correlation between water potential and pore size distribution. (Figure 13) (KUTÍLEK; NIELSEN, 1994; LIBARDI, 2005).

Figure 13: Horizontal liner attenuation coefficient profiles at different times (a-2=0, b-2=48 and c-2=370 hours). The X-axis unit is µm.

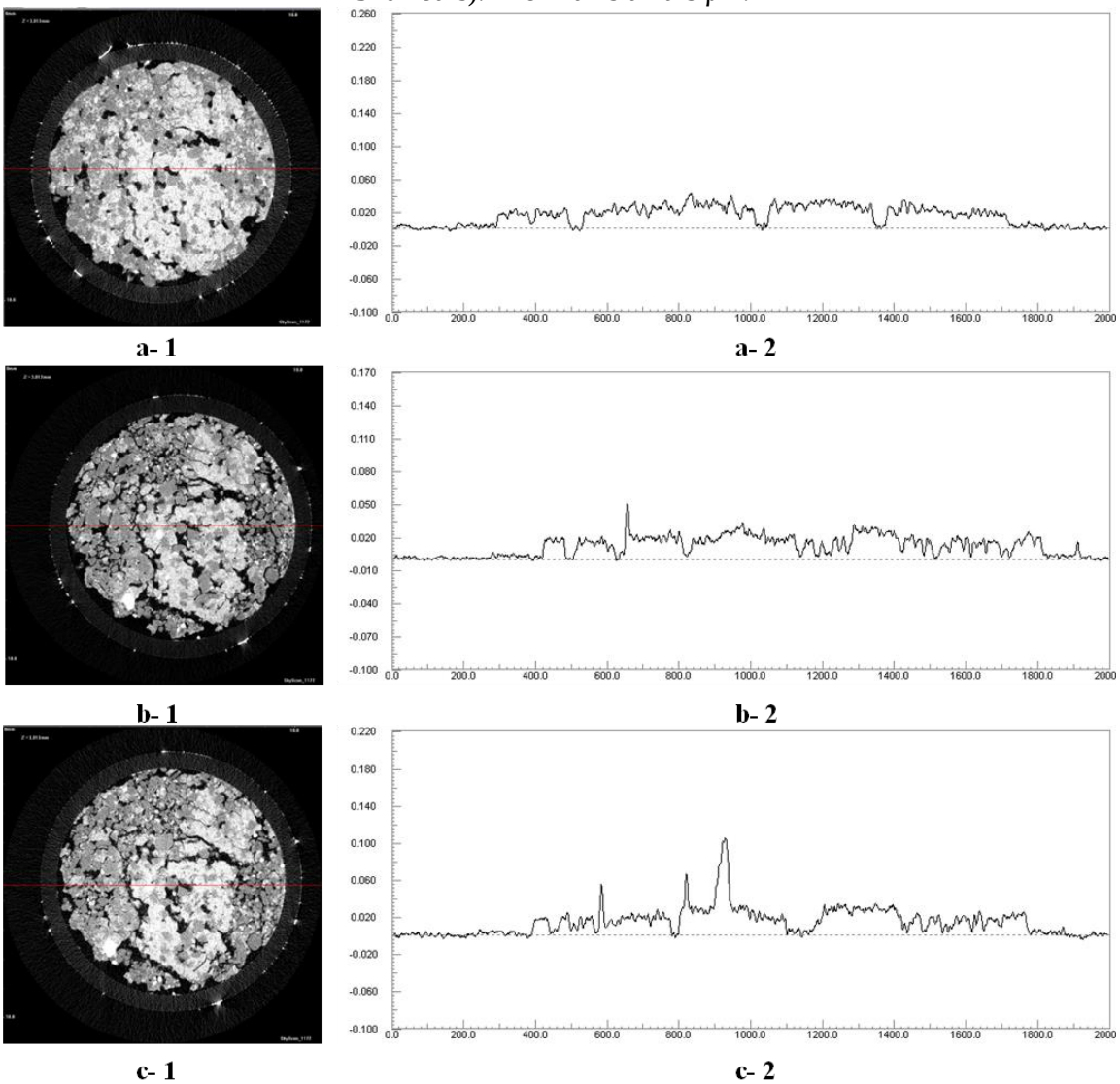

Source: Author (2016)

It should be noted that for future analysis, the movement effect of pore solution should be considered, instead of physical pore, due to the changes related to the image were

consequences of the solution during drying process, also considering hysteresis presence, as it is an irreversible system (Figure 14).

Over time, the solution evaporates, with an increase in the soil potential energy; therefore, the capillary strength dominates, obstructing the water from the sample, even with the increase of the size of empty spaces at the same image profile.

The most common model to estimate water retention curve is consisted by capillary tubes, which also aim to integrate hysteresis in the curve (KUTÍLEK; NIELSEN, 1994). The biggest advantage of microtomography used at soil analysis is the possibility to calculate the porous distribution or empty spaces, in a noninvasive and nondestructive way. Thus, based on preselected images it was calculated the distribution of empty space for each timeframe as from Feret diameter.

Figure 14: Experimental data that simulate indirectly the behavior of a SWRC model through Feret diameter, which is related to diameter of capillary tubes and Ψ

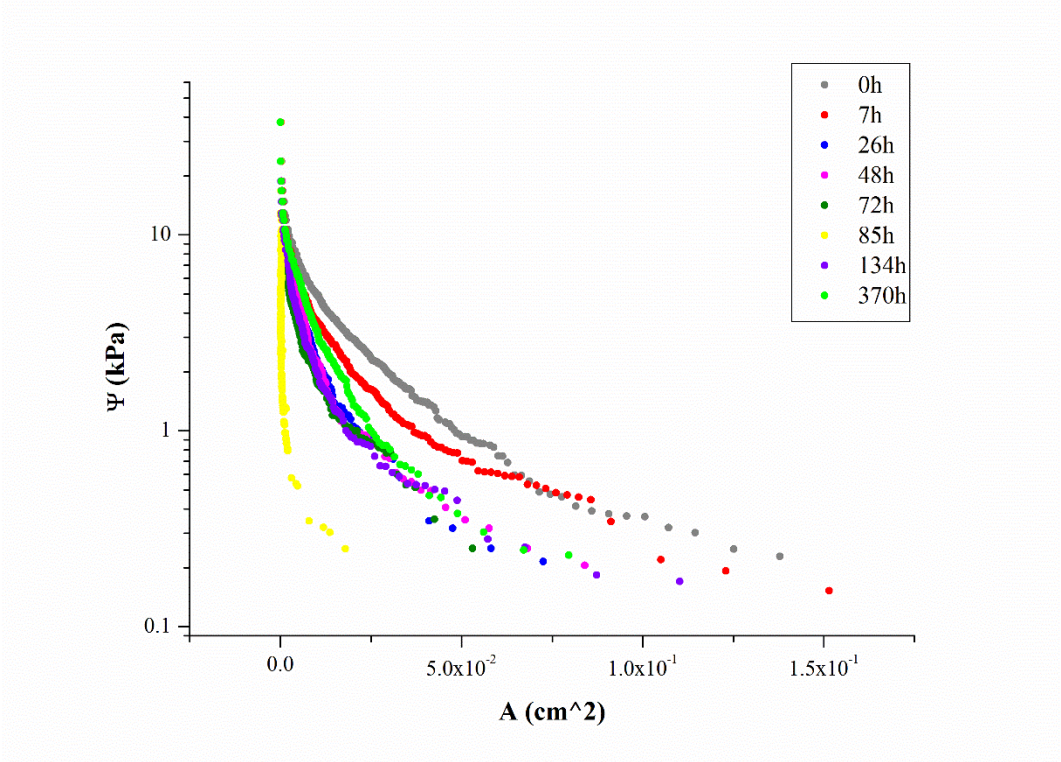

Source: Author (2016)

Thus, from the relation found between Feret diameter and frequency of each diameter it was obtained potential and empty space area curves with similar behavior to a water retention curve. In other words, based on microtomographic experimental data, it is possible to observe

the water transition at different physical states and, it is possible to elaborate a model capable of estimating the water retention curve that involves hysteresis, when process is inverted.

Although the temperature has been constant where the experiment was installed, it was verified a series of oscillation in frequency over time. This generates the possibility to investigate water into the soil at microscopy scale, in relation to time using X-ray microtomography. In general, experiments in this scale are possible with help of synchrotron radiation, showed in recent work by Udawatta et al. (2015), which quantified the consequences of mechanical compaction over porous geometry of two classes of soil aggregates at 9.6 µm.

Ma et al. (2015) evaluated microstructure and stability of two Urtisol aggregates submitted to wetting and drying cycle at 3.7 µm of resolution. Zong et al. (2015) has combined porosimeters and synchrotron X-ray microtomography to characterize pore structure of four types of soil at 3.7µm.

The use of X-ray microtomography based synchrotron radiation allows rapid image acquisition up to the nanometer scale. However, its access is still restricted when compared to benchtop X-ray microtomography system, which is increasingly popular at research environment. Thus, despite of the difficulty to characterize and quantify porosity of hydrodynamic process, it has become more accessible with benchtop X-ray microtomography.

Figure 15: X-ray microtomographic images with 5.48µm spatial resolution over time – (a) 0 hour; (b) 7 hour; (c) 26 hour; (d) 48 hour; (e) 72 hour; (f) 85 hour; (g) 134 hour and (h) 370 hour.

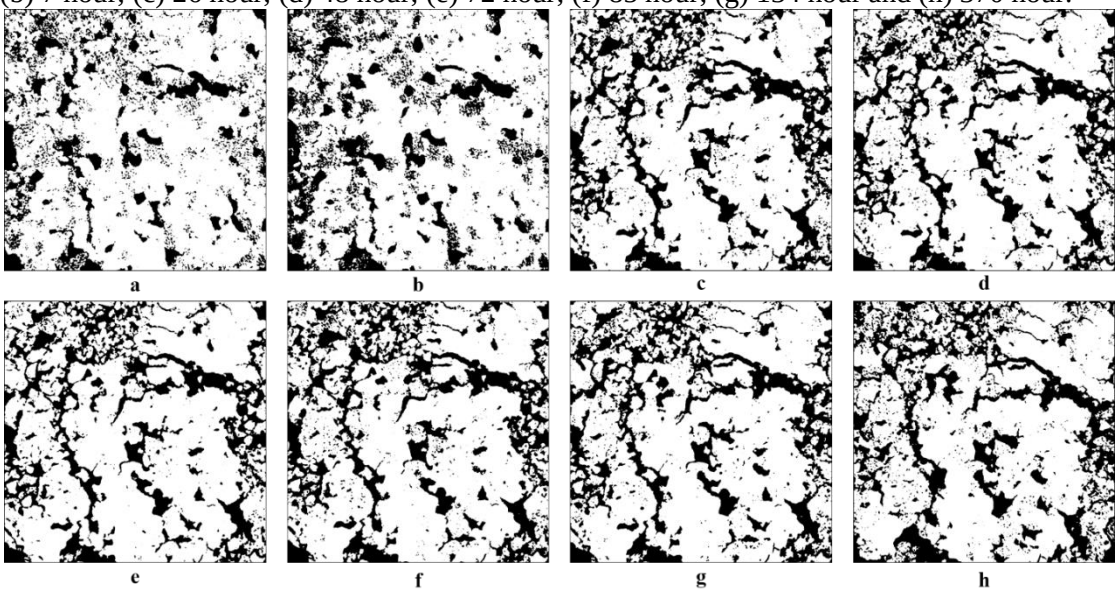

Source: Author (2016)

As time progresses, porosity (%) showed the following changes, i.e. black represents pore space; white is solid and liquid part of the sample (Figure 15 and 16).

a) 0 to 7 hours: There was a small decrease in the free-water porosity (Table 2). This can be attributed to water redistribution (internal drained) in the soil after finishing solution supply. For this reason, there was a slightly reduction, since solution is filling the smaller pores in the soil, searching for a new state of equilibrium;

b) 7 to 26 hours: There was a great increase in the free-water porosity, due to the evaporation, because of capillary rise forces and the gradient potential between soil and external environment;

c) 26 to 48 hours: Once more, water molecules are finding a new state of equilibrium, nevertheless, there was a decrease in its amplitude compared to the first moments;

d) 48 to 72 hours: Despite of a small increase in the Figure 16, which might be understood as the second stage of water redistribution into the soil, the capillary strength starts to act intensely from this interval;

e) 72 to 370 hours: In this stage, capillary strength and adsorption play a relevant role, i.e. it started to attract and "fix" water at solid particles, in such a way that water remains fixed at soil matrix (LIBARDI, 2012).

Table 2: Porosity free water (%)

Time (hour)	0	7	26	48	72	85	134	370
Total Porosity free water (%)	16.13	11.62	29.77	26.55	27.52	29.07	28.64	29.10

Source: Author (2016)

In addition, it was verified that the behavior of porous space into a sample at micrometer scale, observing that in this scale the interface soil-water was oscillatory (Figure 16). Consequently, experimental data was adjusted with a damped sine wave function (Eq. 18). From classic physics point of view, this function is identical to a damped harmonic oscillator (Figure 17), in other words, there is something within the system, which behaves like a pendulum around an equilibrium point and there is a frictional force that reduces its speed over time (TIPLER; MOSCA, 2011). Based on physical principles, water molecules into the soil should also look for an equilibrium position over time, taking into consideration some conditions that prevent water exiting to external environment, such as, temperature (internal energy), capillary strength, solute presence and adsorption effects.

$$y = y_0 + Ae^{-\frac{x}{t_0}} \sin\left(\pi \frac{x - x_c}{w}\right) \qquad (18)$$

where, **y** is the soil porosity (%), **A** is the system amplitude in relation to the time, t_0 is a constant of decay and **w** is the oscillator period.

Figure 16: 3D soil porosity (%) in function of time

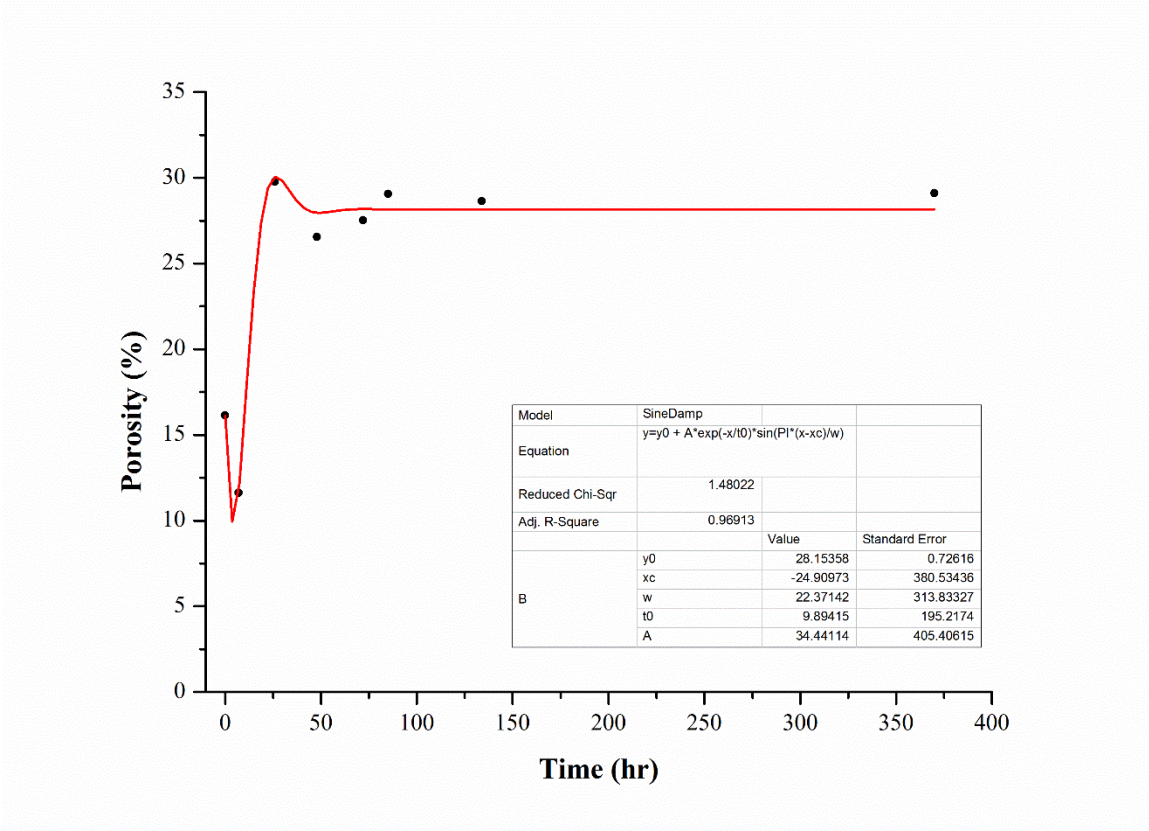

Source: Author (2016)

Consequently, "the drying front" should not occur uniform in the space, because this drying front can be irregular and discontinuous or it can be extended to other region associate with set of water into the small pores, i.e. the water is transported by capillary forces up to the evaporation surface (YANG et al., 2015; WILKINSON; WILLEMSEN, 1983; XU et al. 2008).

Figure 17: a) Representation of damped sine wave over time; b) Damped harmonic oscillator conducted by a restorative force, which is proportional to the displacement d that is time-dependent.

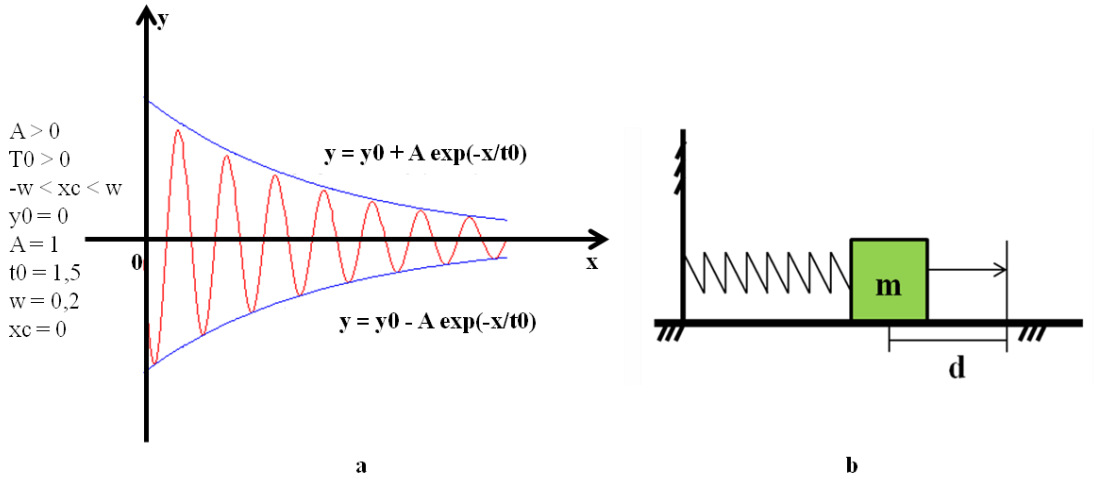

Source: Author (2016)

3.2.4 Lacunarity

Lacunarity refers to spatial pattern distribution of an object. For this study, it is interpreted as the sample fluid dynamic over time (Figure 18). The analysis of lacunarity can be divided in three parts: i) the "gliding box" size (ε); ii) the space fraction occupied by element and iii) the elemental spatial distribution (LUO; LIN, 2009). The maximum gliding box size was observed at time 0 (≈ 0.37), which represents the beginning of the evaporation process, where pore spaces are still filled with solution. Therefore, for time 0, the lacunarity is relatively lower than for other times. In addition, it is possible to observe that although the lacunarity value increased over time, it was characterized by an oscillating behavior. In other words, due to evaporation process from time to time subtly the fluid seeks to reestablish a new equilibrium point with the environment, through its redistribution after macrospores emptying is enabling an indirect estimative of preferential pathway into the soil (LIBARDI, 2005; CRUVINEL; BOTEGA, 2009).

According to Bear and Braester (1972), the REV (Representative Elementary Volume) is defined as the smallest volume, whose measurement variance became independent of its size. Although it hasn't been the focus of this study, it is possible to suggest that when lacunarity decays near 0 or reachs a constant value, the gliding box size is close to the REV (ZENG et al., 1996; LUO; LIN, 2009). Beside, the REV size can be estimated from ln (ε) > 0.7978.

In respect to the curve format, it indicates the degree of spatial heterogeneity and textural self-similarity behavior in practice for both fractal and random (VALOUS et al., 2010). The rapid lacunarity decrease means a random or homogeneous structure, which in general is

represented by a concave down format curve or a straight line (HIDALGO-OLGUÍN et al., 2015; ALLAIN; CLOITRE, 1991). Thus, the structure demonstrated a random behavior, i.e. under evaporation, percolation cluster is notably aleatory.

Figure 18: Lacunarity curve obtained from FracLac (ImageJ plugin), which represents random behavior. λ (lacunarity) versus ε (gliding box size).

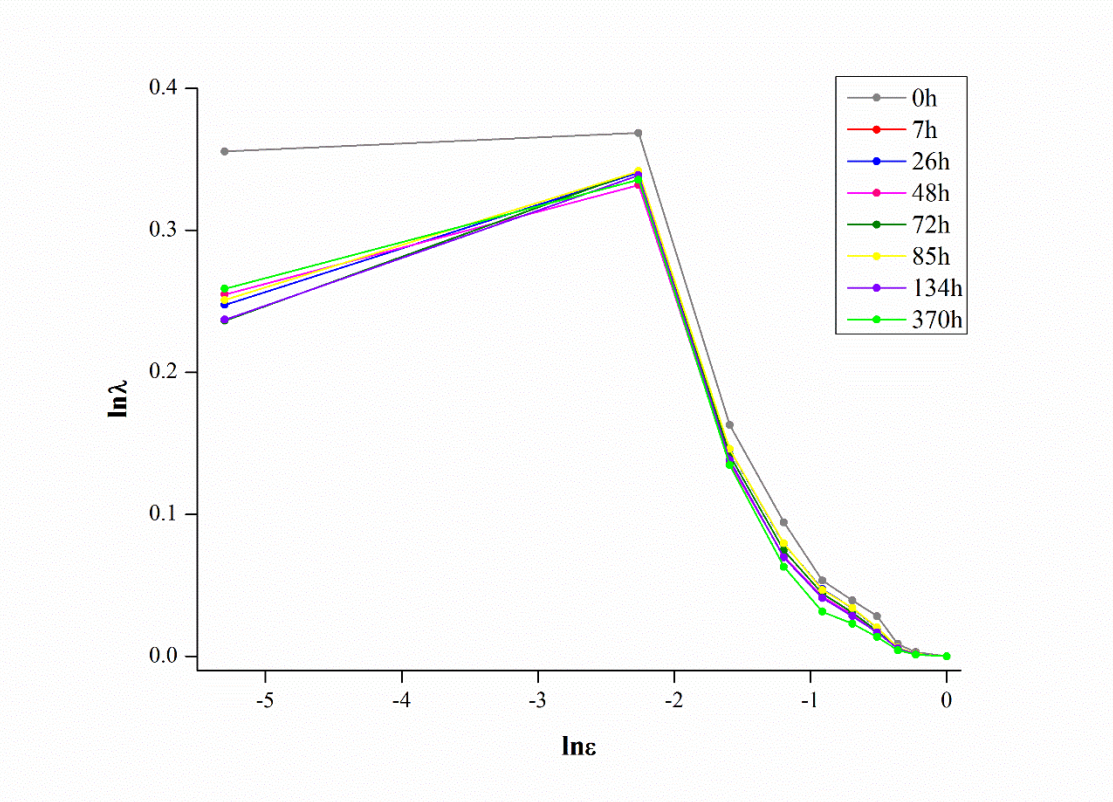

Source: Author (2016)

3.2.5 Euler-Poincaré number

Euler-Poincaré number is one of the most studied indicators, which characterizes connectivity into the object, due to the fact it is a dimensionless number and it is correlated only to the topology (format) of the object in study (RENARD; ALLARD, 2013). Thus, connectivity value between fluid and soil at three dimensions was calculated from this number.

During the 370 hours of experiment (Figure 19), Euler-Poincaré number decayed exponentially, nonetheless, it remained positive. This fact demonstrates that there was a significant increase of soil pore connectivity, due to macropores water loss. Therefore, as higher Euler-Poincaré number is, lower is the connectivity (NAVEED et al., 2016), while on the other hand, part of solution was attached to the soil particles surface, due to temperature and to the adhesive forces between solution and particles.

Thus, it can be generally assumed that the tomographic technique allows to estimate evaporation rate of soils, considering that there is a rigid control of the amount of provided solution, temperature and good spatial resolution, i.e. this part requires a more detailed numerical modeling to determine evaporation rate.

It is also important to point out that those experimental data were adjusted by an exponential curve with decaying rate of R_0 = -0.0794. In other words, this principle is similar to the exponential decay of a radioactive substance (half-life) that follows equation (19), allowing to estimate the time for the solution to reaches up to 50% loss of its original quantity. In this experiment such time was 8.7 hours, which seems reasonable and is in accordance with other results shown here.

$$t_{1/2} = -\frac{\ln 2}{R_0} \qquad (19)$$

Figure 19: Euler-Poincaré number exponential decay over time showing its stablization.

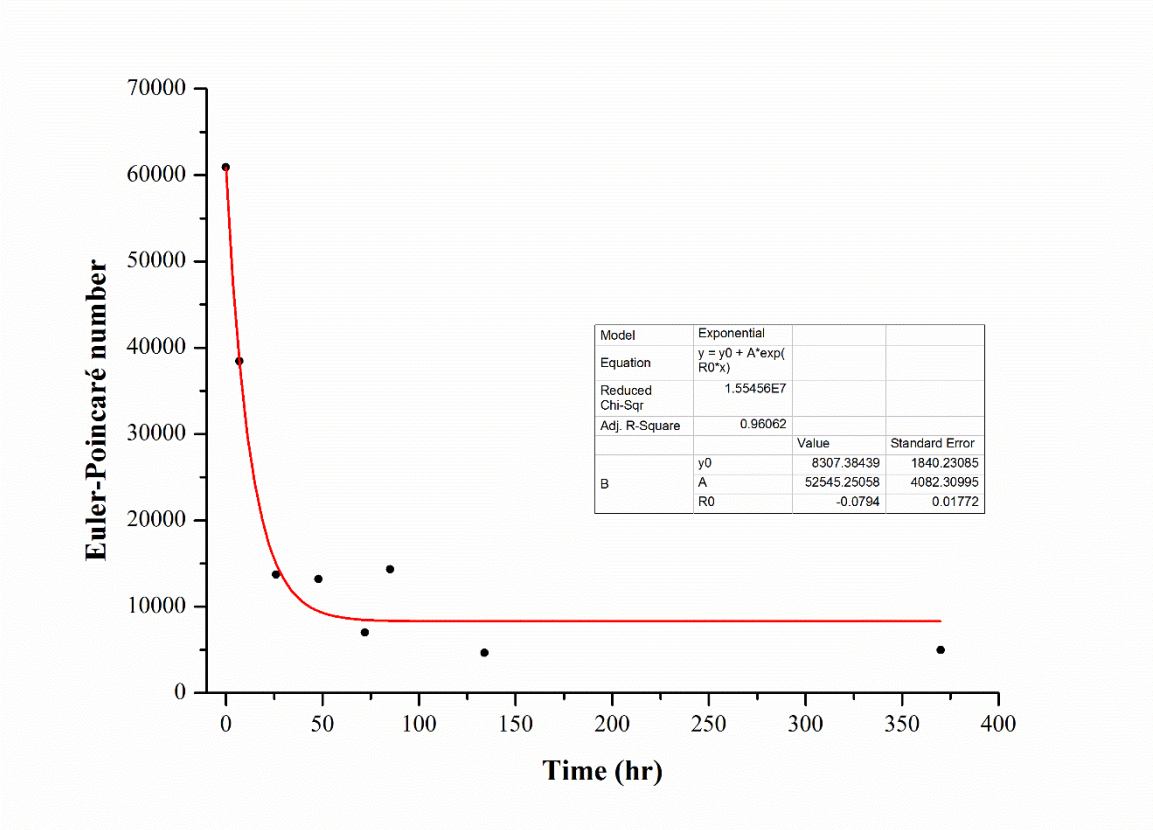

Source: Author (2016)

3.2.6 Degree of anisotropy

The degree of anisotropy (DA) is a measure that determines geometric characteristics in relation to a preferential alignment along an axis (ODGAARD, 1997). It is an important

measure to elucidate a significance of impact in the transport process (GARBOUT; MUNKHOLM; HANSEN, 2013). DA value shows the preferential orientation at macropores level, which directly influence water dynamic into the soil (DAL FERRO et al., 2014; NAVEED et al., 2016; BOTTINELLI ET et al., 2016).

In a first look, it was clearly verified an oscillating behavior. Therefore, the water dynamic into the soil (Figure 20) was adjusted by a damped sine equation, a typical harmonic oscillator in Physics (Figure 17).

Over time, the system energy decayed exponentially. In relation to the system's degree of anisotropy, it can be observed the following points: i) the system in focus seeks over time to attain a equilibrium state within the environment where it is inserted, through a wave function, i.e. harmonic oscillator (Eq 18); ii) over time, the internal energy (capillary and adsorption strength) and external energy (temperature, air moisture, human activities) are counterbalanced; iii) the sum of energy system (internal and external) affect the wave amplitude (DA – isotropic or anisotropic), i.e. towards to preferential direction of transport process.

Considering 0.43906 as cut-off point, it can be verified that at times 26 and 85 hours have similar DA values. At those times the system is more isotropic and probably may predominate the evaporation process, i.e. the solution output to the external environment. At 0, 7, 48, 72, 134, 390 hours they are more anisotropic, seeking rebalance of the solution with external environment with opening porous and its connection at x and y axis. Nevertheless, such hypothesis should be later investigated in more details.

Thus, DA showed to be a great indicator to study preferential direction of flux and when correlate to system energies, it will be possible to formulate a physical model to predict water dynamic into a porous media.

Figure 20: Degree of anisotropy (DA) over time fitted by damped harmonic oscillating function.

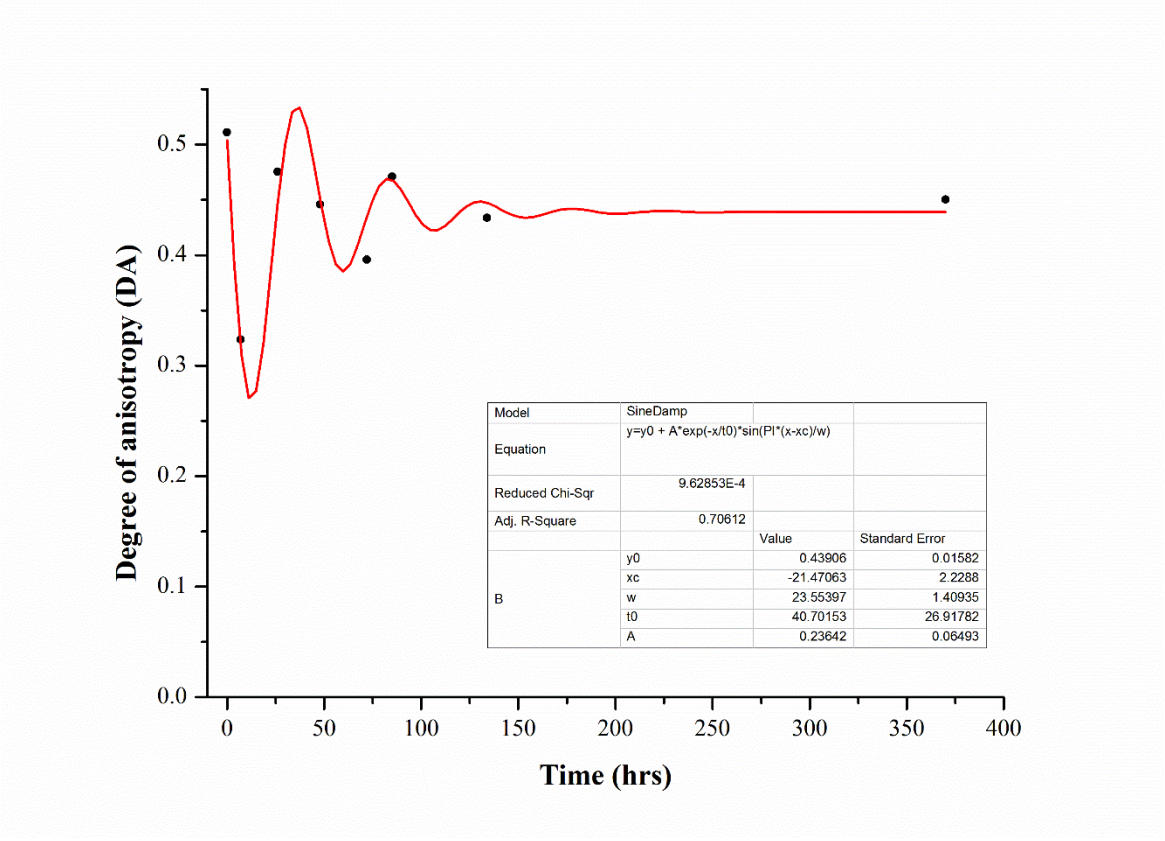

Source: Author (2016)

3.2.7 Tortuosity 2D

When the tortuosity value is near to one, the pathway will be rectilinear because the geodesic distance is equal to Euclidian distance. As furthest it is from 1 the more tortuous will be the pore network (PERRET et al., 1999). For this case, the values obtained over time oscillated between 1.104 and 1.127 (Figure 21), in other words, there was not displacement in straight line, but there was emergence and disappearance of cluster of points, suggesting slight tortuous connections at x and y plane (Figure 22).

In principle, it was expected that tortuosity calculation at two-dimensions could demonstrate the relation between the degree of anisotropy and the main axis propagation ate plane x and y. However, the real pathway of porous is extremely complex and sophisticate and being impossible to represent it in a sole tomographic image.

Even so, this first estimative has already demonstrated a possible relation between tortuosity 2D and degree of anisotropy, which show their similarities. Both are represented by damped sine equations, whose behavior is similar to porosity (%).

Figure 21: Tortuosity in two-dimensions over time.

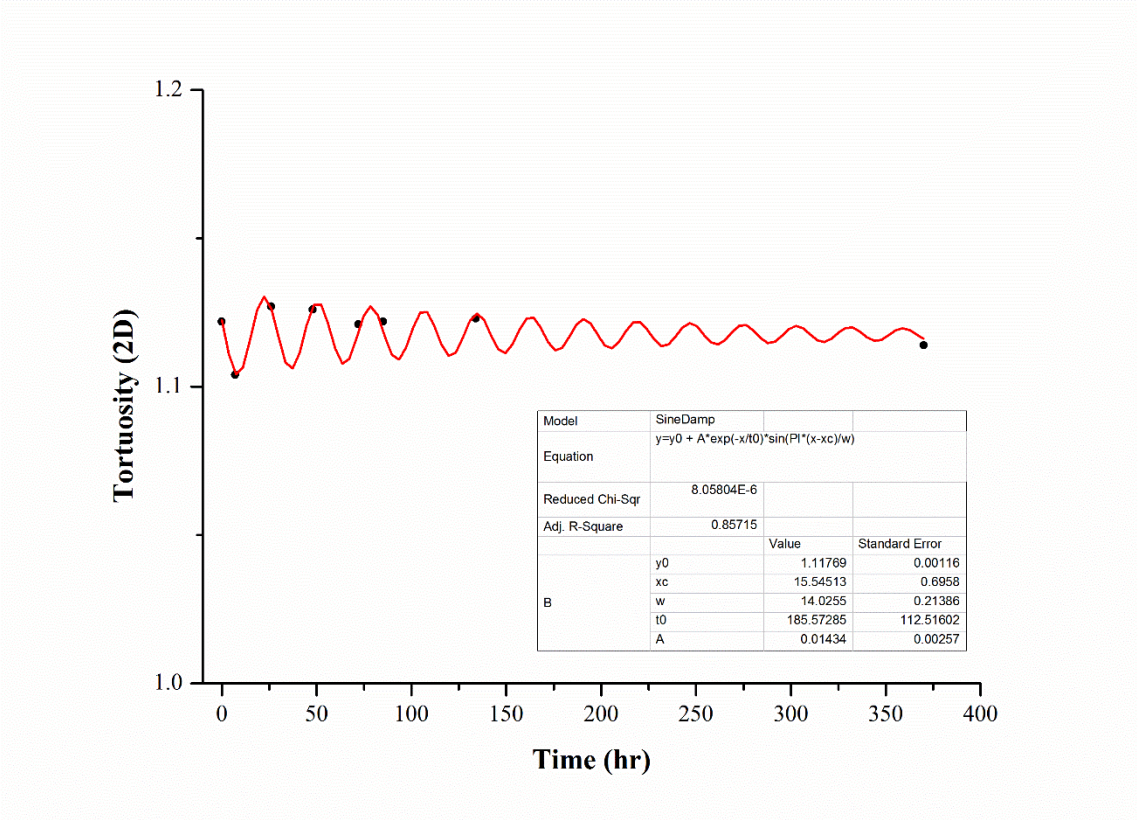

Source: Author (2016)

Figure 22: Tortuosity map in two-dimensions over time - a) 0h; b) 7h; c) 26h; d) 48h; e) 72 h; f) 85 h; g) 134h e h) 370h.

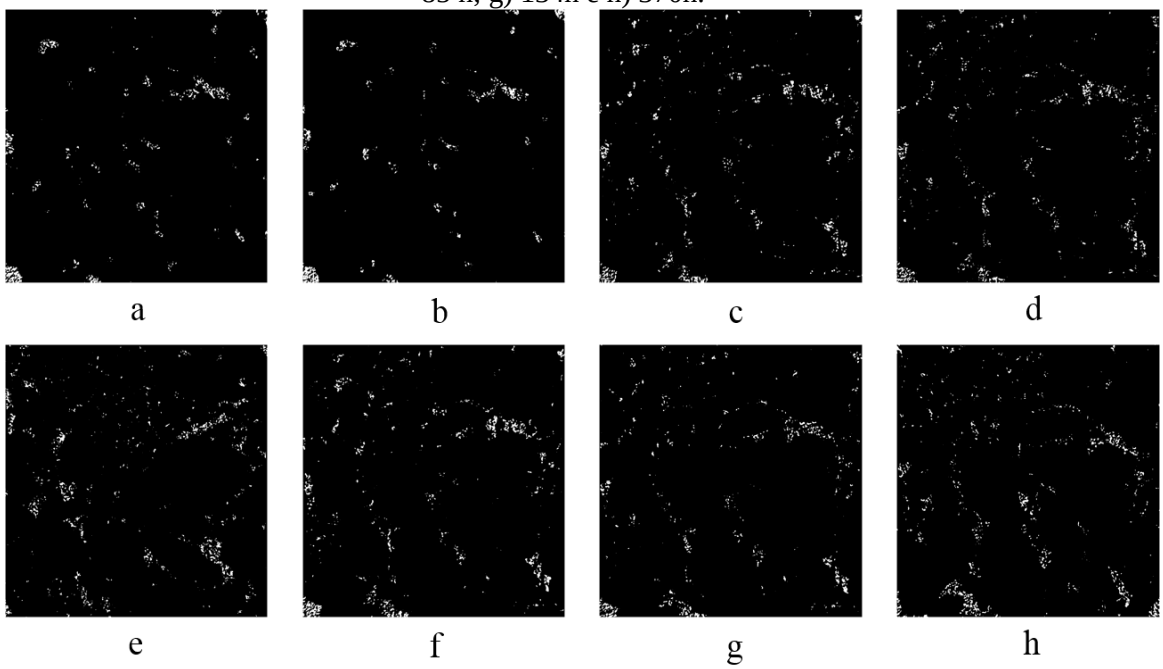

Source: Author (2016)

3.2.8 Tortuosity 3D

The random-walk simulation developed by Nakashima and Kamiya (2007) provides the mean-square displacement $<r^2>$ at x, y and z-axis over time. Besides $<r^2>$ we can calculate tortuosity and simulation of percolated pathway at each time. In the first moment, it was observed that among the analyzed parameters only tortuosity 3D (Figure 23) and Euler-Poincaré number (Figure 20) were ruled by exponential function. Their bases have opposite signs, which differentiate them, i.e. their curves were decreasing and increasing respectively. This observation is coherent, because when Euler-Poincaré number decreases, it means an increase of fluid's interaction quantity. Over time, there was macropores opening, which be came closer to each other and there was presence of fissure due to drying process, providing exchange of fluid into this media.

From the curves, it was possible to see the correlation between tortuosity 3D and Euler-Poincaré number, as well as their behavior, i.e. fluid interaction into the soil increases exponentially at beginning and the over time it stabilizes. Finally, the algorithm also provides a random-walk simulation (Figure 24) showing the restrict diffusion process into the soil.

Figure 23: Tortuosity 3D over time governed by an exponential equation.

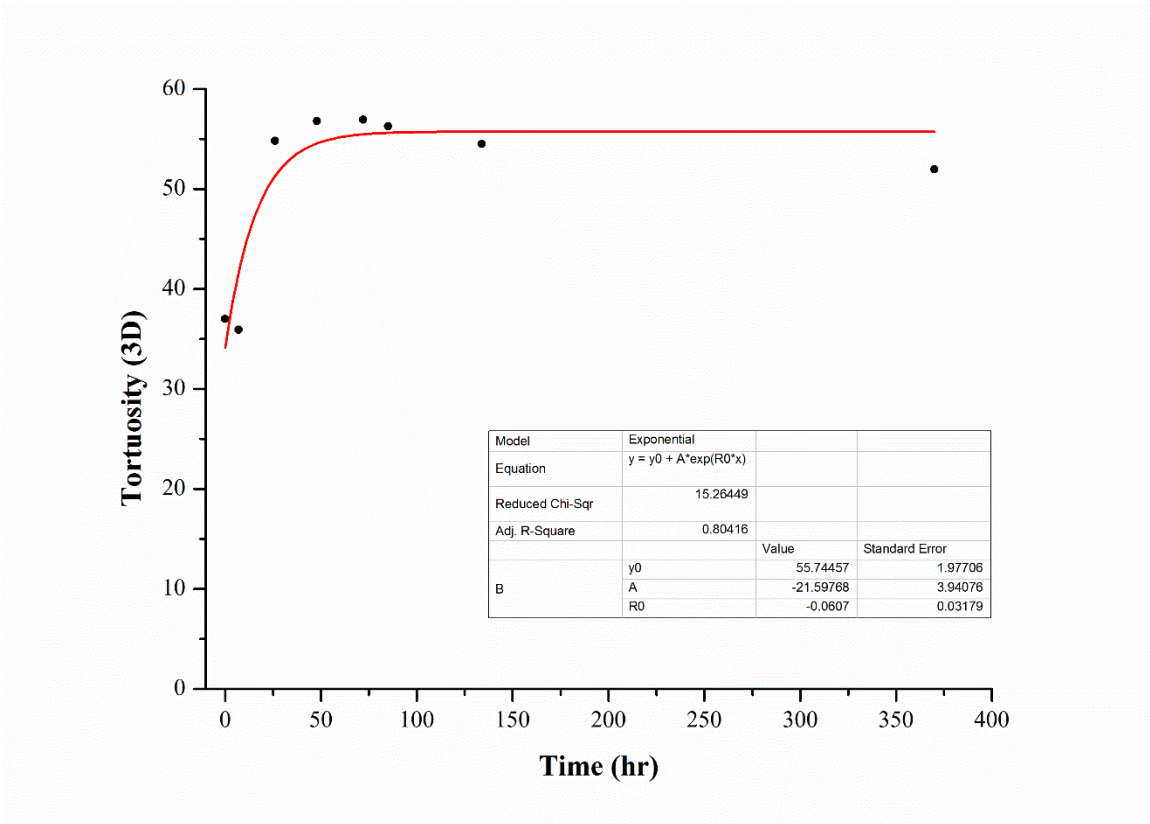

Source: Author (2016)

Figure 24: Example of a random-walk simulation at 150 hours after solution supply suspension. a) plane x-y b) plane y-z c) plane x-z and d) bird's-eye-view trajectory. The total time of steps is 400.00 with the start (τ = 0) and end (τ = 400,000). The initial position is marked by red point and final position by blue, where the random walk dominates at z-axis.

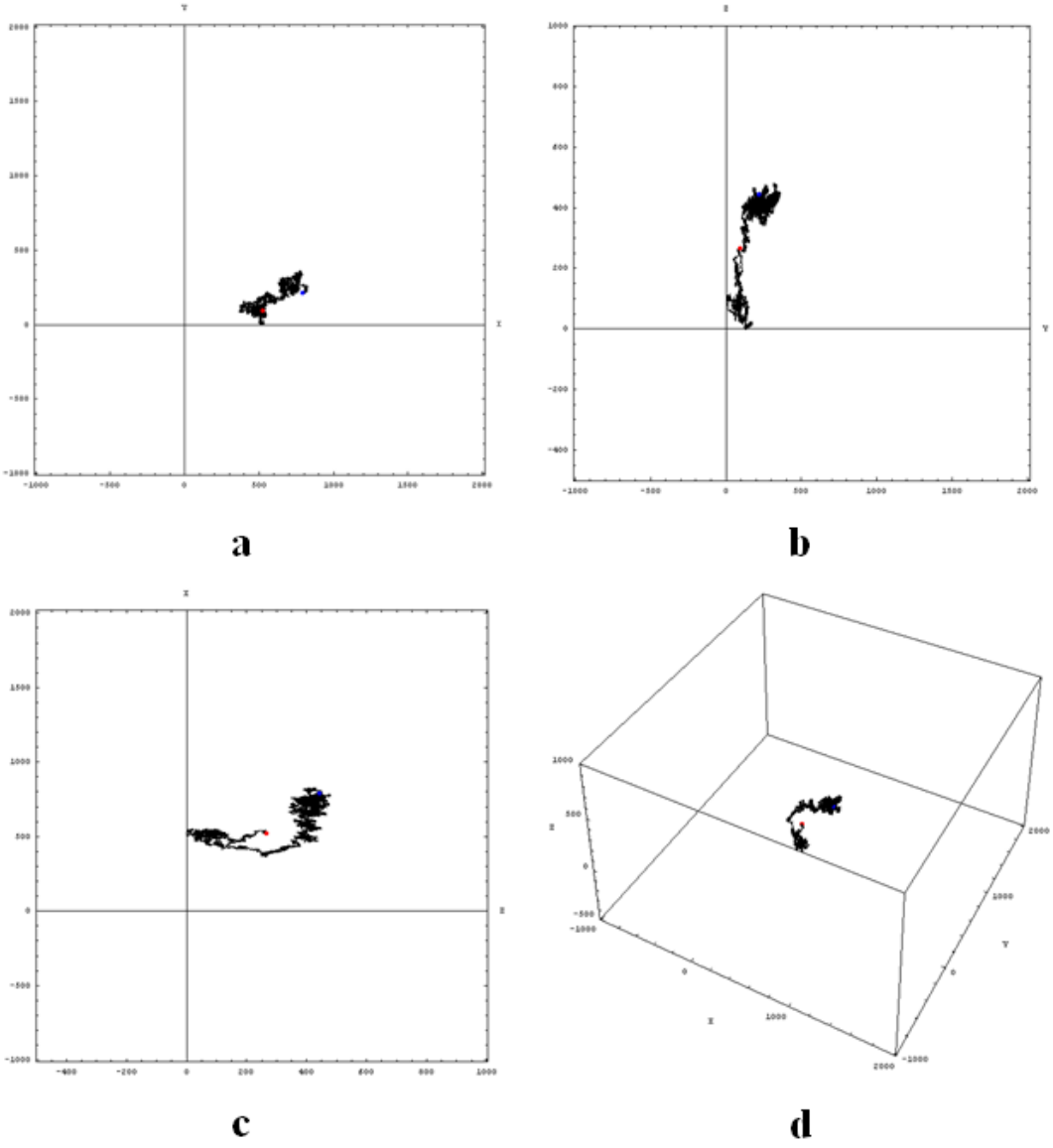

Source: Author (2016)

4. Conclusion

This study achieved its proposed goal, providing quantifying fluid dynamic into the soil over time, through X-ray microtomography. The major results were: **1)** 1% of KI solution was enough to produce contrast in the image and, allowed to detected changes in image at different saturation times; **2)** Among all filter options, the unsharp filter showed the best result, highlighting each phase edge; **3)** Otsu method showed excellent to characterize fluid diffusive process into the soil; **4)** The obtained entropy resulted in a general view about information quantity contained in the image; **5)** The obtained water retention curve was used as reference

to investigate inter-relation between all of physical-hydrological parameters of a tropical soil over time; **6)** It was proved that there was correlation between solution potential and the distribution of porous space's size from the microtomographic, as well as, the possibility to propose a desorption curve model from the image. In addition, it was verified a series of oscillations over time. This fact produces investigation possibility about water into the soil at micrometric scale in function over time of the "drying front"; **7)** Lacunarity is an excellent indicator of spatial heterogeneity degree. The structure of the present study demonstrated a random behavior, i.e. evaporation effect and solution pathway (percolated cluster) are both aleatory; **8)** Euler-Poincaré number decreased exponentially however remained positive. This demonstrates there was a significant increase in connectivity degree of the solid part of the soil sample, due to macropores's water loss; **9)** The timeframe required to the solution reaches up 50% of its initial value and it might be explained by the relation of half-life, i.e. the value was around 6.6 hours after suspension of solution supply in this case; **10)** DA showed itself as a strong indicator to study flux's preferential direction and, when it is correlated to participant energies in the system, it will be possible to provide physical models, capable to predict water dynamic into the soil; **11)** There was no displacement rectilinear in tortuosity 2D, however there was a group of points' emerging and disappearing suggesting slight tortuous connections at the plane x-y; **12)** There is a correlation between tortuosity 3D and Euler-Poincaré number, it fluid interaction in the media increased exponentially at the beginning and after it stabilized itself over time. It is possible to separate all parameters of this study at two groups, according to the analysis: i) Entropy, porosity (%), degree of anisotropy (DA) tortuosity and ii) Euler-Poincaré number and tortuosity 3D. Finally, this study provided new perspective about fluid dynamic, into the soil using an X-ray microtomography, providing several tools for future studies in the soil physics area.

5. Acknowledgements

We extend our thanks to CNPq and CAPES for financial support, to USP for its academic formation, to Embrapa, which made possible the use of its laboratories, developed technologies and technical support, and to Unesp for providing samples and technical support.

References

ALLAIN, C.; CLOITRE, M. Characterizing the lacunarity of random and deterministic fractal sets. **Physical Review A**, v. 44, n. 6, p. 3552-3558, 1991.

ARYA, L. M.; PARIS, J. F. A Physicoempirical model to predict the soil moisture characteristic from particle-size distribution and bulk density data. **Soil Science Society of America Journal**, v. 45, n. 6, p. 1023-1030, 1981.

BEAR, J.; BRAESTER, C. On The Flow of two immscible fluids in fractured porous media. **Developments in Soil Science**, v. 2, p. 177-202, 1972.

BOTTINELLI, N. et al. Macropores generated during shrinkage in two paddy soils using X-ray micro-computed tomography. **Geoderma**, v. 265, p. 78-86. 2016.

BRUNSELL, N. A. A Multiscale information theory approach to assess spatial–temporal variability of daily precipitation. **Journal of Hydrology**, v. 385, n. 1, p. 165-172, 2010.

CRESTANA, S. et al. Calibração e uso de um tomógrafo computadorizado em ciência do solo. **Revista brasileira de ciência do solo**, v. 16, n. 2, p. 161-167, 1992.

CRESTANA, S.; MASCARENHAS, S.; POZZI-MUCELLI, R. S. Static and dynamic three-dimensional studies of water in soil using computed tomographic scanning. **Soil Science**, v. 140, n. 5, p. 326-332, 1985.

CRUVINEL, P.; BOTEGA, L. **Caracterização física de caminhos preferenciais da água em solos agrícolas em ambiente de realidade virtual**. São Carlos: Embrapa Instrumentação Agropecuária, 2009. (Circular Técnica 48).

DAL FERRO, N.; SARTORI, L. et al**.** Soil macro-and microstructure as affected by different tillage systems and their effects on maize root growth. **Soil and Tillage Research**, v. 140, p. 55-65, 2014.

EMPRESA BRASILEIRA DE PESQUISA AGROPECUÁRIA. **Sistema brasileiro de classificação de solos**. 3. ed., Rio de Janeiro: Centro Nacional de Pesquisa de Solos, 2013.

FERREIRA, T.; RASBAND, W. **ImageJ user guide:** IJ1.46r. [S. l.: s.n.], 2012. Disponível em: <http://rsb. info. nih. gov/ij/docs/guide/user-guide.pdf>. Acesso em: 28 jun. 16.

GARBOUT, A.; MUNKHOLM, L. J.; HANSEN, S. B. Tillage effects on topsoil structural quality assessed using X-ray CT, soil cores and visual soil evaluation. **Soil and Tillage Research**, v. 128, p. 104-109, 2013.

GÉRAUD, Y.; SURMA, F.; MAZEROLLE, F. Porosity and fluid flow characterization of granite by capillary wetting using X-ray computed tomography. **Geological Society**, v. 215, n. 1, p. 95-105., 2003.

GERKE, K. M.; KARSANINA, M. V.; SKVORTSOVA, E. B. Description and reconstruction of the soil pore space using correlation functions. **Eurasian Soil Science**, v. 45, n. 9, p. 861-872, 2012.

GONZALEZ, R. C.; WOODS, R. E. **Digital image processing**. Nueva Jersey: Pearson, 2008.

HARRIGAN, T. P.; MANN, R. W. Characterization of microstructural anisotropy in orthotropic materials using a second rank tensor. **Journal of Materials Science**, v. 19, n. 3, p. 761-767, 1984.

HAUSSER, J.; STRIMMER, K. Entropy inference and the James-Stein estimator, with application to nonlinear gene association networks. **Journal of Machine Learning Research**, v. 10, n. Jul., p. 1469-1484, 2009.

HIDALGO-OLGUÍN, D. R.; CRUZ-VÁZQUEZ, R. O. et al. Lacunarity of Classical Site Percolation Spanning Clusters Built on Correlated Square Lattices. **Transport in Porous Media**, v. 107, n. 3, p. 717-729, 2015.

HILLEL, D. **Soil in the environment:** crucible of terrestrial life. Ney York: Academic Press, 2008.

HOSHEN, J.; KOPELMAN, R. Percolation and cluster distribution. I. Cluster multiple labeling technique and critical concentration algorithm. **Physical Review B**, v. 14, n. 8, p. 3438-3445, 1976.

IKEDA, S.; NAKANO, T.; NAKASHIMA, Y. Three-dimensional study on the interconnection and shape of crystals in a graphic granite by X-ray CT and image analysis. **Mineralogical Magazine**, v. 64, n. 5, p. 945-959, 2000.

JANZEN, A.; STEUBE, J. et al. Investigation of liquid flow morphology inside a structured packing using X-ray tomography. **Chemical Engineering Science**, v. 102, p. 451-460, 2013.

KARPERIEN, A. **FracLac v2.5d plug-in for ImageJ**. [S. l.]: Charles Sturt University, [201-?]. Disponível em: <http://rsbweb.nih.gov/ij/plugins/fraclac/fraclac.html>. Acesso em: 14 ago. 2016.

KATUWAL, S.; NORGAARD, T. et al. Linking air and water transport in intact soils to macropore characteristics inferred from X-ray computed tomography. **Geoderma**, v. 237, p. 9-20, 2015.

KOESTEL, J.; LARSBO, M. Imaging and quantification of preferential solute transport in soil macropores. **Water Resources Research**, v. 50, n. 5, p. 4357-4378, 2014.

KUTÍLEK, M.; NIELSEN, D. R**. Soil hydrology:** textbook for students of soil science, agriculture, forestry, geoecology, hydrology, geomorphology and other related disciplines. Cremlingen-Destedt: Catena-Verlag, 1994.

LANDRY, C. J.; KARPYN, Z. T.; AYALA, O. Relative permeability of homogenous- wet and mixed- wet porous media as determined by pore- scale lattice Boltzmann modeling. **Water Resources Research**, v. 50, n. 5, p. 3672-3689, 2014.

LARSBO, M..; KOESTEL, J.; JARVIS, N. Relations between macropore network characteristics and the degree of preferential solute transport. **Hydrology and Earth System Sciences**, v. 18, n. 12, p. 5255-5269, 2014.

LEGLAND, D. **Manuel d'utilisation du plugin «Geodesic» pour ImageJ**. [S l.: s.n], 2016. Disponível em: <http://download2.nust.na/pub4/sourceforge/i/ij/ijtools/ijTools/ijGeodesics/ijGeodesics-2014.02.21/ijGeodesicsManuel.pdf>. Acesso em: 3 ago. 2016.

LÉONARD, A. et al. Image analysis of X- ray microtomograms of soft materials during convective drying**. Journal of microscopy**, v. 212, n. 2, p. 197-204, 2003.

_____. Image analysis of X- ray microtomograms of soft materials during convective drying: 3D measurements. **Journal of microscopy**, v. 218, n. 3, p. 247-252, 2005.

_____. Measurement of shrinkage and cracks associated to convective drying of soft materials by X-ray microtomography. **Drying technology**, v. 22, n. 7, 1695-1708, 2004.

LIBARDI, P. L. **Dinâmica da água no solo**. São Paulo: Edusp, 2012.

LIN, H.. Linking principles of soil formation and flow regimes. **Journal of Hydrology**, v. 393, n. 1, p. 3-19, 2010.

LUO, L.; LIN, H. Lacunaity and Fractal Analyses of Soil Macropores and Preferencial Transport using Micro-X-Ray Computed Tomography. **Vardose Zone Journal**, v. 8, n. 1, p. 233-241, 2009.

MA, R. et al. Partial least squares regression for linking aggregate pore characteristics to the detachment of undisturbed soil by simulating concentrated flow in Ultisols (subtropical China). **Journal of Hydrology**, v. 524, p. 44-52, 2015.

MOHAMMADIAN, S.; GEISTLINGER, H.; VOGEL, H. J. Quantification of gas-phase trapping within the capillary fringe using computed microtomography. **Vadose Zone Journal**, v. 14, n. 5, 2015.

MOLDRUP, P.;OLESEN, T. et al. Tortuosity, diffusivity, and permeability in the soil liquid and gaseous phases. **Soil Science Society of America Journal**, v. 65, n. 3, p. 613-623, 2001.

MORAES, R. M. D. **Transporte de contaminantes inorgânicos em solos tropicais lateríticos: abordagem com cálculo fracionário**. 2013. 120 f. Tese (Doutorado) – Departamento de Engenharia Civil e Ambiental, Universidade de Brasília, Brasília, 2013.

NAIME, J. D. M.; SHINYA, V.; VAZ, C. **Programa para Estimativa Indireta da Curva de Retenção da Água no Solo**. São Carlos: Embrapa Instrumentação Agropecuária, 2004. Disponível em:<https://www.infoteca.cnptia.embrapa.br/bitstream/doc/30172/1/CT602004.pdf>. Acesso em: 3 ago. 2016.

NAKASHIMA, Y.; KAMIYA, S.. **Mathematica programs for the analysis of three-dimensional pore connectivity and anisotropic tortuosity of porous rocks using X-ray computed tomography image data**. Journal of Nuclear Science and Technology, 44, 1233-1247, 2007.

NAVEED, M. et al. Quantifying vertical stress transmission and compaction-induced soil structure using sensor mat and X-ray computed tomography. **Soil and Tillage Research**, v. 158, p. 110-122, 2016.

ODGAARD, A. Three-dimensional methods for quantification of cancellous bone architecture. **Bone**, v. 20, n. 4, 315-328, 1997.

ONODY, R. N.; CRESTANA, S. Experimental studies of the fingering phenomena in two dimensions and simulation using a modified invasion percolation model. **Journal of applied physics**, v. 78, n. 5, p. 2970-2976, 1995.

OTSU, N. **A Threshold selection method from gray-level histograms.** Automatica, 11, 23-27, 1975.

PACHEPSKY, Y. A.,; RAWLS, W. J. Accuracy and reliability of pedotransfer functions as affected by grouping soils. **Soil Science Society of America Journal**, v. 63, n. 6, p. 1748-1757, 1999.

PERRET, J. et al. Three-dimensional quantification of macropore networks in undisturbed soil cores. **Soil Science Society of America Journal**, v. 63, n. 6, p. 1530-1543, 1999.

PETH, S. Applications of microtomography in soils and sediments. **Developments in Soil Science**, v. 34, p. 73-101, 2010.

PLOTNICK, R. E. et al. Lacunarity analysis: a general technique for the analysis of spatial patterns. **Physical review E**, v. 53, p. 5461, 1996.

POT, V. et al. Three-dimensional distribution of water and air in soil pores: Comparison of two-phase two-relaxation-times lattice-Boltzmann and morphological model outputs with synchrotron X-ray computed tomography data. **Advances in Water Resources**, v. 84, p. 87-102, 2015.

RAB, M. A.; HALING, R. E., et al. Evaluation of X-ray computed tomography for quantifying macroporosity of loamy pasture soils. **Geoderma**, v. 213, p. 460-470, 2014.

RENARD, P.; ALLARD, D. Connectivity metrics for subsurface flow and transport. **Advances in Water Resources**, v. 51, p. 168-196, 2013.

ROZENBAUM, O.; BRUAND, A.; LE TRONG, E. Soil porosity resulting from the assemblage of silt grains with a clay phase: New perspectives related to utilization of X-ray synchrotron computed microtomography. **Comptes Rendus Geoscience**, v. 344, n. 10, p. 516-525, 2012.

SILVA, A. M. da. **Construção e uso de um tomógrafo com resolução micrométrica para aplicaçãoes em Ciências do Solo e do Ambiente**. 1997. 129 f. Tese (Doutorado) - Centro de Recursos Hídricos e Ecologia Aplicada, Escola de Engenharia de São Carlos, Universidade de São Paulo, São Carlos,1997.

SHANNON, C. E.. A mathematical theory of communication**. ACM SIGMOBILE Mobile Computing and Communications Review**, v. 5, n. 1, p. 3-55, 2001.

SHANTI, N. O. et al. X-ray micro-computed tomography and tortuosity calculations of percolating pore networks. **Acta Materialia**, v. 71, p. 126-135, 2014.

SHOKRI, N.; OR, D. Drying patterns of porous media containing wettability contrasts. **Journal of Colloid and Interface Science**, v. 391, p. 135-141, 2013.

BRUKER. **Morphometric parameters measured by Skyscan™ CTanalyser** software. [S. l.: s. n.], 2015. Disponível em: <http://bruker-microct.com/next/CTAn03.pdf>. Acesso em: 28 jun. 16.

STAUFFER, D.; AHARONY, A. **Introduction to percolation theory**. Boca Raton: CRC Press, 1994.

TIPLER, P. A.; MOSCA, G. P. Física para cientistas e engenheiros : física moderna: mecânica quântica, relatividade e a estrutura da matéria. Rio de Janeiro: LTC, 2011.

TRACY, S. R.; DALY, K. R. et al. Three- dimensional quantification of soil hydraulic properties using X- ray Computed Tomography and image- based modeling. **Water Resources Research**, v. 51, n. 2, p. 1006-1022, 2015.

TSENG, C. L. et al. Uso de tomógrafos de raios-x em resolução nanométrica e micrométrica para investigar, em duas e três dimensões, o espaço poroso e a água no interior de amostras de solo. In: SIMPÓSIO NACIONAL DE INSTRUMENTAÇÃO AGROPECUÁRIA, 2014, São Carlos. **Anais…** São Carlos: Embrapa Instrumentação, 2014. Disponível em: <https://ainfo.cnptia.embrapa.br/digital/bitstream/item/115646/1/341siagro-2014print01.pdf.>. Acesso em: 28 jun. 2016.

UDAWATTA, R. P. et al. Synchrotron microtomographic quantification of geometrical soil pore characteristics affected by compaction. In: EGU General Assembly Conference Abstracts, 2015, Vienna. **Proceedings…** Vienna: [s.n.], 2015. vol. 17, p. 1834).

VALOUS, N. A., SUN, D. W. et al. The Use of lacunarity for visual texture characterization of pre-sliced cooked pork ham surface intensities. **Food Research International**, v. 43, n. 1, p. 387-395, 2010.

VAN GENUCHTEN, M. T. A Closed-form equation for predicting the hydraulic conductivity of unsaturated soils. **Soil Science Society of America Journal**, v. 44, n. 5, p. 892-898, 1980.

VAZ, C. M. P. et al. Validation of the Arya and Paris water retention model for Brazilian soils. **Soil Science Society of America Journal**, v. 69, n. 3, p. 577-583, 2005.

VAZ, C. M. P. et al. Desempenho de 3 equipamentos da TDR para a medida da umidade e condutividade elétrica dos solos. In: CONGRESSO BRASILEIRO DE CIÊNCIA DO SOLO, Ribeirão Preto, 2003. **Anais...** Ribeirão Preto: [s.n.], 2003.

VAZ, C. M. P.; TULLER, M. et al. New perspectives for the application of high-resolution benchtop X-ray microCT for quantifying void, solid and liquid phases in soils. In: TEIXEIRA, W. G. et al. (Eds.). **Application of soil physics in environmental analysis**. [S.l.]: Springer, 2014. p. 261-281.

VAZ, C. M. et al. Evaluation of an advanced benchtop micro-computed tomography system for quantifying porosities and pore-size distributions of two Brazilian Oxisols**. Soil Science Society of America Journal**, v. 75, n. 3, p. 832-841, 2011.

VOGEL, H. J. Topological characterization of porous media**.** In: MECKE, K. R.; STOYAN, D. (Eds.). **Morphology of condensed matter:** physics and geometry of spatially complex systems. [S.l.]: Springer, 2002. p. 75-92.

WANG, W. Comparison of image segmentation methods in simulated 2D and 3D microtomographic images of soil aggregates. **Geoderma**, v. 162, n. 3, p. 231-241, 2011.

WILDENSCHILD, D.; SHEPPARD, A. P. X-ray imaging and analysis techniques for quantifying pore-scale structure and processes in subsurface porous medium systems. **Advances in Water Resources**, v. 51, p. 217-246, 2013.

WILKINSON, D.; WILLEMSEN, J. F. Invasion percolation: a new form of percolation theory**. Journal of Physics A: Mathematical and General**, v. 16, n. 14, p. 3365-3376, 1983.

WU, Y. et al. Local Shannon entropy measure with statistical tests for image randomness. **Information Sciences**, v. 222, p. 323-342, 2013.

YANG, F. et al. Visualization of water drying in porous materials by X- ray phase contrast imaging**. Journal of Microscopy**, v. 261, n. 1, p. 88-104, 2015.

YANG, F. et al. Extraction of pore-morphology and capillary pressure curves of porous media from synchrotron-based tomography data. **Scientific reports**, v. 5, 2015.

ZENG, Y. et al. Fractal dimension and lacunarity of bulk density determined with X-ray computed tomography**. Soil Science Society of America Journal**, v. 60, n. 6, p. 1718-1724, 1996.

ZHANG, X.; CRAWFORD, J. W.; YOUNG, I. M. A Lattice Boltzmann model for simulating water flow at pore scale in unsaturated soils. **Journal of Hydrology**, 538, p. 152-160, 2016.

ZONG, Y. et al. Characterizing soil pore structure using nitrogen adsorption, mercury intrusion porosimetry, and synchrotron-radiation-based X-ray computed microtomography techniques. **Journal of Soils and Sediments**, v. 15, n. 2, p. 302-312, 2015.

CHAPTER VII

Final Remarks

1. Main remarks

The intended purpose for this thesis was successfully reached, based on the results and analysis. It was possible to provide greater knowledge and quantification of the soil in the environment through nonconventional methods in order to investigate soil architecture submitted to different managements and to evaluate fluid dynamic within the soil along the time.

In Chapter 2, it was organized a tool package from nonconventional methods that allowed the investigation of soil architecture through correlation between the geometric, morphometric and energy characteristics. Two equipment were used: X-ray microtomography and gamma-ray granulometry analyzer; and eight software: Qualissolo, CT-Analyser, ImageJ, R, MASS, Dendrogram, Mathematica and CT-Vox.

In Chapter 3, part of the tools clearly showed the geometry difference among the six different types of management by means of physical parameters, such as porosity, form factor and lacunarity.

In Chapter 4, through soil physical analysis tool package of this work, it was possible to differentiate the soil managements in the morphometric scope and the structural differences were shown from the degree of anisotropy, Euler-Poincaré number, Shannon entropy. At the same time, it was possible to relate those structural parameters to the water retention curve and the tridimensional simulation of the soil managements.

In Chapter 5, with help of tool package of this work, it was possible to generate the soil management multifractal spectrum for two different planes and three depths. By using the spectrums, it was possible to perform the characterization of the management through entropy, degree of multifractality and asymmetry of the system.

In Chapter 6, it was quantified the behavior of a soil from the native forest of Cerrado during the drying process; the physical parameters used were: Shannon entropy, porosity, lacunarity, Euler-Poincaré number, degree of anisotropy and, tortuosity. These parameters allowed the characterization of the process and, by associating them with the 3D random-walk simulation it was obtained original results related to the fluid dynamic within the soil along the time.

From these results, it was verified that the hypothesis proposed in the beginning of this thesis were proved: the nonconventional methods are really important and efficient tools for soil study in the environment, for both evaluation of management recovery status and for the study of water dynamic within the soil along the time.

2. Suggestions for future research

Throughout this thesis elaboration, it was verified some interesting points to continue soil studies in the environment.

a) A better adaptation of form factor used in this study for tropical soil, i.e., more application to larger quantities of samples and different classes of Brazilian soil;
b) To associate lacunarity with REV (Representative Elementary Volume);
c) To extend the methods and physical parameters to deeper layers of the soil and, thus, having a better understanding of its interactions with the environment;
d) Further investigation of the oscillatory behavior of soil-water dynamic along the time in the energy scope through the multifractal analysis;
e) To investigate soil behavior at nanometric scale;
f) To correlate soil architecture, involving physical, chemical and biological properties through artificial neural network;
g) To associate the interactions that occur in the soil applying the dynamic system theory.

APPENDIX I

Application of computed tomography technique at micro and nanometric resolution in soil matrix investigation

TSENG, C. L., FERNANDES, C. P., MOREIRA, A. C., VAZ, C. P. M., CRESTANA, S.

APPLICATION OF COMPUTED TOMOGRAPHY TECHNIQUE AT MICRO AND NANOMETRIC RESOLUTION IN THE INVESTIGATION OF SOIL MATRIX

Tseng, C. L.[a], *Fernandes, C. P.* [b], *Moreira, A. C.* [b], *Vaz, C. P. M.* [c], *Crestana, S.*[c]

[a]Universidade de São Paulo, USP, Avenida Trabalhador São-carlense, 400, 13566-590, São Carlos, SP - Brazil

[b] Universidade Federal de Santa **Catarina**, UFSC, Laboratório de Meios Porosos e Propriedades Termofísicas-EMC, 88040-900, Florianópolis, SC - Brazil

[c]Embrapa Instrumentação, Rua Quinze de Novembro, 1452, Centro, 13560-970, São Carlos, SP - Brazil

---

ABSTRACT

The computadorized tomography techniques has shown as a useful tool to study soil in a nonconventional way. The present work looks investigate the soil matrix and to characterize the solid, liquid and gaseous phases in bi and three dimension. Recently, the advance of technology, the commercial high-resolution tomograph in laboratories has become more popular, facilitating an increase of soil study at micrometer scale; At nanometer scale, there is still a shortage for both: sample preparation technique and image acquisition. Due to this fact, it was explored two techniques of soil sample preparation and acquisition of the first image within the soil at 64nm. Finally, the preliminary results provided new opportunities for qualitative and quantitative soil studies using nonconventional technology, at multiscale - nanometer to micrometer.

Keywords: X-ray microtomography, x-ray nanotomography, porosity, water.

1. Introduction

The tomographic technique is a valuable tool for soil investigation, because it provides the measurements of several physical properties in a nonconventional way. In this context, it is highlighted X-ray micro and nanotomograph as advanced tools aiming this purpose.

Currently, the use of X-ray nanotomograph in soil researches is still scarce at international level (HELLIWELL et al., 2013), due to its cost and availability. Highlighting some works related to use of synchrotron to soil analysis, Peth et al. (2014) located the organic matter in soil aggregates; Rozenbaum, Bruand and Le Trong (2012) showed that x-ray sinchrotron microtomography can analyze with more precision, soil porosity of an assemblage of silt grain and clay phase than the conventional methods. In rock studies it can be found many research work; recently, Kuva et al. (2015) combined the same nanotomograph used in this study and SEM/EDS (Energy-dispersive X-ray spectroscopy) to analyze the effects of changes in monomineral samples.

Cnudde and Boone (2013) highlight some advantages of microtomophy such as to allow visualization and the tridimensional analysis of opaque objects as a non-destructive technique. However, it also presented some limitations such as, they still depend on operators for the image acquisition; there is noise and artefact presence in the image. It is believed that in a near future a series of limitations might be reduced as technology and research improve.

Vaz et al. (2011) used x-ray microtomograph – Skyscan (Belgium) to quantify the porosity and its distribution of two Brazilian soils. Wang et al. (2012) characterized intra-aggregated pores by using X-ray microtomograph; Hernández Zubeldia et al. (2015) from the University of Brasília used tomography image at micrometric scale, and dimensional automate cellular to generate artificial porous media; Dal Ferro and Morati (2015) combined microtomography and 3D print technology to evaluates reproduction and the hydraulic properties of original soil; Marchine (2015) used microtomography as one of the indicators, to investigate if the adopted soil management are recuperating. Passoni et al. (2015) characterized soil block's macroporous by using a medical microtomograph. Pires, et al. (2017) studied soil structural changes induced by tillage.

The aim of this present study was show the technique potential and a preliminary test of X-ray micro and nanotomography application for the visualization of dry and humid soil. It is expected with this work to provide new opportunities for qualitative and quantitative soil studies by using nonconventional technology at multiscale - nanometer to micrometer.

2. Material and method

2.1 Soil

The study area is characterized by remnant of Ilha Solteira Hydroelectric implantation, where it was removed 8.6m of soil in the 1960s, since then the area was exposed. The soil in study is a dystrophic Red Latossol (Brazilian oxisol), its textural class is sandy clay loam, highly weathered, it is a typical soil of equatorial clime (EMBRAPA, 2013).

2.2 Equipment

The projection acquisition and bi dimensional image reconstruction were made by using three equipment: 1) Xradia nanotomograph, model Ultra XRM-L200; 2) Xradia microtomograph, model Versa XRM-500, both belonging to Laboratório de Meios Porosos e Propriedades Termofísicas (LMPT), Federal University of Santa Catarina, campus Florianópolis; 3) Skyscan X-ray microtompgraph, model 1172 granted by Embrapa Instrumentation, São Carlos city.

2.3 Sample preparation methods

For the execution of the experiment in Xradia nanotomography, it was necessary the sample to go through a previous preparation. This step is divided into two lines of preparation: **I** – laser ablation and **II** – soil grain selection. Line **I** consisted of two steps: 1) gluing the soil sample to the sample holder with cyanoacrylate (Super Glue); 2) insertion of sample in the equipment and starting laser ablation three times until it reaches “stair” format (Figure 1), which are considered mechanically more resistant than a simple cylinder. Line **II** also consisted of two steps: 1) soil sieving by using a 2mm sieve and 2) gluing of soil into tomograph sample holder.

Figure 1 - Soil sample “stair” format

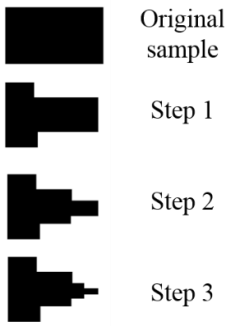

Source: Author (2014)

In the multiscale analysis it was used Xradia microtomograph, model Versa XRM-500. The samples were collected with acrylic tube and sealed with plastic film, and finally they were fitted directly in sample holder in the tomograph.

2.4 Parameter setting for image acquisition and reconstruction

In the case of nanotomograph, the radiation source was 40kV and 1.2kW. It was selected the region of interest in the soil sample, then it was performed the alignment and 40 images with 120 seconds of exposure time as reference measurement were acquired; finally, the sample was replaced to acquire tomographic projections. The projections reconstruction were performed from a reference image with best beam hardening factor and smoothing setting, thus obtaining the images with 64nm resolution.

In the Xradia microtomograph, model Versa XRM-500, initially, it was necessary to perform thermal stabilization of the X-ray tube for approximately one hour obtaining 1601 reference projections with sample alignment; the magnifying optical lens, spatial resolution, beam hardening filter, transmission and exposure rate were adjusted according to each sample. In the end, the X-ray source was configured to 40kV and 74μA for all experiment. The image reconstruction was the same as of the nanotomographic.

3. Results and discussion

3.1 Technique potential

The multiscale experiment (Figure 2) was intended to verify the technique potential, as well as to choose the more adequate resolution for qualitative and quantitative analysis, considering equipment, image quality and acquisition time. Therefore, the two best resolution that represent the morphology within the soil were 2 μm obtained at UFSC and 5 μm from Embrapa Instrumentation.

It was observed at microtomography that the presence of pure water (Figure 2) within the soil is not so evident visually as the potassium iodide solution (KI, 1%) (Figure 2). Therefore, it was more advantageous the insertion of KI solution in the soil sample differentiating the different phases that are in contact with the part solid of soil matrix. Although other studies are still necessary, it is possible to anticipate that the results are very important for the qualitative and quantitative research in respect to porous space and its occupation with water and solutes.

Figure 2 - Sample morphological analysis of a dried soil at multiscale: 24µm; 5µm e 2µm and wetted soil with water and KI 1% solution.

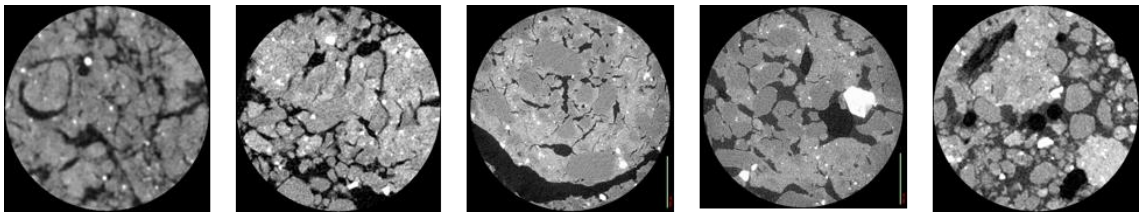

Source: Author (2014)

3.2 Sample preparation for x-ray nanotomography

3.2.1 Laser ablation

Although the sample preparation method used for the nanotomograph has possibly caused disturbances in the soil, it was possible to obtain tomographic images with 64 nanometers resolution, showing the presence of empty space within the aggregate or solid structure (Figure 3). It may be considered as a promising result, as they certainly involve phenomenon that haven't been explored yet in this scale of experimentation. For the next step, a more natural soil sample will be prepared, in order to investigate it by using nanotomograph.

Figure 3 - Morphologic analysis at different planes of a soil nanotomography with 64nm of spatial resolution and 3D reconstruction

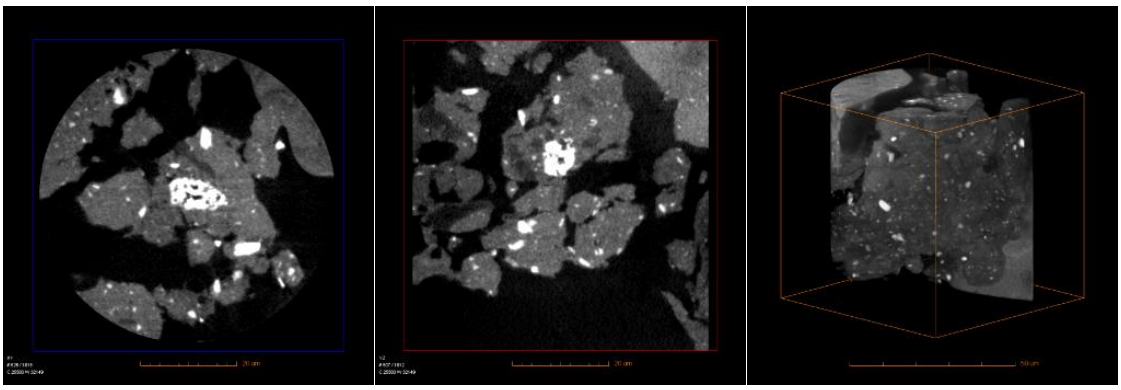

Source: Author (2014)

3.2.2 Natural soil grain

By opting for image acquisition with natural soil grain, it was preserved the integrity of it; by the image, it was detected that in the soil grain there are empty space, i.e., there is presence of pores in some nanometers and also there is was bottleneck and connection between the

empty spaces. This is an original result for the Soil Science, as from this observation, a new frontier is open to investigate phenomenon that haven't been explored in this scale.

Figure 4 - Soil nanotomography morphological analysis at plane XY and YZ with 64 nm spatial resolution

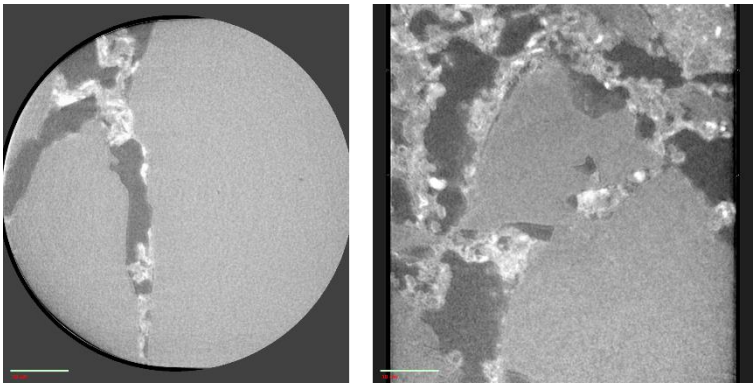

Source: Author (2014)

4. Final consideration

The aim of this study was successfully reached, it can be concluded that X-ray micro and nanotomography are tools with great potential to investigate the soil's three phases; in term of sample preparation for X-ray nanotomography, it is better if the soil is not deformed instead of using laser ablation to disturb its originality. Therefore, the preliminary results brought new opportunities to soil study using nonconventional techniques at multiscale in a satisfactorily way.

Reference

CNUDDE, V.; BOONE, M. N. High-resolution X-ray computed tomography in geosciences: A review of the current technology and applications. **Earth-Science Reviews**, v.123, p.1-17, 2013.

DAL FERRO, N.; MORARI, F. From real soils to 3D-printed soils: reproduction of complex pore network at the real size in a silty-loam soil. **Soil Science Society of America Journal**, v.79, n.4, p.1008-1017, 2015.

EMPRESA BRASILEIRA DE PESQUISA AGROPECUÁRIA (EMBRAPA). **Sistema brasileiro de classificação de solos**. 3th ed. Rio de Janeiro: Centro Nacional de Pesquisa de Solos, Rio de Janeiro, 2013.

HELLIWELL, J. R. et al. Applications of X-ray computed tomography for examining biophysical interactions and structural development in soil systems: a review. **European Journal of Soil Science**, v.64, n.3, p.279-297, 2013.

HERNÁNDEZ ZUBELDIA, et al. Cellular automata and x-ray microcomputed tomography images for generating artificial porous media. **International Journal of Geomechanics**, v.16, n.2, 2015.

KUVA, J. et al. Pore and mineral structure of rock using nano-tomographic imaging. In: **MRS Proceedings**, 1744, p. 235-240, 2015.

MARCHINI, D. C. et al. Matéria orgânica, infiltração e imagens tomográficas de Latossolo em recuperação sob diferentes tipos de manejo. **Revista Brasileira de Engenharia Agrícola e Ambiental**, 19, p.574-580, 2015.

PASSONI, S. et al. Three dimensional characterization of soil macroporosity by X-ray microtomography. **Revista Brasileira de Ciência do Solo**, v.39, n.2, p.448-457, 2015.

PETH, S. et al. Localization of soil organic matter in soil aggregates using synchrotron-based X-ray microtomography. **Soil Biology and Biochemistry**, v.78, p.189-194, 2014.

PIRES, L. F. et al. Soil structure changes induced by tillage systems. **Soil and Tillage Research**, v.165, p.66-79, 2017.

ROZENBAUM, O.; BRUAND, A.; LE TRONG, E. Soil porosity resulting from the assemblage of silt grains with a clay phase: New perspectives related to utilization of X-ray synchrotron computed microtomography. **Comptes Rendus Geoscience**, v.344, n.10, p.516-525, 2012.

VAZ, C. M. et al. Evaluation of an advanced benchtop micro-computed tomography system for quantifying porosities and pore-size distributions of two Brazilian Oxisols. **Soil Science Society of America Journal**, v.75, n.3, p.832-841, 2011.

WANG, W. et al. Intra-aggregate pore characteristics: X-ray computed microtomography analysis. **Soil Science Society of America Journal**, v.76, n.4, p.1159-1171, 2011.